Alkaline Battery Division

GULTON INDUSTRIES, INC.

Metuchen, N. J.

DESIGN, DEVELOPMENT AND MANUFACTURE OF STORAGE BATTERIES FOR FUTURE SATELLITES

* * * * * *

NASA - FINAL REPORT - JULY 1, 1963

NATIONAL AERONAUTICS AND SPACE ADMINISTRATION

CONTRACT NO. NAS 5-809

GODDARD SPACE FLIGHT CENTER

GREENBELT, MARYLAND

PREPARED BY

R. C. SHAIR, Director of Research

H. N. SEIGER, Asst. Director of Research

H. COHEN, Research Chemist

A. LYALL, Research Chemical Engineer

G. RAMPEL, Senior Chemist

E. KANTNER, Senior Chemist

GULTON INDUSTRIES, INC.
212 DURHAM AVENUE
METUCHEN, NEW JERSEY

TABLE OF CONTENTS

TABLE OF CONTENTS (Continued)

TABLE OF CONTENTS (Continued)

LIST OF FIGURES

LIST OF FIGURES (Continued)

LIST OF FIGURES (Continued)

LIST OF FIGURES (Continued)

REFERENCES

1. H. N. Seiger and R. C. Shair; Paper presented at the Electrochemical Society Meeting, Detroit, Oct. 1961.
2. Gulton Industries, Final Report, S. L. Conti No. DA 36-039 SC-8539, June 1962
3. J. E. Wynn, Paper delivered at E.C.S. Meeting, Detroit, 1961
4. W. Latimer, Oxidation Potentials, Prentice Hall, N. J., 1952
5. M. Barak, et alia, Paper delivered at E.C.S. Meeting, Detroit, 1961
6. Gulton Industries, Inc., Signal Corps, 6th Quarterly Report, Contract No. DA 36-039 SC-85390 Dec. 1961
7. M. Breiter, J. Electrochem. Soc. 109, 425 (1962)
8. R. A. Jeanine, Patent 2,646,455, July, 1953
9. G. Neumann and V. Gottesmann, U.S. Patent 2,571,927, Oct. 1951
10. E. Baars, Paper presented at the Electrochem. Soc. Meeting, Boston, 1954.
11. E. Baars, Proceedings 12th. Annual Power Sources Conference
12. W. Berl, Trans. Electrochem. Soc. 83, 253 (1943).
13. A. Fleischer, Private Communication
14. K. Dehmelt and H. von Dohren, Proceedings 13th. Annual Power Sources Conf.
15. M. Quintin and R. Viltange, Compt rendu 250, 840 (1960)
16. Gulton Industries, Inc., Signal Corps, Final Report, June 1962, DA 36-039 SC-85390
17. Gulton Industries, Inc., AF Tec. Doc. Report No. ASD-TDR 62-67, April, 1962
18. Unpublished data obtained in these laboratories
19. Gulton Industries, Inc. Signal Corps Report, 4th. Quarterly, June, 1961 DA 36-039 SC-85390

20. G. Bianchi, et alia, U.S. Government Research Reports AD 278690, abstract,

21. D.A. Sama, et alia, J. Electrochem. Soc. 109, 884 (1962)

22. S. Hoshizawa and Z. Takehara, Electrochem. Acta., 5, 240 (1961)

23. Z. Szklarska-Smialowska and M. Smialowski, J. Electrochem. Soc. 110, 44 (1963)

24. J. Wells, J. Amer. Chem. Soc. 33, 504 (1911)

I. ABSTRACT

The work originally contemplated under this contract was divided into three phases:

Phase I Fabricate and Test Advanced State of the Art Hermetically Sealed Nickel-Cadmium Cells

Phase II Establish a Pilot Line for the Exclusive Fabrication of Hermetically Sealed Cells for Space Applications

Phase III Perform Fundamental Studies on Hermetically Sealed Cells

The initial effort was directed at fabricating the VO-6 HS cell so as to yield a mechanically sound and uniformly reproducible product. Initially the cell closure was achieved by heliarc welding but this caused a large percentage of losses of the ceramic-to-metal seal. An attempt was made to reduce thermal stresses by use of a cadmium solder, but the degradation of the solder in the caustic oxidizing environment plus the undesirable high vapor pressure of cadmium caused this technique to be abandoned. Experimentation in heliarc welding techniques coupled with methods to heat sink the cells during welding led to a final perfected all welded can. For the VO-6 HS cell a drawn can was developed to reduce cell dimensions and to provide a more uniform package.

VO-6 HS cells were fabricated and their electrical performance observed in continuous repetitive 100 minute cycling routines. At 77^{o}F, at a depth of 70%, 1500 cycles were achieved and at a depth of 50%, 4900 cycles have been reached and the tests continue.

Large size hermetically sealed nickel-cadmium cells were fabricated and tested. The VO-50 HS cell is the largest space cell available today. It has a capability of 18.4 watt-hours per pound. Mechanically it has been optimized for heat transfer and it contains a heavy duty ceramic-to-metal terminal closure.

Thin plate cells were fabricated and found to have enhanced properties for those cases where the performance is dependent on current density. The thin plate cells did not, however, offer any advantages in their watt-hour-per-pound performance.

The thermal aspects of hermetically sealed cells were studied. Temperature profiles were determined for several different temperatures and operating rates. A mathematical analysis was made to determine the optimum cell geometry based on thermal considerations. This was applied to the design of the VO-50 HS.

Studies were made of electrode impregnation techniques to improve plate loading without decreasing the coefficient of utilization of active materials.

A detailed fundamental study was made of the charge efficiency of sealed cells. Studies were made both of the negative and positive plates at various rates of charge and at various temperatures.

Fundamental research was carried out on the mechanism of oxygen reduction at the cadmium electrode. A new theory was advanced, postulating that the reduction is a chemical reaction between the oxygen and absorbed hydrogen generated on the nickel matrix of the negative plate. Experimental evidence was collected which substantiates the theory.

II. ESTABLISHMENT OF A PILOT LINE FOR THE FABRICATION OF HERMETICALLY SEALED CELLS

The basic philosoph for the establishment of a pilot line for the fabrication of hermetically sealed cells for space applications was to provide extreme quality control and 100 percent inspection of all items, and at every phase of manufacture. The cells were to be carefully checked for the hermetic seal, for mechanical perfection, for satisfactory capacity, resistance and voltage characteristics, for assurance of working overcharge capability (and hence low internal cell pressure), and for assurance of the absence of internal shorts. Each cell was to be precycled ten times to assure its functional capability, and to weed out incipient cell failures that might show up early in life.

The design and establishment of a pilot production line required certain fundamental prerequisites. This line was designed to produce reasonable quantities of the cell specifically in mind at its conception, and it was also to have a flexible capability of producing cells of other designs. The processes developed in the Pilot Plant have had considerable bearing upon the design of future cells.

The pilot line consists essentially of several separate but parallel lines joining for the final assembly as shown in Figure 1. Each triangular operation is an inspection. Since this is a Pilot Plant, equipment is grouped more for convenience in installation and segregation of types of operations rather than on a material flow basis. It is assumed that variations in cell construction will from time to time alter the material flow within the Pilot Plant.

This Pilot Plant area is completely enclosed and air-conditioned for the preservation of cleanliness, reduction of humidity, and control of temper-

ature during the assembly of hermetically sealed cells for satellite applications.

Two key steps in the manufacture of satellite cells are the manufacture of the ceramic-to-metal seal and the final electrical and mechanical check-out of the cell. The basic equipment used to make and evaluate the seals are the Kinney Vacuum systems with their furnaces and the Veeco Mass Spectrometer Helium Leak Detector.

The Kinney PW-400 Vacuum system, with a 40 volt power supply and specially designed furnaces, has been the major equipment for developing and producing ceramic-to-metal seals. This little unit was purchased first for its flexibility in performing the desired operations. Figure 2 is a picture of this machine. The one drawback to this machine was the vibration transmitted through the vacuum connections from the mechanical pump to the bed of the machine.

When it became evident that a larger machine was needed to handle anticipated demands for production, a Kenney P-2 Vacuum system best met the requirements and was installed. This machine is presently assembled with two groups of 8 furnaces each, giving a total of 16 furnaces which can be loaded simultaneously and fired in rotation from two 40 volt power supplies. The actual flow of metal at each seal may be observed by the operator so that uniform products may be produced.

The development of the furnaces played an important part in obtaining good seals. Each furnace must give an even heat so that each part of the seal will flow at nearly the same time. Any shorting of coils by vacuum deposited materials from the sealing operation results in subsequent rejections of seals. A ceramic covering for the heating element which shielded it from deposits and yet was not a substantial heat barrier was developed, and is now being used on all furnaces.

Each seal which passes a visual inspection is carefully checked for leakage. The Veeco MS 9ABC Helium Leak Detector has proven to be an excellent machine for testing these seals. A seal, properly fixtured on this machine, can be tested for a leakage rate of the order of 10^{-10}cc of helium per second. The test procedures have been set up so that if there is any detectable leakage, even though it is of an order which could be tolerated, the seal is rejected. This eliminates seals which have any detectable flaws which could become enlarged under service conditions.

The Veeco leak detector, Figure 3, is also used to check the final closure of a cell. The entire cell may be fixtured under a bell jar which is connected to the detector. The cell is evacuated and back filled with helium. Any helium that leaks from the cell to the bell jar is detected. Any cell that can pass this test with a pressure of 20 psia of helium inside is considered a good cell.

While the closure of a cell is of utmost importance, the elements within the cell are also important. A good container is of no value if the element within is capable of generating pressures that exceed the capacity of the container. To this end, two requirements must be met: the cell must be capable of recombining the oxygen formed at the positive plate during overcharge, and hydrogen evolution must be completely supressed during normal operation. To attain this objective, considerable care must be given to the formation cycle for the electrodes.

A formation pack consists of 8 positive plates and 9 negatives with a Dynel and Viskon separator wrapped as shown in Figure 4. By handling the plates in small groups, it is possible to handle large quantities and still individually assess the quality of all the plates. The formation setup is

shown in Figure 5. If the capacity of any one plate is low, the entire pack containing this plate is discarded. Prior to formation, all plates are given a close inspection for any defects, particularly on the edges.

Following the formation cycles, the plates are thoroughly washed in a spray bath which removes all of the potassium hydroxide from the plates. The timing of this bath is critical since the plates must be washed clean, but must be removed from the wash before any corrosion occurs along the edges of the steel foundation of the plates. The plates are rushed from the wash into drying ovens where they are rapidly dried at a temperature of 50°C.

Until the plates are required for cell assembly, they are stored in plastic containers. Plate tabs are cut to length during this time, the positive tabs being one length, the negatives a different length. This makes it virtually impossible for electrode assemblies to be made in a mixed manner, or for the plates to be connected to terminals in improperly reversed polarity. The difference of plate length would certainly be spotted at one of the many inspections prior to the final closure of the cell.

The use of proper fixtures for cutting tabs, welding combs to packs, straightening combs after welding, and inserting the separator material greatly facilitates the final assembly. Some of these are shown in Figures 6 and 7. All electrode stacks of hermetically sealed cells are heavily compressed. This compression is necessary for the proper functioning of the cell, particularly on overcharge when oxygen is formed at the positive electrode but remains dissolved and transfers to the negative plate by diffusion through the flooded separator. The diffusion path should be as short as possible for maximum overcharge capability, and therefore the separator is compressed between the electrodes. The case is so designed that the electrode stack must be compressed to be inserted. While under maximum compression, the pack is checked for shorts.

With the pack inserted, the cell is now closed, using careful welding techniques and an Arcofix heliarc welding machine. Proper heat sinking protects the internal structure of the cell and the ceramic-to-metal seal.

The back-filling station of the Veeco MS9-ABC unit is now used to check the seal of the entire cell. The cell is fixtured, by means of the pinch tube, to the manifold outlet of the back-fill station, and tested as previously outlined. Successful cells are then filled with a carefully controlled amount of electrolyte. Valve and gauge assemblies are then attached to every cell by means of a collet fitting on the pinch tube.

At this point the assembled cells are conditioned and then processed through an elaborate electrical and mechanical checkout. For this purpose, a 50 volt 300 ampere power supply has been installed and an automatic cycling panel is programmed to give each cell at least ten cycles of 25% depth.

The final steps in the manufacture of the cells consist of closing the pinch tubes, removing the gauge unit, welding the pinch tube tight, and making final electrical tests and leak checks on the finished cell prior to shipment. Each cell is supported in a clamp during processing as shown in Figure 8. Prior to shipment the cells are removed from the clamp to check for bulging and for dimensional conformity. The cells are then cleaned, labeled and shipped with the clamps for the convenience of the customer.

Each cell is shipped with a data sheet certifying that the cell has been mechanically and electrically checked out. Capacity, voltage, overcharge voltage, overcharge pressure, and absence of electrical shorts are shown. Each cell receives several capacity checks including a final one after it has been sealed off.

The elaborate inspection and electrical checkout takes more processing time than actual cell fabrication, but ensures the acceptability of the cell for reliable satellite application.

At the present time, the Pilot Plant processes prismatic cells of the 1, 3, 6, 12, 20 and 50 ampere-hour size, and cylindrical cells of the 1, 2, and 3 ampere-hour size.

III. FABRICATION OF VO-6HS HERMETICALLY SEALED NICKEL-CADMIUM CELLS

A. WELDED CANS

At the start of this program, the electrochemical considerations of the operation of the nickel-cadmium system were pretty well defined and understood. This information had been obtained in laboratory cells which were sealed by gasketing methods.

The problems involved in the production of hermetically sealed cells centered mainly about the generation of the ceramic-to-metal seal and the associated problems of joining the terminal to the plates and the header to the cell case.

The basic solution to the problem of joining the plates to the terminal was solved by designing a terminal and comb system whereby the plates are joined to a comb by heliarc welding the projections of the plate tabs through the slots in the comb. The comb could then be joined to the terminal base by spot welding methods. This resulted in a light weight terminal construction of minimum vertical development and adequate electrical path.

The problem of generating a satisfactory ceramic-to-metal seal was divided into two problems. The first problem, naturally, was to generate a sound seal; the second problem was to determine that a sound seal had actually been produced. Actually, the second problem had to be solved first.

The submerged bubble check was found to show up gross leaks, but was too slow when looking for a leak in the order of 10^{-6} cc/sec of helium. The first attempt at the leak detector was the use of a halogen detector using freon as the tracer fluid. The combination of the sensitivity of the detector and the size of the freon molecule made this method unsatisfactory. The solu-

tion was found in the application of the mass spectrometer helium leak detector. The techniques for using this apparatus were worked out to test individual seals and finally completed cells.

The solution to the problem of generating good ceramic to metal seals was found largely in the refinement of the techniques of firing the seal. Since the seals were produced by the active metal process, all the heating and cooling was carried on in a high vacuum chamber where the transfer of heat from the coils of the furnace to the parts being brazed is entirely by radiation. Some of the seal parts are white and poor conductors of heat, while the metal parts are gray with good conduction. In addition, there are slight differences in the thermal coefficient of expansion between parts at the brazing temperature. Therefore, the heating cycle is important so as to bring both surfaces to be joined up to the brazing temperature at the same time that the brazing alloy melts. Refinements of the heating cycle finally resulted in acceptable seals being produced.

With the advent of the satisfactory ceramic-to-metal seal, problems in the final closure of the cell which had previously been masked by the imperfect seal became evident. It was found that stresses set up in the cover by the welding operation joining the cover to the case were fracturing the ceramic. The first attempt to correct this was to use a cadmium solder to join the cover to the case. This solder melted below the temperature at which the expansion coefficients of the ceramic and the cover diverge. What was not considered at the time was the fact that the joints, which were heated by a torch, were not being evenly heated with the result that uneven stresses were set up within the cover resulting in seal fracture. In addition, the solder joint did not retain the internal battery environment of caustic and oxygen.

The solution to this problem, of joining the cover to the case, was found in applying the heliarc process of welding again, but with the cover de-

signed to keep the area being welded out of the plane of the ceramic-to-metal seal. In addition, careful heat sinking of the cell during welding prevented overheating.

Testing of the ceramic-to-metal seal is conducted at several stages in the manufacture of the cell. A mass spectrometer detecting helium leakage is the apparatus used to conduct the tests. The seals are first checked individually upon removal from the furnace. Another check is made when the plates have been joined to the terminals. A third test is conducted upon the cell after the cover has been joined to the container, but before electrolyte is added to the cell. A final test is made after the cells are tested electrically and the pinch tube sealed. This final test may be conducted in two manners: first, helium may be introduced to the cell before the final pinch is made and, second, the cell may be exposed to a high-pressure helium atmosphere and checked for any traces which leak in and then back out. The former method is the surest method.

B. DEEP DRAWN CELL CONTAINERS

The development of deep drawn cell containers came about with the need to improve hermetically sealed cells for space applications. Three major factors make the drawn can a superior container over the present weldment. First, the drawn container dimensionally can be made to closer tolerances. Second, the strength of a drawn unit is approximately three (3) times greater than that of a welded unit of the same material. Third, there are fewer seams that might normally allow the possibility of leakage. Aside from the above mentioned improvements, the question of weld slag contaminating the cell always arises. Deep drawn cans minimize this since only one weld occurs - the final weld of the header to the can.

To meet existing dimensional requirements, the deep drawn container had to be similar to the welded can used. This required special tooling not normally found in establishments doing this type of work. The corners and radii had to be held to close tolerances as well as the depth of draw. To accomplish this, eight (8) separate developments had to be made. This proved to be a trial and error operation, to flow the material to the proper location for the next draw. After each drawing operation the material must be annealed because it work hardens during the preceding operations. The final dimensions of the VO-6HS cell with drawn case are shown in Figure 9.

The final finish of the surface of the cans caused more of a problem than anticipated. The sides and faces had to be smooth and free from any disfigurations. To accomplish this, the side had to be ironed first and then annealed. Then the faces had to be ironed. The annealing, after ironing the faces, was eliminated to retain added stiffness in that portion of the can which would normally tend to bulge with any internal pressure.

At the present time, the deep drawn container for the VO-6 HS cell has been perfected and is being used in normal production. Figure 10 shows the drawn case.

During the past two years the uniformity of cell characteristics has improved to the point where normal production of VO-6 yields the bulk of the cells having capacities between 6.3 and 7.1 ampere-hours as shown in Figure 11.

IV. ELECTRICAL PERFORMANCE OF VO-6HS CELLS

A. CYCLING TO 70% DEPTH

Six laboratory cells of the VO-6 type were fabricated and electrically checked out by charging them at 0.6 amps for 5 days, and discharging them to 1.00 volts at a 3.0 ampere rate. This was repeated and the capacities were determined. The average capacity was 6.67 ampere hours with a spread of 0.70 ampere hours.

The cells were fully charged and overcharged for two days at 0.6 amps (C/10) after which they were placed on a 70% depth of discharge cycle consisting of a 60 minute discharge at 4.2 amperes followed by a 120 minute charge at 2.4 amperes. This charge was found to be insufficient and was increased after a few cycles to 2.5 amps or a 19% overcharge.

These cells continued cycling for 560 cycles. A typical cycle curve for one of these cells at cycle number 500 is shown in Figure 12. A three hour cycle had been selected because of a lack of cycling data on this size cell, but since they were responding normally to this cycle, it was decided to change the cycle to a 90 minute cycle. At the end of the 560th. cycle, the average end of charge voltage was 1.50 with a spread of 0.03 volts. The cells were taken off cycle at the end of charge and placed on 0.6 amps for two hours and then discharged at 3.0 amps (C/2). The average capacity was 4 ampere hours with a spread of 0.2 ampere hours. The cells were exhibiting the "memory effect" and at 70% depth were exhibiting just the capacity being cycled. Some cells were below 1.0 volts at the end of discharge. The cells were shorted after discharging to 0.60 volts and left shorted for 16 hours. They were recharged at 0.6 amps and 16 hours. They were recharged at 0.6 amps and left on

overcharge for 5 days. The average overcharge voltage was 1.39 with a spread of 0.04 volts.

The cells were then put on a 90 minute cycle consisting of a 35 minute discharge at 7.2 amps and a 55 minute charge at 5.5 amps or a 20% overcharge.

After 800 cycles, it was noted that the end of discharge voltage of one of the cells was down to 0.50. Cycling was stopped at the end of charge after 800 cycles and the cells placed on a 0.6 amp overcharge for 16 hours. The capacities were checked at a C/2 rate. Two cells had 6.2 ampere hours, two had 6.0 ampere hours, and one had 5.7 ampere hours, and one cell had 3.9 ampere hours. This cell was the same one that had an end of discharge voltage of 0.50 volts. Upon returning the cells to a 0.6 ampere charge, this cell indicated a partial short. The cell was disassembled and a burned spot found in the edge of the separator between plates.

The remaining cells were recharged at 0.6 amps and overcharged for 5 days at the same rate. The capacities were again determined at 3.0 amp discharge rate, and the average capacity was 5.72 ampere hours with a spread of 1.0 ampere hours. The cells were recharged again and put back on cycle.

At about the 850th. cycle one of the cells was observed to exhibit a decreasing end of discharge voltage and a rising end of charge voltage. This continued with increasing magnitude. At the 926th. cycle this cell indicated a short and it was removed and disassembled for failure analysis. The separator was very dry and there was a short burned through the separator at one of the corners. At the 960th. cycle another cell similarly failed.

The remaining three cells continued on cycle, and at the end of 1500 cycles the end of charge voltages average 1.57 and the end of discharge voltages average 1.00. A change in charge current of .05 amps was detected and

corrected so that the end of discharge voltages returned to the 1.04 volts which is the usual level for this cycle.

At cycle 1587 one of the cells dried out and failed during the week-end. The remaining two cells developed high pressures since the balance of the charge-discharge current was upset. When one cell failed, the other two were discharged at a lower current and charged at a higher current rate, resulting in too much overcharge, and at too high a charge rate with the resulting high pressure.

The cells were removed at the end of a charge cycle, checked for capacity at the C/2 rate, and found to be 3.63 and 4.8 ampere hours. After treating the cells as described in the following section on 50% depth of discharge, the capacities were 6.5 and 6.6 ampere hours respectively. After a second treatment followed by a C/10 overcharge for 7 days, the capacities were each 7.6 ampere hours and the overcharge pressures were less than 10 psig.

B. CYCLING TO 50% DEPTH

Another set of VO-6 HS cells that was placed on an automatic 50% depth cycle August 20, 1962, have completed over 4850 cycles. This cycle consists of a 35 minute discharge at 5.15 amperes or 3.0 ampere hours, followed by a 55 minute charge at 3.86 amperes, which corresponds to an 18% overcharge based on the capacity removed. The voltage of a typical cell are plotted in Figure 13 for cycles number 2, 1440, 2825, and 4634.

This set of curves shows two prominent features of cell voltage during cycling. During the early cycle life the cell is being discharged midway through a normal C rate discharge (approximately C rate) and the end of discharge is on the 1.2 volt plateau. Likewise, the end of charge voltage is

typical for a C/2 overcharge at temperatures close to 100°F which is the expected range based on experimental work done in this laboratory. As the number of cycles increases, the end of discharge voltage starts to decrease and the end of charge voltage starts to show the sudden rise to a short plateau during the overcharge period (beyond 81.6 minutes of the cycle) of the charge cycle. The deviation found in the curves of cycle numbers 1440 to 4634 can be better attributed to temperature differences than to any peculiar characteristic of cycle life.

A plot of the average end of charge voltages and end of discharge voltages versus cycle number is shown in Figure 14. The fluctuation in end of discharge voltage at the beginning was due to instability in the cycling current. Since at this depth of cycle, only 18% overcharge is necessary to maintain an end of discharge voltage above 1.00 volts, instead of 20% overcharge, it is also more critical to maintain the current constant. A drop of 0.06 amps on charge means a change from 18% overcharge to 16% overcharge which is not enough. If the overcharge is increased above 18% to allow a greater safety factor, the end of charge voltages are higher. It is desirous to maintain the lowest practical charge current to keep the pressure low without losing capacity.

There is a continuous increasing of the end of charge voltage and a continuous decrease in the end of discharge voltage. Between 3800 and 4000 cycles there was some mechanical difficulty with the relay on the charge circuit, but since this has been fixed, the end of discharge voltage has stabilized at slightly above 1.00 volts. It is impossible with this cycle to reduce the end of charge voltage without lowering the end of discharge voltage too. Because of the "memory effect" these cells have essentially a 3.0 ampere hour capacity and will discharge down to 1.0 volts. Since the period of the charge cycle is fixed, any increase in overcharge must be accomplished by increasing the current,

and this will result in high pressures. If the cell is removed from cycle while charged and given a C/10 overcharge for 24 hours, the capacity comes back to almost the full capacity. If the cell is discharged to 1.0 volts, then shorted through a one ohm resistor to 0.1 volt, then given a dead short for two hours, followed by a C/10 charge for 24 hours, the full capacity is usually recovered. A second such treatment has always resulted in recovery of the full capacity.

As has been noted in other tests, continuous repetitive cycling does not result in irreversible loss of capacity. Even though the cycled cells assume a capacity about equal to the depth of the cycle routine, the full nominal capacity is recoverable after a C/10 overcharge. Separator failure (shorted cell) still appears to be the most likely cause of cell failure.

V. FABRICATION AND ELECTRICAL CHARACTERISTICS OF VO-50 HS HERMETICALLY SEALED NICKEL-CADMIUM CELLS

Because of the trend toward larger satellite power levels, a design was made for a 50 AH cell. Cells of this size were constructed and tested electrically.

The major areas for consideration for 50 AH cells were the electrical capacity, the mechanical design of both the package and the ceramic-to-metal seals, and the thermal parameters.

A. CAPACITY

Electrodes which have an active area of 4.6 inches wide by 4.5 inches high have a theoretical positive plate capacity of 3.76 AH per plate. With 15 positive electrodes, the design capacity was calculated to be 56.4 AH, which, allowing for all variations, was considered to be a conservative design for the VO-50 HS.

The dimensions of the cell using this configuration, with a compact composit terminal, has the following outside dimensions as shown in Figure 15.

Thickness	1-9/32 inches
Width	4-7/8 inches
Height (over case)	5-41/64 inches

Cell V = 34.8 $in.^3$

The electrode stack is shown in Figure 16 along with a VO-6 HS electrode stack.

B. THERMAL CONSIDERATIONS

From the heat transfer analysis of Section VII, the critical dimensions to be avoided were as follows:

Thickness of Cell	$X = .602 \times V^{1/3}$	$= .602 \times 3.26 = 1.96$ inches
Width of Cell	$Y = 1.028 \times V^{1/3}$	$= 1.028 \times 3.26 = 3.35$ inches
Height of Cell	$Z = 1.62 \times V^{1/3}$	$= 1.62 \times 3.26 = 5.28$ inches

As seen from the above figures, the only dimension approaching the critical dimension was the height; the others being decidedly on the favorable side.

A more detailed thermal analysis for the 50 ampere-hour cell is included in Section VII - C.

C. MECHANICAL CONSIDERATIONS

As shown in Figure 15, the VO-50 HS cell is 1-9/32 inches thick, 4-7/8 inches wide, and 5-41/61 inches high.

The thickness of the cell is close to the maximum considered practical for unsupported cell sides in a cell of this size. With cell walls of .0319 stock, a maximum cell thickness should be in the order of 1-1/4 inches. This cell is within 0.036 inch of this figure and is considered practical.

Design-wise, the 50 AH hermetically sealed cell differs in several ways from the smaller cells. Normally, the hermetic seal was formed by making a ceramic-to-metal bond between the cover and the ceramic insulator, in addition to between the terminal and ceramic insulator. In the present design, neither of the two terminal posts forms part of the hermetic seal. This allows freedom in the choice of materials from which the terminal can be made. The material that has been chosen is copper, which allows good heat transfer and has better electrical conductivity.

For the hermetic seal at the positive terminal, the upper end of the ceramic insulator has a seal ring attached by a ceramic-to-metal bond. At the

lower end, the lower seal ring is also attached by a ceramic-to-metal bond. Both these seals are compression seals. The copper terminal, which passes through the center of the insulator is silver soldered to the terminal base. The upper face of the terminal base is heliarc welded to the bottom face of the lower seal ring completing the hermetic seal. At the lower end of the terminal base is a plate which is slotted parallel to the direction of the electrodes. The tabs of the nickel electrodes are notched so that they can be slipped into the slots and welded, thereby allowing a reduction in case height compared to the usual method of using combs.

The negative terminal is grounded to the case so that the copper terminal is silver soldered to the cover. The electrodes are welded into the comb and the comb is attached to the cover by a comb support. The cover is made by drawing, and the case is fabricated and heliarc welded.

D. ELECTRICAL CHARACTERISTICS

Table I shows the test histories of VO-50 HS cells fabricated and tested under this program.

Figure 17 shows a typical discharge characteristic, and Figure 18 shows overcharge voltage.

TABLE I.

TEST HISTORIES OF GULTON VO-50 H.S.

HERMETICALLY SEALED CELLS FOR

N A S A

CELL NUMBER	OVERCHARGE FOR 24 HOURS AT 5.0 AMPS. VOLT.	PRESS.	ON CYCLE FOR 10 CYCLES CONSISTING OF: 36 MINUTE DISCHARGE AT 20.0 AMPS. 64 MINUTE CHARGE AT 13.5 AMPS. ON CYCLE PRESSURE	OVERCHARGE FOR 24 HOURS AT 5.0 AMPS. VOLT.	PRESS.	DISCHARGED AT 25.0 AMPS. TO 1.0 V PRESS.	A.H.	OVERCHARGE FOR 24 HOURS AT 5.0 AMPS. VOLT.	PRESS.	DISCHARGED AT 25.0 AMPS. TO 1.0 V PRESS.	A.H.	SHORTED FOR 16 HRS. CHARGED 5 MINUTES AT 5.0 AMPS ON OPEN CIRCUIT STAND FOR 24 HOURS O. C. V.	OVERCHARGE FOR 24 HRS. AT 5.0 AMPS. VOLT	DISCHARGE AT 25.0 AMP. TO 1.0 V. A.H.	OVERCHARGE FOR 24 HRS. AT 5.0 AMP. VOLT	DISCHARGED AT 25.0 AMP. TO 1.0 V. A.H.
100	1.40	39	5	1.39	35	-14	59.20	1.40	46	-10	59.17	1.19	1.42	60.83	1.41	60.83
101	1.40	41	4	1.39	41	-19	58.90	1.40	50	-20	58.91	1.19	1.42	61.08	1.41	61.26
102	1.40	69	13	1.38	59	-10	56.67	1.40	39	-15	56.25	1.20	1.40	58.34	1.41	58.75
103	1.40	60	13	1.38	54	- 5	59.17	1.40	39	-12	59.58	1.20	1.40	60.00	1.41	61.26
104	1.40	47	7	1.39	44	- 9	58.34	1.40	19	-20	58.34	1.20	1.40	59.58	1.41	60.00
107	1.42	49	6	1.38	22	3	56.67	1.38	40	5	55.00	1.17	1.39	61.68	1.39	59.17
108	1.43	15	-25	1.38	18	-29	63.34	1.38	22	-25	62.51	1.18	1.40	66.25	1.39	64.18
109	1.41	30	- 2	1.38	25	- 8	58.34	1.38	23	- 5	56.25	1.16	1.40	61.26	1.39	59.17
111	1.41	35	0	1.38	31	- 9	58.76	1.38	30	- 2	56.67	1.17	1.40	62.09	1.38	60.01
115	1.42	46	2	1.38	38	- 5	57.51	1.38	38	- 2	55.42	1.19	1.40	60.43	1.38	58.76
116	1.41	39	8	1.40	31	-15	61.25	1.41	38	-14	62.45	1.20	1.40	62.08	1.40	62.91
117	1.40	39	+ 5	1.39	31	-17	57.08	1.41	33	-15	58.33	1.18	1.39	59.58	1.39	60.00
118	1.41	31	+ 5	1.39	26	-15	61.63	1.41	32	-12	62.08	1.19	1.39	62.81	1.39	62.08
119	1.41	23	- 5	1.39	26	-15	57.50	1.41	20	-12	58.33	1.18	1.39	60.00	1.39	59.58
120	1.41	25	+ 8	1.39	20	-15	56.25	1.41	22	-12	56.67	1.18	1.39	57.50	1.39	59.58
121	1.41	24	+ 8	1.39	21	-15	57.91	1.41	28	-14	58.75	1.18	1.39	59.58	1.39	60.41
123	1.40	28	- 8	1.39	21	-15	58.33	1.41	34	-12	58.58	1.18	1.40	60.41	1.40	61.66
124	1.41	30	+ 5	1.39	26	-15	59.16	1.41	27	-14	60.00	1.18	1.40	60.41	1.40	61.66
125	1.41	30	+ 5	1.39	24	-12	60.83	1.41	36	-12	61.66	1.19	1.38	61.66	1.39	62.08
126	1.40	25	- 8	1.39	21	-13	57.50					1.18	1.40	59.58		
127	1.40	15	-18	1.39	15	-22	58.48					1.18	1.40	61.25		
128	1.40	34	+ 7	1.39	32	-10	59.16					1.18	1.40	62.08		
129	1.40	22	-12	1.39	17	-12	58.48					1.18	1.40	61.25		
130	1.40	20	-12	1.39	25	-12	60.00					1.17	1.40	62.08		
131	1.40	20	-11	1.39	23	-12	58.48					1.18	1.40	60.41		

VI. THIN PLATE CELLS

A. DESIGN AND FABRICATION

In order to determine if there were any possible advantages to using thinner electrodes in prismatic sealed cells, two special 5 plate laboratory cells were fabricated from specially prepared thin sintered plates. The plates were .025 inches thick, which is 73.5% of the thickness of our standard plates which are .034 inches thick. A series of discharges were conducted, and the capacities obtained correspond to 75 to 77 percent of the standard plate. Based on the volume of the plate, there is an apparent gain of available capacity of 2 to 4 percent. From this information six cells were assembled using the thin plates in a construction similar to that of the VO-6 HS cell. The thin negative and positive electrodes which were employed had thicknesses of 0.025 inch and 0.027 inch respectively. The porosity in the dry discharged state is 21% as compared to 17% for the standard thickness. The VO-6 HS can was used, but the overall height was 0.25 inch less. The cells contained 11 positive and 12 negative plates, and the separator was non woven nylon. The amount of electrolyte for the cell to function as a hermetically sealed cell was calculated to be 13.5 ml based on porosity measurements for the plates and separator. Sufficient electrolyte was added to completely flood both the plates and the separator between them.

B. ELECTRICAL CHARACTERISTICS

Because the porosity of the thin plate electrodes was 25% greater than that of the thicker plates, it was found that separate tank formation of the electrodes was not necessary. Therefore, after assembly the five cells were filled with 13.5 ml of electrolyte, evacuated, and sealed.

1. Overcharge Characteristics

The cells were charged at 0.5 amperes and then put on overcharge at the same rate. At the steady state, the voltages and pressures were recorded while the cells were maintained at 25 $\pm$0.5°C in an oil bath. The overcharge current was increased to 0.75 amperes until the steady state was again reached. Then the overcharge current was increased to 1.0 ampere and maintained until the steady state was obtained. The observed pressure versus overcharge current is shown in Figure 19. The overcharge current is expressed as a fraction of the cell capacity. The slope of the line representing the average of the five thin plate cells is given as 40 ma/psi.

In addition, Figure 19 also gives the observed pressure versus the overcharge current for typical VO-6HS and VO-20H nickel-cadmium cells. As shown, not only is the slope less for the VO-5X cell, but the overall pressures are lower.

Figure 20 illustrates the cell voltage as a function of the overcharge current. The overcharge current is expressed as a fraction of cell capacity. In addition, the curves for a typical VO-6HS and VO-20 HS nickel-cadmium cell are given for comparison.

2. Initial Cycling

After the overcharge, the cells were discharged at the C/2 rate. The capacity to 1.0 volts was 5.75 AH. They were then recharged manually at 0.5 amperes and put on cycling which discharged the cells to a 40% depth and returned 120%. The discharge portion was 3.9 amperes for 35 minutes, 2.28 AH, while the charge portion was 3.0 amperes for 55 minutes, 2.74 AH. The cells were cycled 31 times. Table II gives

the beginning of discharge, end of discharge, beginning of charge, and the end of charge voltages for cycle 1, cycle 14, and cycle 31.

TABLE II.

CELL VOLTAGES AS A FUNCTION OF CYCLE NUMBER

	Charge Voltages		Discharge Voltages	
Cycle Number	Beginning	End	Beginning	End
1	1.30	1.46	1.29	1.22
14	1.20	1.47	1.35	1.19
31	1.27	1.48	1.34	1.18

3. Charge-Discharge Characteristics

After the 31 cycles, the cells were placed on a 0.5 ampere continuous charge for 24 hours. A C/2 rate discharge was conducted and the capacity obtained was 4.62 AH. The cells were recharged at 0.5 amperes and then overcharged at 1.0 ampere.

A C rate, 5.0A, discharge was conducted, and the capacity obtained was 4.74 AH to 1.0 volt. Figure 21 illustrates the performance. For comparison a C rate discharge for a typical VO-6 HS cell is added to the same figure.

Figure 22 shows the discharge voltage of the thin plate cell as a function of the discharge rate. In Figure 23 is shown the voltage characteristic and capacity for several discharge rates.

4. Extended Cycling

The effect of extended cycling on the VO-5X cells has been studied. The five cells were subjected to 1987 cycles at 35% depth. Each cycle

corresponds to a 90 minute orbit. The cells were discharged at 3.0 amperes for 35 minutes (1.75 AH) and charged at 2.19 amperes for 55 minutes. In Table III below, data is given to cycle No. 1537. The average cell voltages at the beginning and end of the discharge as well as the beginning and end of charge are tabulated. In addition the cell pressures were monitored throughout the test. The average cell pressures and the range are given at the end of both the discharge and charge of the recorded cycles.

The end of discharge voltage is shown as decreasing with cycle life. Except for cycle 17, the data shows relatively stable pressures on both the charge and discharge portions of cycle throughout the test. It should be noted that for the five cells the range at no time exceeds 4.0 pounds. The pressure drop between the average end of charge and the average end of discharge ranges between 6.7 pounds and 12.1 pounds.

TABLE III.

CYCLING CHARACTERISTICS FOR THE VO-5X THIN PLATE CELLS

	DISCHARGE				CHARGE			
	Cell Voltage		Pressure psia		Cell Voltage		Pressure psia	
Cycle No.	E_o	E_{35}	Av.	Range	E_o	E_{35}	Av.	Range
17	1.35	1.21	10.7	10.3 - 11.3	1.27	1.46	16.7	15.7 - 17.2
515	1.36	1.17	21.9	20.2 - 24.2	1.24	1.49	30.1	28.7 - 32.2
1012	1.35	1.14	15.3	14.2 - 16.2	1.23	1.48	22.9	21.7 - 23.7
1537	1.35	1.07	17.7	16.7 - 19.2	1.25	1.48	29.8	28.2 - 31.7

5. Extended Overcharge

After cycle 1987 the cells were discharged and one ohm resistors were connected across the terminals of each cell. They remained in this state, in a constant temperature bath for 56 days to simulate dead storage conditions. In order to see how these conditions affected the cells, they were charged at 500 ma for 99 days. Throughout the test the cell voltages and pressures were monitored. The data is illustrated in Figure 24. It shows that the voltage rose rapidly initially, and then it started to decay after 2 days. The pressure shows a maximum at 10 days followed by a decay.

After the extended overcharge the cells were discharged at 5 amperes, the C rate. The average capacity to 1.00 volts was 4.65 AH. The C rate discharge previous to cycling gave 4.74 AH. The difference between the two capacities is within experimental error. Therefore, no indication of reduction in capacity has been observed due to cycling or extended overcharging.

C. COMPARISON OF THIN PLATE CELLS TO STANDARD SEALED CELLS

In order to ascertain the advantages of this cell, a comparison is given below of some of the characteristics of the VO-5X, VO-6 HS and VO-20 HS nickel-cadmium cells.

	VO-5X	VO-6 HS	VO-20 HS
WEIGHT (LBS.)	0.47	0.62	1.9
CELL DIMENSIONS (in)			
LENGTH	2.09	2.09	2.98
WIDTH	0.81	0.81	0.89
HEIGHT	2.91	3.67	6.58

	VO-5X	VO-6 HS	VO-20 HS
VOLUME in^3	4.92	6.15	17.44
WATT-HOURS	5.63	8.28	23.5
WATT-HOURS/LB.	12	12	13
WATT-HOURS/in^3	1.1	1.4	1.4

D. DISCUSSION

The thinner plates represent a 28.6% reduction in overall thickness and a 23.4% reduction of active matrix. The ratio of plate thickness to separator thickness was ~ 3.9 for conventional plates and 2.8 for the thinner plates. The same separator was used. It can be seen, therefore, that for a given capacity more electrodes and separator material were required. The VO-5X was constructed in a cut down VO-6 HS container. Nine (9) positive and ten (10) negative are used in the VO-6 HS, whereas 11 positives and 12 negatives could be inserted using thinner electrodes. The porosity of the thinner positives was 25% greater than the thicker positives, which fact made it possible to operate VO-5X cells without prior electrical formation. It was also observed that an extended stand of 56 days did not cause passivation of the electrodes, resulting in overpressuring when the cells were placed on charge at C/10.

The overcharge voltage and pressure characteristics which are dependent on current density showed improvement in the thin plate cells as might be expected because of the greater porosity of the plates and the greater surface available for electrochemical reaction.

However, due to the increased separator bulk, no enhancement was seen in the watt-hour per pound or watt-hour per cubic inch capability.

VII. THERMAL ASPECTS

A. THEORETICAL APPROACH

The first phase of this study was to mathematically derive a heat transfer equation applicable to the general configuration of the Gulton hermetically sealed cell.

ASSUME UNIDIMENSIONAL HEAT TRANSFER

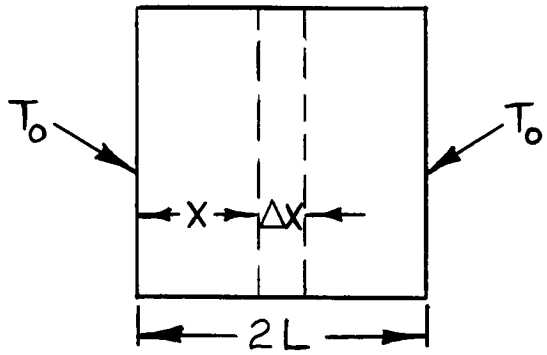

Heat Conducted Through Left Face During Time $\Delta\theta$ + Heat Generated by Sources in Element During Time $\Delta\theta$ = Heat Conducted Through Right Face During Time $\Delta\theta$

$$(1) \quad -KA \frac{dt}{dx}\Big|_X \Delta\theta + \dot{q}(A\Delta X)\Delta\theta = -KA \frac{dt}{dx}\Big|_{(x+\Delta X)} \Delta\theta$$

where $\dot{q}$ = $\frac{\text{Heat Source Strength}}{\text{Unit Volume, Unit Time}}$

Using the Mean Value Theorem

$$f(x + \Delta x) = f(x) + \frac{d}{dx}(f(x))_M \Delta x$$

where M is located between (x) and (x + Δx)

$$\therefore \frac{dT}{dx}\Big|_{(x+\Delta x)} = \frac{dT}{dx}\Big|_x + \left[\frac{d}{dx}\left(\frac{dT}{dx}\right)\right]_M \Delta x$$

Substituting into Equation (1)

$$-KA\frac{dT}{dx}\Big|_x \Delta\theta + \dot{q}\,(A\Delta X)\Delta\theta = -KA\frac{dT}{dx}\Big|_X \Delta\theta - KA\frac{d^2T}{dx^2}\Delta x\Delta\theta$$

$$\therefore \dot{q} = -K\frac{d^2T}{dx^2} \quad \text{or} \quad \frac{d^2T}{dx^2} = -\frac{\dot{q}}{K}$$

Integrating with the following boundary conditions, substituting and rearranging

a. $T = To, \quad x = 0$

b. $T = To, \quad x = 21$

(3) $$K = \frac{\dot{q}\,L^2}{2\,(T\ \text{internal} - To}$$

Where K = Thermal Conductivity $\frac{BTU}{Hr.\ ^oF\ Ft.}$

L = Distance (Ft.)

T Internal = Internal Cell Temperature (^oF)

To = Mean Skin Temperature (^oF)

$\dot{q}$ = Internal Heat Generation $\frac{BTU}{Hr.\ Ft.^3}$

Using equations (3) and the analogy of heat flow and current flow, one may obtain the following equations which determine the amount of heat flowing in the three mutually perpendicular planes of the cell.

(4) a.
$$\dot{q}_x = \frac{L_x^{\frac{1}{2}}}{L_x^{\frac{1}{2}} L_y^{\frac{1}{2}} L_z^{\frac{1}{2}}}\,\dot{q}$$

(4) b.
$$\dot{q}_y = \frac{L_y^{\frac{1}{2}}}{L_x^{\frac{1}{2}} L_y^{\frac{1}{2}} L_z^{\frac{1}{2}}}\,\dot{q}$$

(4) c. $$\dot{q}_z = \frac{\frac{1}{L_z^2}}{\frac{1}{L_x^2} + \frac{1}{L_y^2} + \frac{1}{L_z^2}} \dot{q}$$

The values of q, T, L, and To are measurable values by which K, the thermal conductivity of the cell can be calculated.

B. VO-6 HS CELLS

Test Objective

The primary objective of the test was to determine a mean thermal conconductivity of a VO-6 HS cell as a function of charge, overcharge, and discharge current in an ambient environment of 80°F.

Test Procedure

Two cells were fabricated with the necessary instrumentation to study the heat transfer characteristics of the VO-6 HS cell. The instrumentation consisted of a thermocouple placed within the electrode stack, near its geometric center, and 24 thermocouples welded to the exterior surface of the cell case, as per Figure 25, so that the temperature pattern at the surface could be studied.

The insertion of the internal thermocouple is a very difficult operation, requiring the removal of material from the center plate of the stack to make room for the thermocouple and its leads. A cell fabricated in this manner has a laboratory life expectancy of only 2 to 4 weeks.

The cells were placed into an ambient environment of 80°F and charged at .25, .50, .75, 1.0, and 2.0 amperes until 115% of capacity was put into the cell. The cells were then overcharged at .25, .50, .75, 1.0, and 2.0 amperes until the internal temperature remained constant. Once constant temperature was reached, the cells were discharged at .25, .50, .75, 1.0, and 2.0 amperes

until the internal cell temperature remained constant. During the charge, overcharge, and discharge at constant current, internal temperature, skin temperatures, and cell electrical characteristics were continuously monitored.

Analysis of Data

It was noted from the data that as the overcharge rate increased from .25 amperes to 2.0 amperes, the internal temperature changed from $86^{o}F$ to $89^{o}F$, while the mean skin temperature remained in the range of $82^{o}F$ - $83^{o}F$. The thermal conductivity of the cell increased as the overcharge current increased because the amount of heat generated by the cell increased at a greater rate than the thermal gradient. This is evident from the previously derived equation where

$$K = \frac{\dot{q} \, L^2}{2 \, (T_{int} - T_{skin})}$$

in which

K = Thermal Conductivity $\frac{BTU}{HR \, FT \, {}^{o}F}$

$\dot{q}$ = Internal Heat Generation $\frac{BTU}{FT^3 \, HR}$

$(T_{int} - T_{skin})$ = Thermal Gradient ^{o}F

$\frac{L^2}{2}$ = Constant FT^2

It can be seen from this, that the thermal conductivity is not a constant, but it is a function of overcharge rate. From other studies carried on at Gulton, but not connected with this contract, it has been found that thermal conductivity is also a function of ambient temperature.

In Figure 26, there is a plot of thermal conductivity versus overcharge current at an ambient temperature of $80^{o}F$. It is presumed that this curve will move downward as the ambient temperature is increased, and upward

as the ambient temperature is decreased, resulting therefore, in a family of curves for thermal conductivity.

The important significance of these curves is that once knowing the overcharge current and the ambient temperature, one can determine the thermal conductivity and predict the thermal gradient in the cell.

Beside the study of the heat transfer directly from the cell, means of transferring heat from the cells within a battery pack were studied. The use of aluminum sheets of approximately 1/32 inch thick, coated in such a manner as to make them good electrical insulators without reducing thermal transfer too greatly, have shown great promise in transferring heat. These sheets were placed between cells in lieu of the regular insulators and, connected to a heat sink, reduced the operating temperature of an internal cell as much as $40^{o}F$.

For the VO-20 HS cells, Figures 27 and 28 show a plot of internal cell temperature versus time, as well as electrical cell characteristics versus time for ambient conditions of $83^{o}F$ and $104^{o}F$, respectively. It can be seen in both cases, that during the charging cycle, the internal cell temperature of the cell remains constant. However, once the cell is fully charged, the internal temperature begins to increase, and the cell goes into an overcharge condition at the 8 ampere charge rate. Looking at the electrical characteristics, one again sees a constant terminal voltage until a state of overcharge is reached, at which the terminal voltage begins to increase and reach a plateau at a higher voltage. When the cells were placed on the 1.4 ampere overcharge, the internal temperature decreased to a constant value, and remained there for the remainder of the test cycle.

Three dimensional thermal gradients were constructed for the cell during the charge, discharge and overcharge segments of the cycle.

It was observed that during charge-discharge the upper half of the cell is warmest. This is due to the fact that all of the current enters the cell through the top and I^2R losses are greater at the top. During overcharge the lower half of the cell is warmest. This is due to the fact that the upper one-third of the cell has the empty space for the terminal connections, and therefore the overcharge heat which is uniformly generated in the electrode stack is concentrated in the lower regions of the cell.

C. LARGE CELLS, VO-20 HS, VO-40 HS AND VO-50 HS

Objective

The primary objective of the analytical analysis was to predict the thermal gradient in a VO-40 HS, and VO-50 HS cell.

Procedure

Using thermal data accumulated for the VO-6 HS and VO-20 HS cells, as well as employing the assumptions that the thermal conductivity of the cells are alike, and the terminal voltages will be equal for all the cells at the same $\frac{\text{Overcharge Rate}}{\text{Capacity}}$ (this is current expressed as the "C - rate"), one will be able to use the equations derived to predict the thermal gradient.

Analysis of Data

Looking at the tabulation of results (Tables IV, V, and VI), and the curve of thermal gradient versus $\frac{\text{Overcharge Rate}}{\text{Capacity}}$ (Figure 29), one can see that the rate of increase of the thermal gradient for a VO-50 HS is much greater than that of a VO-40 HS and a VO-20 HS. This can be attributed to the fact that at the same $\frac{\text{Overcharge Rate}}{\text{Capacity}}$ for all the cells, the larger cap-

acity cells will be producing more heat. Since the heat produced by the larger cells must traverse a greater path, the geometry of the larger capacity cells being larger than the smaller capacity cells, it also produces an increase in the thermal gradient.

TABULATED RESULTS FOR VO-50 HS

TABLE IV.

OVERCHARGE CURRENT (AMPS)	ESTIMATED TERMINAL VOLTAGE	TOTAL HEAT GENERATED (q) BTU/HR	TOTAL HEAT GENERATED PER UNIT VOL. (q) BTU/HR in^3	HEAT TRANS. in x DIR. q_{x_3} BTU/HR in^3	HEAT TRANS. in y DIR q_{y} BTU/HR in^3	HEAT TRANS. in Z DIR q_{z} BTU/HR in^3	(T internal -T skin mean ^{o}F
2.0	1.310	8.96	.245	.1785	.0571	.0094	13.52
3.0	1.385	14.19	.388	.283	.0904	.0146	21.40
4.0	1.428	19.51	.533	.389	.1241	.0199	29.00
5.0	1.450	24.75	.676	.493	.1575	.0255	37.35
6.0	1.458	29.90	.817	.596	.1904	.0306	45.15
7.0	1.460	34.91	.954	.695	.222	.037	52.60
8.0	1.465	40.00	1.093	.797	.254	.042	60.40

TABULATED RESULTS FOR VO-40 HS

TABLE V.

OVERCHARGE CURRENT (AMPS)	ESTIMATED TERMINAL	TOTAL HEAT GENERATED (q)	TOTAL HEAT GENERATED PER	HEAT TRANS. in x De q_{x_3} BTU/HR in.^{3}	HEAT TRANS in y DIR. $_3q_y$ BTU/HR in^3	HEAT TRANS in Z DIR. $_3q_z$ BTU/HR in^3	(T int. $-T_{mean}$ skin ^{o}
2	1.350	9.26	.324	.250	.0613	.0127	14.38
3	1.420	14.61	.512	.391	.0969	.0241	21.25
4	1.450	19.91	.698	.539	.132	.027	31.00
5	1.463	25.15	.881	.680	.1665	.0345	39.11
6	1.465	30.15	1.055	.814	.1995	.0415	46.82
7	1.470	35.32	1.237	.955	.234	.048	54.45

TABULATED RESULTS FOR A VO-20 HS

TABLE VI.

OVERCHARGE CURRENT (AMPS)	ESTIMATED TERMINAL VOLTAGE	TOTAL HEAT GENERATED ($\dot{q}$) BTU/HR	TOTAL HEAT GENERATED PER UNIT VOL. ($\dot{q}$) BTU/HR in ^{3}	HEAT TRANS. in x DIR. ($\dot{q}_x$) BTU/HR in^3	HEAT TRANS.in y DIR. ($\dot{q}_y$) BTU/HR in	HEAT TRANS.in z DIR.($\dot{q}z$) BTU/HR in	ΔT(T int.) -T mean skin ^oF
1	1.35	4.63	.238	.209	.0233	.006	5.62
2	1.45	9.94	.510	.449	.050	.011	12.1
3	1.465	15.1	.774	.681	.0759	.0171	18.35
4	1.47	20.2	1.035	.912	.1015	.0165	24.6

D. THERMAL RESISTANCE

It was noted from previous data that the mean skin temperature on all six sides of a cell were identical at a specific environmental condition and overcharge rate. This caused the temperature difference from the center of the cell to the skin to be the same in all three directions. An experimental investigation was undertaken to determine the magnitude of the thermal resistance in the three directions. This was accomplished by placing a known heat source on one face of the cell and insulating it and four other faces so that the flow of heat would be unidimensional. The thermal gradient in the direction of heat flow was measured which enabled one to determine the thermal resistance in one direction. The same procedure was followed to determine the thermal resistance in the other two directions. It was found that the thermal resistances in the x, y, and z directions are 0.377 $\frac{HR\ ^{o}F}{BTU}$, 1.175 $\frac{HR\ ^{o}F}{BTU}$, and 2.22 $\frac{HR\ ^{o}F}{BTU}$, respectively. It was also found that the resistance was such as to produce an identical temperature differential along each of the three axes of the cells.

In a further investigation it was found that a minimum of $\left(\frac{1}{Rcq}\right)$ existed in which the worst possible dimensions are obtained. Within practical means, consistent with current manufacture practice, this configuration is to be avoided. It can be seen from this that the flat cells offer much less thermal resistance than do the squat cells.

E. EFFECT OF CELL DIMENSIONS ON HEAT TRANSFER RATES - A MATHEMETICAL ANALYSIS

An attempt was made to ascertain whether there exists one set of cell dimensions which would minimize the heat resistance out of the cell in

the three dimensions are shown in the figure. The effect of cell dimensions on heat transfer was analyzed mathematically.

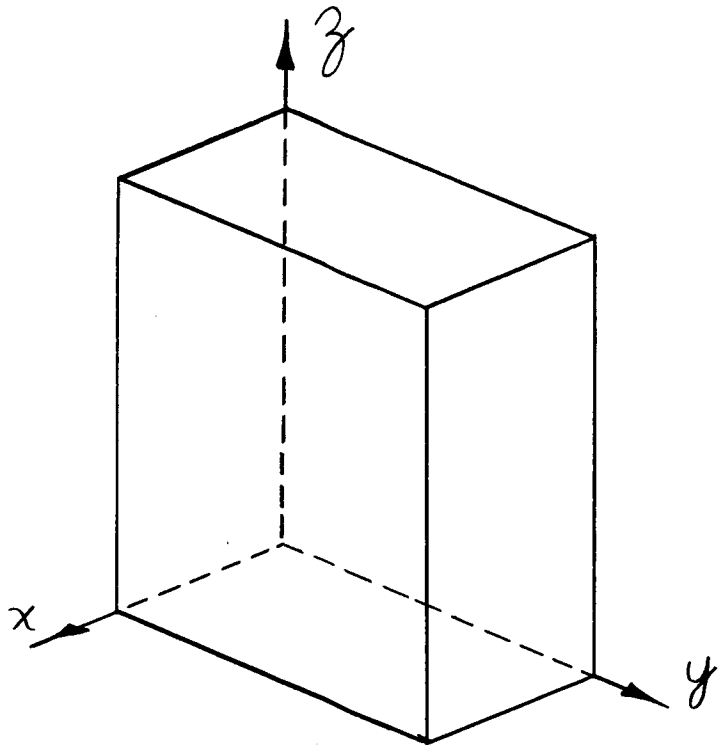

$$q_x = \frac{K_x A \Delta T_x}{\Delta x} = \frac{\Delta T}{\frac{\Delta x}{K_x A}}$$

This is analogous to

$$I_x = \frac{E}{R}$$

$$R_x = \frac{\Delta x}{K_x A} = \frac{x}{K_{xyz}}$$

$$R_y = \frac{y}{K_y X_z}$$

$$R_z = \frac{z}{K_z X_y}$$

Since the temperature potential in all three mutually perpendicular directions is the same, ($\Delta T_x = \Delta T_y = \Delta T_z$; or $E_x = E_y = E_z$) we can simulate the heat flow phenomenon by an equivalent electrical circuit.

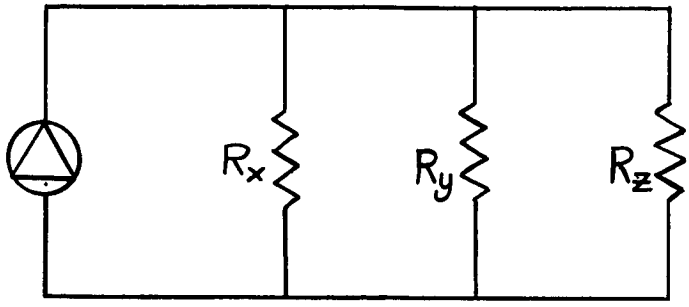

To get an equivalent resistance.

$$\frac{1}{Req} = \frac{1}{R_x} + \frac{1}{R_y} + \frac{1}{R_z} = \frac{R_yR_z + R_xR_z + R_xR_y}{R_xR_yR_z}$$

$$\frac{1}{Req} = \frac{\cancel{yz}}{K_yK_zx^2\cancel{yz}} + \frac{\cancel{xz}}{K_xK_z\cancel{x}y^2\cancel{z}} + \frac{\cancel{xy}}{K_xK_y\cancel{xy}z^2} \Bigg/ \frac{\cancel{xyz}}{K_xK_yK_z\,x^2y^2z^2}$$

$$\frac{1}{Req} = K_xK_yK_zxyz \left\{ \frac{1}{K_yK_zx^2} + \frac{1}{K_xK_zy^2} + \frac{1}{K_xK_yz^2} \right\}$$

$$\frac{1}{Req} = \frac{K_xY\,z}{x} + \frac{K_y\,x\,z}{y} + \frac{K_z\,x\,y}{z}$$

The system obeys the equation and has the following equation of restraint.

$$\therefore V = Const = x\,y\,z$$

We can use the method of Lagrange to obtain the maximum or minimum and later test to see which we have.

We must differentiate the main function and the restraining equation, set them both equal to zero, multiply the differentiated restraining equation by a Lagrange multiplier (λ), collect all terms with the same differential.

1. $\lambda yz - K_x \frac{y\,z}{x^2} + K_y \frac{z}{y} + K_z \frac{y}{z} = 0$

2. $\lambda xz - K_y \frac{xz}{y^2} + K_x \frac{z}{x} + K_z \frac{x}{z} = 0$

3. $\lambda xy - K_z \frac{xy}{z^2} + K_x \frac{y}{x} + K_y \frac{x}{y} = 0$

4. $xyz - V = 0$

We have four equations and four unknowns

Solving equation (1) for λ we have

$$\lambda = \frac{K_x}{x^2} - \frac{K_y}{y^2} - \frac{K_z}{z^2}$$

Substituting λ in equation (2)

$$\frac{K_x\,xz}{x^2} - \frac{K_y\,xy}{y^2} - \frac{K\,xz}{z^2} - \frac{K_y\,xz}{y^2} + K_x \frac{z}{x} + K_z \frac{x}{z} = 0$$

$$\therefore \cancel{K_x \frac{z}{x}} = \cancel{K_y \frac{xz}{y^2}}$$

$$\frac{K_x}{K_y} = \frac{x^2}{y^2}$$

2a. $$\text{or } \frac{x}{y} = \sqrt{\frac{K_x}{K_y}} = \beta$$

Substituting into equation (3) we have

$$K_x \frac{x\ y}{x^2} - \cancel{K_y \frac{x\ y}{y^2}} - K_z \frac{x\ y}{z^2} - K_z \frac{x\ y}{z^2} + K_x \frac{y}{x} + \cancel{K_y \frac{x}{y}} = 0$$

$$\cancel{\partial} K_x \frac{\cancel{y}}{\cancel{x}} = \cancel{\partial} K_z \frac{x \cancel{y}}{z^2}$$

$$\frac{K_z}{K_x} = \frac{z^2}{x^2}$$

3. a or $\frac{z}{x} = \sqrt{\frac{K_z}{K_x}} = \partial$

We now have three equations three unknowns

2a. $y = \frac{x}{\beta}$

3a. $z = \partial x$

4. $xyz = V$

Substituting equations 2a and 3a into equation (4)

$$x \left(\frac{x}{\beta}\right) (\partial x) = V$$

$$x^3 = V \frac{\beta}{\partial}$$

$$\boxed{x = \sqrt[3]{\frac{\beta}{\partial}}\ V^{1/3}}$$

Substituting for x in equation 2a.

$$y = \sqrt[3]{\frac{1}{\alpha\beta^2}} \; V^{1/3}$$

Substituting for x in equation 3a.

$$z = \sqrt[3]{\beta\alpha^2} \; V^{1/3}$$

From previous experimental data for a nickel-cadmium battery

K_x = .136 BTU/HR in ^oF

K_y = .394 BTU/HR in ^oF

K_z = .986 BTU/HR in ^oF

$$\beta = \sqrt{\frac{K_x}{K_y}} = \sqrt{\frac{.136}{.394}} = .587$$

$$\alpha = \sqrt{\frac{K_z}{K_x}} = \sqrt{\frac{.986}{.136}} = 2.69$$

$$\sqrt[3]{\frac{\beta}{\alpha}} = \sqrt[3]{\frac{.587}{2.69}} = .602$$

$$\sqrt[3]{\frac{1}{\alpha\beta^2}} = \sqrt[3]{\frac{1}{(2.69)\ (.597)^2}} = 1.028$$

$$\sqrt[3]{\beta\alpha^2} = \sqrt[3]{(.587)\ (2.69)^2} = 1.62$$

cell is warmer.

In the data obtained from the VO-6 HS cells, it was noted that as the overcharge rate increased from .25 amperes to 2.0 amperes, the internal temperature changed from 86°F to 89°F, while the mean skin temperature remained in the range of 82°F - 83°F. The thermal conductivity of the cell increased as the overcharge current increased, because the amount of heat generated by the cell increased at a greater rate than the thermal gradient. It can be seen from this that the thermal conductivity is not only a function of environmental temperature but also of overcharge rate. In the plot of thermal conductivity versus overcharge current, at an ambient temperature of 80°F, it is presumed that this curve will move downward as the environmental temperature is increased, and upward as the ambient temperature is decreased, resulting therefore, in a family of curves. The significance of these curves is that once knowing the overcharge current and the environmental temperature, one will be able to determine the thermal conductivity and predict the thermal gradient in the cell.

The thermal information which has been collected will facilitate designs of cells and batteries to ensure their proper thermal operation.

The data and methods of analysis were applied to the VO-50 HS cell described in Section V, and its design was predicated on the knowledge of the thermal characteristics of the smaller cells. Several cell configurations have been constructed and analyzed both experimentally, and both results agree quite favorably. For example, in a special configuration, the temperature differential in the x direction was calculated to be 2.02°F whereas,

experimentally it was $3^{o}F$. In the y direction the calculation showed a constant temperature gradient which was again proven to be true experimentally. The calculated temperature gradient in the z direction was $10.9^{o}F$ whereas experimentally it was $10^{o}F$.

In the mathematical analysis to determine the effect of cell dimensions on heat transfer rates it was found that a minimum of $(\frac{1}{R_{eq}})$ existed in which the worst possible dimensions are obtained. Within practical means, consistent with current manufacturing practice, this configuration is to be avoided. It can be seen from this that the flat cells offer much less thermal resistance than do the squat cells. This information will aid the battery manufacturer in not only designing a cell for electrical characteristics, but also for thermal considerations.

VIII. IMPROVED ELECTRODES

Research and development efforts on nickel-cadmium cell electrodes were aimed at improving the energy to weight and energy to volume ratios, with the primary emphasis placed on the former. It was felt that an increase in the ampere-hour capacity of an electrode of a fixed size and weight, would result not only in a better weight efficiency, but an improved volume efficiency as well. Our approach was such that an improvement in one area meant an improvement in the other one also.

The Gulton VO-HS series cells which have been designed specifically for space applications are such that about 55% to 60% of the total cell weight represents the weight of the positive and negative plates. Consequently, about 0.061 to 0.066 ampere-hours/gm of plate are required to achieve a 20 watt-hour per pound ratio for a cell (0.061 AH/gm are required for the VO-20 HS cell and 0.066 AH/gm are required for the VO-6 HS cell to achieve the 20 watt-hours per pound). For these reasons results will be discussed in terms of weight gain or AH capacity achieved per unit weight of plate.

Development efforts to achieve higher plate loading have been concentrated on techniques to effectively load more dissolved nickel and cadmium into the sintered carbonyl nickel plaques. Nickel nitrate and cadmium nitrate were dissolved in low surface tension solvents in such concentration that one cc of solution contained one gram of the salt. The plate was immersed in the solution, dried, and the nitrate converted to the corresponding hydroxide by treatment with KOH. The plate was then washed to remove excess KOH and dried. This cycle was repeated until the desired pickup was achieved. The impregnated plates were then assembled into vented, flooded cells and charge-discharge

cycled at the two hour rate to determine the AH capacity.

In the early phases of this program impregnation of plates using molten salts were also examined. Cd $(NO_3)_3$-$4H_2O$ (m.p. 59.4°C) and $Ni(NO_3)_2 \cdot 6H_2O$ (m.p. 56.7°C) were heated to 80°C and used in the impregnation cycle described above. However, after two trials, the results achieved by this technique were so poor compared to the low surface tension solvent method that this approach was abandoned.

If the active materials are used with a 100% efficiency 3.46 gms of $Ni(OH)_2$ and 2.72 gms of $Cd(OH)_2$ (the active material while the cell is in the discharge state) are required for one AH of capacity. Earlier work had shown that while the positive active material can be utilized with a 100% efficiency, the negative one is only 80% efficient. This means that 3.40 gms of Cd $(OH)_2$ are required for one AH of capacity. In addition, for successful sealed cell operation, an excess negative capacity is desirable. Assuming that a 30% excess negative capacity is required for overcharge capability, the amount of Cd $(OH)_2$ needed for one AH is increased to 4.42 gms. That brings the total amount of active material required to 7.88 grams/AH for a sealed cell.

Results of active material impregnation using low surface tension solvents, are summarized in Figures 30 to 32.

Figure 30 shows the positive active material pickup as a function cycles. As may be seen, the pickup is uniform for the first three cycles, but as the plate becomes loaded, the pickup diminishes. As the figure indicates, a continuation of the impregnation cycling would in all probability result in an even greater pickup. However, our aim has been to achieve a certain plate loading, and after this goal had been achieved, the process was stopped.

Figure 31 shows the active material pickup for negative plates. As may be seen, a much higher loading is possible for an equivalent negative plate. In fact, four to five cycles would have been sufficient to match the desired capacity based on the available positive capacity. Any excess negative capacity beyond that which is required merely serves to reduce the watt-hour per pound ratio of the cell.

Figure 32 shows the actual AH capacity achieved when the cells were cycled at the two hour rate. Values are based on the weight of both positive and negative plates, assuming that the weight distribution between positive and negative plates are divided in a ratio of 45 to 55. As may be seen, we have achieved a figure of 0.0658 AH/gm of plate, or 20 watt-hours per pound of cell when discharged at the two hour rate to 1.0 volt per cell.

IX. CHARGE EFFICIENCY

The nebulous term charge efficiency has been more rigorously defined. In a general way, the charge efficiency of any electrochemical system is dependent upon the characteristics of the individual electrodes.

During the charge of an electrode, some of the current causes undesirable side reactions. If the charge current is I and the current causing the side reaction is i, then a charge current efficiency may be defined by equation 1:

$$(1) \quad E_i = 1 - \frac{i}{I} \quad .$$

As an example of this kind of charge efficiency, consider the following reactions that occur during the charge of the $Ni(OH)_2$ electrode:

$$(2) \quad Ni(OH)_2 + OH^- \xrightarrow{i_1} NiOOH + H_2O + e^-$$

$$(3) \quad Ni(OH)_2 + XOH^- \xrightarrow{i_2} A_1 + X\ e^-.$$

$$(4) \quad 4OH^- \xrightarrow{i_3} O_2 + 2H_2O + 4\ e^-.$$

The charge current I is equal to $\sum_{n=1}^{3} i_n$, but only i_1 results in a completely useful reaction. The charge current efficiency for the charge process is therefore,

$$(5) \quad E_i = 1 - \frac{i_2 + i_3}{I} = \frac{i_1}{I} \quad .$$

There is some time during the charge process that a side reaction, or even a new process, becomes the dominant electrode process observed. This particular change is a passivation of the electrode. In some cases, such as the Cd electrode of our particular system, passivation is accompanied by a potential change. In other cases, and our NiOOH electrode is a most important example, the change in process

is not accompanied by any significant potential change. The operating potential of the $NiOOH/Ni(OH)_2$ potential is above the theoretical oxygen electrode potential, so that the only required potential step is concerned with overvoltage. The overvoltage here is oxygen evolution overpotential on NiOOH. Apparently this value is already exceeded at the $NiOOH/Ni(OH)_2$ electrode so that there is no accompanying potential change during passivation.

Passivation phenomena are dependent upon current and temperature. The dependence of passivation of the $Ni(OH)_2$ and $Cd(OH)_2$ half-cells on these factors differ and result in a complicated relationship for the cell. For example, at room temperature it is found that the higher the charge rate, the later (with respect to ampere-hours input) the passivation of the positive electrodes. The negative electrodes show a converse characteristic. At very high charge rates, an early passivation of nickel-cadmium cells is observed and, because hydrogen is found in the cell, is related to passivation of the negative electrodes. At very low charge rates there is also an undue early passivation which was traced to the positive electrodes. An optimum charge rate region is, thusly, found.

The utilization coefficient is the discharge capacity obtained after a complete charge in relation to the theoretical capacity, i.e. C_d/C_t. The theoretical capacity is based on the weight gain during impregnation. The discharge capacity is a function of the temperature, rate and charge input used on the previous charge as well as a function of the rate and temperature of the discharge. The work reported here is carried out at only one discharge rate, and the utilization coefficient is not of primary interest.

The problems under investigation are two-fold. One is to determine the side reactions, and, which mechanisms prevail in the side reactions. This work was aimed at the positive electrode which is responsible for the degradation of capacity at the low charge rates. Two postulated side reactions are given in equations 3 and 4. In equation 4 it is immediately seen that the oxygen is produced by anodic oxidation of hydroxyl ion to oxygen. The compound A_1 is unstable and releases oxygen. A_1 has not been identified chemically, but its existance was determined by its ability to release oxygen. It is one aim to determine whether the reaction represented by equation 3 or equation 4 or both contribute to the charge current inefficiency. These measurements also yield information on the current efficiency. Consequently, current efficiencies of the nickel oxide electrodes were measured by means of special cells which contained positive electrodes and unimpregnated negatives. For a given current a theoretical oxygen consumption rate can be calculated. Deviations of the experimental values from the theoretical values indicate the amount of current going into a side reaction.

The second set of measurements are of the passivation as noted by the beginning of the large pressure rise observed. These were determined as a function of temperature, the current during constant current charge, and the voltage of a controlled potential charge.

A. PRESSURE CHANGES AT THE END OF CHARGE

As a result of the work done on the charge efficiency of the nickel oxide-cadmium alkaline system several curves were obtained which were indeed interesting. These were the curves of the pressure changes in a cell after charging and evacuation.

The typical aspects of these curves were that the pressures at first increased rapidly, then they leveled off and finally started to decrease. These curves are to be expected on the basis of the self-discharge processes that the positive electrodes exhibit, and the oxygen reduction process that occurs at the negative electrode.

Such experimental data can, at least in principle, afford information on the overcharge process and charge efficiency of the positive electrode. This was one of the objectives in the contract. In addition, information can be gained on the self-discharge processes. This can be used as an adjunct to some information already available on these processes. A third area of information will be on the oxygen reduction process. This last process was also part of the objectives of the work, and separate experiments are reported in another section of this report.

In order to obtain maximum information from these data, (it is necessary to eliminate the effects of the second consecutive self-discharge process and the oxygen consumption process) a method is needed. This method is supplied by a theoretical consideration of the system we are studying. The law that describes the self-discharge is known as is the law that describes

oxygen reduction. By using these laws in differential form to explain the pressure behavior and solving for the initial rates, the derived function is the method used for analyzing the experimental data.

1. Theory

The oxygen evolution processes from charged nickel oxide electrodes have been shown to consist of an oxygen source which yields oxygen in two consecutive processes. The first process has a rate constant approximately 10^{-2} per minute while the second is approximately 1/20 of this rate.[1]

The oxygen reduction process is independent of the state of charge of the negative electrode, at least above about 2/3 atmosphere partial pressure of oxygen.[2] Above this pressure the reaction is first order with respect to oxygen. Below 2/3 atmosphere oxygen is still reduced, but the specific velocity constant is considerably less than for unflooded cells*.

It can be shown that the pressure change in a cell after interruption of charge, provided it is in overcharge for a sufficiently long period, is given by:

(6) $\text{Rate}_{\text{initial}} = \frac{\alpha A^o}{C} (k_1 + k_2) - P_o k_g.$

where A^o = amount of oxygen source material at the instant of current interruption,

*The rate constant is that of a heterageneous reaction so that changes may be effective changes corresponding to different surface areas or reaction sites.

C = capacity of the positive electrode expressed in the same units as A^o,

k_1, k_2 the rate constants for the two oxygen evolution processes, units of reciprocal time

t = time

α is the conversion factor to pressure units,

k_g is the rate constant for oxygen reduction from the gas phase

P_o is the pressure at to

Consider equation (6). If the positive electrodes are isolated, kg is then set equal to zero since oxygen reduction can not occur. Also, as P_o is increased in magnitude, the effect of the other terms on the right hand side is diminished. That is to say, that the maximum pressure rise is decreased as P_o is increased. It also follows that the time to reach a maximum pressure is decreased as P_o is increased. At high enough values of P_o, the time to reach the maximum pressure will be zero.

2. Results

a. Oxygen Decay Curves

In order to obtain an order of magnitude for k_g under various conditions, oxygen pressure decay curves were determined on a cell when in an unflooded condition, and also later when flooded. The effective rate constant for an unflooded cell is approximately 50 times greater than for a flooded cell in the

higher pressure region above 2/3 atmospheres.

b. Unflooded Cells

The pressure changes encountered in sealed cells are expected to follow equation (6).

The initial pressure rise as a function of P_o is shown in Figure 33. The equation that fits the straight line shown in this Figure is:

(7) $R_{init} = 0.070 - 0.053\ P_o$.

Equation (7) has the same form as (6).

The data for initial pressure rise at several low temperatures are plotted versus the charge rate in Figure 34. Three charge rates were used. Since a cell that is not charged at all can not have a pressure rise, these data were extrapolated to the origin. These data will satisfy equation (6) when P_o is set equal to zero. Since the initial pressure rise at each temperature is dependent upon the charge rate, A^o must be dependent upon the charge rate. The slope of each line is therefore given by $(c/\ )(k_1+k_2)$. But $k_1 \approx 20\ k_2$, and the activation energy of the rate constant k_1 may be obtained by taking the slope of a plot of the relative slopes against the reciprocal of absolute temperature. This is shown in Figure 35. This slope corresponds to an activation energy of 3.92 kcal/mode.

c. Flooded Cells

Since the oxygen consumption rate is decreased by an order of magnitude or more when a cell is flooded, equation (6) becomes simplified. The last term may be

neglected while taking the initial rate data.

Cells were flooded until the electrolyte was above the level of the plates. A pressure transducer was used to record the changes. The results obtained at a 0.6A charge rate at 77°F are given in Table VII. It is seen that the initial pressure increase rate is essentially independent of the initial oxygen pressure. The total amount of rise is also virtually independent of the initial pressure. These are the results to be expected for flooded cells on the basis of the theory developed.

B. BLANK ELECTRODE CELLS

The blank electrode cells were described earlier. They are identical with the previously described cells, but the negatives are unimpregnated. These cells are pressured with oxygen and then placed on charge. Oxygen will then be consumed during charge. If the oxygen consumption rate is less than theoretical, the difference is ascribed to oxygen generation at the positives which decreases the current efficiency of the system.

The results reported here are preliminary in nature. Internal checks on the method were obtained using a silver anode in place of the $Ni(OH)_2$ anode. These cells were constructed primarily for an investigation of the oxygen reduction reaction. Several were constructed with reference electrode. These data are presented elsewhere in this report.

TABLE VII

PRESSURE RISE AS A FUNCTION OF INITIAL OXYGEN PRESSURE CHARGE AT 0.6A FLOODED CELL 77°F

INITIAL PRESSURE atm.	INITIAL RATE OF PRESSURE RISE atm/min.	MAXIMUM PRESSURE RISE atm
0.01	0.032	0.41
0.20	0.034	0.43
0.40	0.035	0.41
0.59	0.029	0.31
0.78	0.034	0.39
0.94	0.040	0.44
Average	0.036	0.40

1. Theory

When current is passed through a $Ni(OH)_2$ - blank or Ag-blank cell there are electrochemical processes occurring at both electrodes. For the $Ni(OH)_2$ electrode we have postulated the following:

(2) $Ni(OH)_2 + OH^- \xrightarrow{i_1} NiOOH + H_2O + e^-$.

(3) $Ni(OH)_2 + OH^- \xrightarrow{i_3} A_1 \quad e^-$.

(4) $4\ OH^- \xrightarrow{i_2} O_2 + H_2O + 4e^-$

Equation (2) is the conversion of the discharged material into active material. Equation (4) represents the possibility of the direct evolution of oxygen by an electrochemical process. Equation (3) is the electrochemical formation of the unstable oxygen source.[1] This source decays into a second source, A_2, with the simultaneous evolution of oxygen. A_2 decays again releasing additional oxygen. These decompositions may entirely account for the oxygen found, eliminating the necessity of postulating the oxidation of hydroxyl ion given in equation (4). Regardless of the particular mechanism, any current going into the reactions 3 or 4 will be evidenced as oxygen. It is this fact that makes the method of study used here a feasible method.

At the silver anode, the following reactions occur sequentially:

(8) $2\ Ag + 2OH^- \xrightarrow{i} Ag_2O + H_2O + 2e^-$

(9) $Ag_2O + 2OH^- \xrightarrow{i} 2AgO + H\,O + 2e^-$.

Equation 3 is postulated as a possible side reaction, especially during charge at the upper plateau corresponding

to equation (9). The potential will determine the processes occurring. Equation (8) occurs at a potential less anodic than equation (2), but equation (9) requires a more anodic potential than equation (2) increasing the likelihood of the oxidation of hydroxyl ion. Of course, this must be tempered by the overvoltage of oxygen upon the electrode involved.

Consider the experimental cell. It has a gas volume V, is charged at I amperes at an absolute temperature T, and is pressured with oxygen to P atmospheres. When the oxygen is consumed at the negative blank electrode, it must do so at a rate proportional to the current. Using the ideal gas law, we may write the pressure decay as:

$$(10) \quad \frac{dP}{dt} = \frac{RT}{V} \frac{dn}{dt} ,$$

where n is the number of moles of oxygen consumed and the other symbols have their usual significance. Multiplying by the number of electrons required to produce a molecule of oxygen, 4 N, and using the relationship (N = Avogadro's number)

$$(11) \quad I = zF \frac{dn}{dt} ,$$

where F is the faraday of electricity,

$$(12) \quad \frac{dP}{dt} = \frac{RT}{4FV} I.$$

Equation (12) therefore represents the theoretical rate of oxygen consumption, and is expected to hold until the oxygen pressure decreases to the point where this process no longer occurs. At this time it is expected that the potential will

increase as the blank electrode changes from an oxygen consumption electrode into a hydrogen evolution electrode.

The pressure rise during hydrogen evolution should occur at approximately twice the rate at which oxygen is consumed, since only 2N electrons are required to produce a mole of hydrogen.

2. Results

Several cells were prepared for this work. The volumes were determined by a gas expansion procedure. A cell case and cover with a pressure gauge were used to form a pressure vessel. Its volume was determined with water. It was pressured with N_2 (He gave the same results), connected to the evacuated cell, the volume of which was being determined. From the pressure drop, the volume of the cell was determined.

The cells were evacuated, then pressured with oxygen to approximately 50 PSIG. During a 0.6A charge, the pressure decay rates were measured manually, and data taken corresponding to oxygen consumption, and finally into the region of hydrogen evolution. The terminal voltage was simultaneously measured.

Typical data for a nickel-blank cell are shown in Figure 36 and for a silver-blank cell are shown in Figure 37. During the oxygen consumption period the cell voltage is fairly stable, even at the lower pressure region. The sharp rise in voltage occurs in the neigh-

borhood of the hydrogen evolution region. The flattening of the curve at the higher oxygen pressures is not unexpected. The Nernst equation for a hydrogen electrode leads one to expect the voltage to be proportional to the logarithm of hydrogen pressure, which accounts for the relatively low rate of change of terminal voltage with increasing pressure.

The pressure behavior is, in most respects, that which was predicted in the theoretical section. Oxygen is consumed at a rate approximately related to current. Hydrogen is evolved later at approximately twice the rate for oxygen consumption.

The first cell investigated in this manner was initially used for other experiments, and it turned out that the positives were nearly fully charged. The charge efficiency is given in terms of the deviation of the slope from the theoretical slope. It averaged 27% low.

A cell using silver anodes and blank cathodes was next investigated in both the oxygen consumption and hydrogen evolution region. These results are given in Table VIII. A second nickel oxide-blank cell was made. In this case the electrodes were discharged initially so that changes in efficiency could be determined as a function of the state of charge. These data are also in Table VIII.

These data are considered preliminary in nature. The error in measuring volume and current is small enough to

TABLE VIII

DEVIATION OF OXYGEN CONSUMPTION AND HYDROGEN EVOLUTION RATES FROM THEORETICAL VALUES (BLANK CELL DATA).

CELL	EXP. NO.	DEVIATION OF O_2 CONSUMPTION, %	DEVIATION OF H_2 EVOLUTION, %
Ni Blank (1)	3/12 -1	-28	-32
Ni Blank (1)	3/13 -2	-24	-24
Ag Blank	3/13 -1	-4	-12
Ag Blank	3/14 -2	-3	-8
Ni Blank (2)	3/15 -1	-7	-4
Ni Blank (2)	3/15 -2	-14	-4
Ni Blank (2)	3/15 -3	-18	-23

be ignored. The pressure measurement error from which the rate determinations are made is estimated to be about 3%. Another source of error is in the use of the ideal gas law, and may also be a few percent.

The rate determination errors should be random. The use of the ideal gas law will yield results that are low, so that the net result is that Table VIII would have negative signs indicating negative deviations.

As a first approximation we may neglect the errors, and give the charge efficiency of the positive electrodes as shown in Figure 38. These three points, represent the average values of oxygen consumption deviation from theoretical in the intervals indicated by the horizontal arrows. These are for V0-6 HS type positive electrodes charged at 75°F at C/10. These points do indicate that the current efficiency of the positive electrodes is always less than unity and is dependent upon the state of charge. The decreasing efficiency indicates further the need for overcharge in order to completely convert the $Ni(OH)_2$ into the higher oxide.

C. PASSIVATION OF CELLS

1. Constant Current Charge

The charge data indicated, that in general, as the charge current was increased the cells tended to gas at progressively lower inputs. At temperatures above 50°F, low charge currents (0.6 and 1.2 amperes), the cells produced oxygen.

When high charge currents were employed (3.0 and 6.0 amperes), hydrogen was present in large quantities. Under the experimental conditions, steady-state pressures were reached only with the lower currents, namely C/10 and C/5. However, at the higher currents, hydrogen was formed early in the charge, indicating passivation of the negatives, and the pressure increased steadily to the gauge limit of 150 psi.

At temperatures of 50° and 25°F the charge input for initiation of gas evolution decreased with increase in charge rate and decrease in temperature, as found in the high temperature test results. But, as the temperature is further decreased, first to 0°F and then to -15°F, the order of dependence on charge rate for the onset of gas evolution is inverted. The charge input required for initiation of gas evolution increases as the charge rate is increased at these low temperatures. As the temperature is decreased, the input for the onset of gas evolution is also decreased. It was noted also, that the gases in the various cells during charge, except at the 0.15A rate at 50°F, were found to contain hydrogen, even when steady state pressures were attained.

The charge input required to produce gas is plotted as a function of charge current in Figure 39. The graph shows that the input to produce gas varies considerably with charge rate and temperature. At 25° and 50°F, progressively greater inputs are associated with the onset

of gas evolution as the charge rate is decreased and the temperature is increased. However, at 0° and 15°F, although the dependence of input for gas formation upon temperature is the same as given above, the order according to rate is reversed. The 0° and 15°F isotherms show that progressively greater inputs are obtained as the charge rate is increased. This phenomenon indicates that there is an inversion point between the 0° and 25° isotherms. This inversion point is clearly shown in Figure 40 where the charge input to start pressure rise is plotted versus temperature. The inversion temperature is in the vicinity of 10°F.

The cell capacities obtained after discharge at 3A to 1.0 volt are listed in Table IX.

2. Controlled Potential Charge

The curves relating charge input for pressure rise to the experimental temperatures and potentials are given in Figures 41 and 42. It may be seen that the charge input required to produce gas decreases as the charge potential is increased, while the input increases as the temperature is decreased from 50° to 25°F. However, at the 0° temperature, the order of gas initiation is reversed with regard to charge input, that is, charge input for gas onset decreases as charge potential is decreased. At -15°F the order is again reversed and is the same as is given for the 50° and 25° temperatures.

TABLE IX

CELL CAPACITIES AFTER 3 AMPERES DISCHARGE TO 1.0 VOLT
AFTER CONSTANT CURRENT CHARGE

CHARGE RATE Amperes	TEMPERATURE, °F, OF CHARGE (Discharge at Room Temperature, after 3 days stand)			
	-15	0	25	50
0.15	6.2	6.2	6.3	6.3
0.3	6.4	6.4	6.2	6.5
0.6	7.0	7.1	6.3	6.7
	77	90	100	120
0.6	6.6	6.9	6.4	6.1
1.2	6.6	7.0	6.7	6.4
3.0	7.4	7.3	6.4	6.5
6.0	7.5	7.3	6.3	6.3

Thus two inversion points were obtained which may be again implied from an examination of Figure 42, where charge potential is plotted versus charge input to start pressure rise. The inversions are indicated clearly by the near-asymmetry of the 0^{o} to 50^{o}F isotherms and the displacement of the -15^{o} isotherm, which is out of sequence. There appears to be an inversion charge potential in the vicinity of 1.553 volts. In Figure 42 where temperature is shown as a function of charge input for gas production, the graph is more informative than Figure 41. The equipotential contours intersect in two points, corresponding to two inversions in the sequence of charge input. The inversion temperatures are at approximately +10 and -10^{o}F. It should also be noted that the gases evolved (shown at the dotted line isotherms in Figure 42) was oxygen at 50 and 0^{o}F and hydrogen at 25^{o}F and -15^{o}F.

Steady state pressures and/or pressure rise to 150 PSIG were obtained throughout the tests. The data showed that the magnitudes of the developed cell pressures increase with increasing charge potential and temperature. This applies to steady state cases as well as those in which 150 PSIG was reached during charge.

The capacities of the cells upon discharge at 3.0 amps to 1.0 volt are given in Table X.

TABLE X

CAPACITIES OF CELLS CHARGED AT CONSTANT POTENTIALS

DISCHARGES AT 3A TO 1.0 VOLT
*Capacities in Ampere-Hours

CHARGE POTENTIAL volts	50°F	25°F	0°F	-15°F
1.45	6.2 (8.3)	5.9 (8.4)	5.2 (5.5)	3.0 (4.6)
1.50	6.8 (13.6)	7.0 (9.4)	6.8 (10.2)	5.8 (7.6)
1.55	7.0 (14.3)	7.2 (9.3)	7.1 (11.7)	5.7 (8.6)
1.60	7.4 (11.1)	7.8 (14.8)	6.7 (14.3)	6.9 (11.5)

*Charge inputs are in parenthesis

D. DISCUSSION

The theory developed to help interpret the pressure change data obtained after charge did yield mathematical expressions that are in agreement with experiments. From application of this theory it is deduced from Figure 34 that the amount of the first unstable nickel oxide formed is dependent directly upon the charge current and is also dependent upon temperature.

The blank cell work shows that there is a side reaction that is responsible for a current efficiency of less than unity. The efficiency does appear to be dependent upon the state of charge of the positive electrodes. This indicates the need for an overcharge in the nickel-cadmium system in order to obtain full capacity.

It has been previously reported[2] that at low charge rates the capacity of Ni-Cd cells is decreased. A plot of these data is shown in Figure 43. If this fall-off of capacity at the lower charge rates is due to formation of unstable oxides, then one would expect at lower charge rates to find more of these oxides present. Experiments have shown that less of these oxides are formed. It is therefore presumed that the parasitic reaction responsible for the lessened capacity at low charge rates is due to the generation of oxygen as given in equation (4). If the negative deviations given in Table VIII for the silver electrode are real, instead of containing an error of comparable magnitude due to use of the ideal gas law, then

one would presume that equation (4) also occurs in this system. Generally, the charge efficiency of the silver-cadmium system is high, 96 to 98%. The agreement between the results of others on the charge efficiency tends to provide additional support for the conclusion that hydroxyl ion converted electrochemically to oxygen and water is the side reaction responsible for the lowered charge efficiency of the positive electrodes.

Charge efficiencies of less than unity may be due to (1) the oxidation of water at the positive to form oxygen, or an equivalent electrochemical reaction (2) the reduction of water at the negative to yield hydrogen, as given above by equations

$$4OH^- \longrightarrow 2H_2O + O_2 + 4e^- \quad \text{and}$$

$$2H_2O + 2e^- \longrightarrow 2OH^- + H_2$$

During the charging of the cells in the experimental scheme, both reactions were in evidence as shown by the tests for hydrogen and oxygen. At high charge rates, hydrogen was always formed at a point during the charge when the input was less than the rated cell capacity. Therefore, it is seen that low efficiency, even at elevated temperatures is primarily due to a charge efficiency of less than unity at the negative electrode. The positive electrode, at these relatively high charge rates must then be significantly more efficient than the negative. If the positive was significantly less efficient than the negative, the evolved oxygen would travel to the negative

and depolarize it by reaction with hydrogen to form water.

For example, at low temperature constant current charge, hydrogen is obtained, except for 50°F, where oxygen is found at the 150 ma rate and a mixture of hydrogen and oxygen is found at the 300 ma rate. At the low temperatures and relatively high charge rates hydrogen is evolved at the onset of pressure rise. This implies a decrease in charge efficiency for the negative electrodes under these conditions. Of equal significance is the appearance of steady states with hydrogen, obtained for the first time in these tests. This shows that oxygen has reached the negative, as in the high temperature tests. One way to express this interaction between the positive and negative electrodes is to say that the positive is not inefficient enough to enhance depolarization of the negative. Another way of stating this concept would be (since predominantly hydrogen is produced as the temperature is lowered) to say that even at these low charge rates, the negative is first passivated and then depolarized.

There is an increase in self-discharge* (oxygen evolution) rate with charge rate and temperature for the positives. This causes the capacities of the positives to reach a maximum. Therefore, the higher charge rates do not result in a more efficient charge.

*The self-discharge processes involved are the fast processes which have half-times of 8 minutes and 150 minutes, approximately. There is no experimental evidence for a faster self-discharge of BNiOOH, and, in our opinion, no such evidence will ever be found.

The low temperature inversion phenomenon found indicates that the net effect of decreasing temperature and charge rate may serve to decrease the efficiency of the negative relative to that of the positive.

The results obtained during self-discharge at low temperatures were similar to those obtained during the high temperature tests. The initial self-discharge rates indicate that these rates are charge dependent as well as temperature dependent. As the charge rate is doubled in steps, going from 0.15 to 0.30 to 0.60 amperes, the decay rates also essentially double. The initial self discharge rate approximately doubles for at 40 to 50°F temperature rise.

The cell capacities in these tests do not give information regarding cell efficiency, since the charge input for each cell was different. These discharges were carried out at room temperature after a 3-day stand. At these lower temperatures the capacities still remain above 6 AH. It does appear that the lower the temperature the more effective is a higher charge rate. For instance, at 0° and -15°F the cells charged at 0.6 A yielded 7 AH at room temperature. This is similar to the data obtained for 3 and 6 A charges at 77 and 90°F. In a sense, the meaning of a high charge rate depends upon temperature. At 77°F the C/10 rate is not a high charge rate which it is at 0°F.

The controlled potential charge method is considerably more complex in analysis than the constant current method.

However, if the controlled potential charge curves are characterized by their component parts, the factors affecting cell behavior under controlled potential charge conditions will be uncovered.

The controlled potential charge curves are separable into three parts: (1) a limiting current region, which is in reality a constant current charge; (2) a current decay portion; and (3) a plateau region, which may be regarded as a second constant current charge (Figure 44). These curves should be in many respects similar to a step-type charge, and indeed this is supported by the data. It was found during the course of the tests that each portion of a given curve varied with charge potential and temperature in a specific manner independent of the remainder of the curve, but in a definite relation to other curves in the group(s). Thus, it was found that region 1 in this figure increased in length as the potential and temperature increased; the slope of region 2 increased in magnitude with increasing potential and temperature; the current associated with regions (1) and (3) increased with increasing potential and temperature. Thus, the initial portion, region 1 corresponds to a high rate constant current charge, which undergoes a transition (region 2) to a low rate constant current charge corresponding to region 3.

X. FUNDAMENTAL STUDY OF THE REDUCTION OF OXYGEN AT THE CADMIUM BIELECTRODE

When oxygen is consumed in a fuel cell, the potential of the electrode is approximately -.02 volts versus the Hg/HgO, KOH electrode.[3] The oxygen consumption reaction in the nickel-cadmium battery occurs at the cadmium electrode at a potential of -0.90 volts versus the Hg/HgO, KOH electrode.

The potential -0.90 volts is that of the cadmium electrode which is tabulated in Latimer[4] as -0.80 volts*, the difference being that the Hg/HgO, KOH electrode is about 0.1 volt more positive than the basic hydrogen electrode.[5]

Because the potentials at which the reduction of oxygen occurs in these two systems is so different, one is led to suspect that the mechanisms may be as different as the potentials. Also, the electrode material upon which a reaction is occurring may have specific catalytic effects. For instance, two oxygen reduction waves were found at the dropping mercury electrode in 7.2M aqueous potassium hydroxide. No such waves were observed, however, at a rotating gold electrode.[6] Instead, with small cathodic polarization a maximum in current was observed similar to that observed by Breiter[7] during the reduction of oxygen adsorbed on Pt by dissolved hydrogen.

An understanding of the mechanism governing the reduction of oxygen at the cadmium electrode is pertinent because this reaction is operative in the hermetically sealed nickel-cadmium cell. Basically, one needs to know whether the reaction is rate controlled by oxygen

* The signs in this report are based on the Gibbs-Stockholm Convention.

transfer, or by the electrochemical process. Application of this knowledge will result in a greater overcharge capability.

It is important to note how such commercial cadmium electrodes are fabricated. A nickel powder having a density of approximately unity (the metal itself has a density of 8.9) is sintered upon a conductive grid. The grid is usually nickel plated cold rolled steel. The porosity of the sintered mass is in the order of 80%. Cadmium salts are impregnated into the sinter and converted into cadmium hydroxide. The resultant porosity after processing is reduced to approximately 50%. Thus, the cadmium electrode is to be regarded as a bielectrode consisting of an inert metal electrode and the $Cd/Cd(OH)_2$ electrode.

It is well-known that a charged Cd electrode removed from the electrolyte and held in air ignites while drying out. It is also well-known that a vented type cell that contains a one-way valve in a flexible case becomes concave several days after charge. This concavity is presumed due to a reaction between the atmosphere within the cell and the electrodes, particularly the negative electrode. It should be noted that hydrogen and oxygen are evolved from such cells and will sweep out the air.

Jeanine[8] reported that sintered nickel electrodes, not containing active material, closely spaced evolved less than the theoretical quantities of gases.

Neumann and Gottesmann[9] reported that oxygen is transferred by the gas phase and provided for "electrolyte free gas passages" in the separator, but neglected to provide a method for determining their presence.

Baars[10] put forth a theory that included both gaseous transport of oxygen, or, in the case of small interelectrode distances, a bridge which constitutes a short circuit of such magnitude as to support the current and the existing (it is presumed) pressure in the cell. These shorts were to burn themselves out on current interruption. This theory was later abandoned by Baars[11] in favor of a peroxyl mechanism similar to that of Berl[12] for the fuel cell oxygen electrode. It should be noted that Baars did not report an experimental finding of peroxide. Fleischer[13] using the sensitive titanate test was not able to detect peroxide.

Following Baars, Dehmelt and von Dohren[14] concur in a peroxide mechanism theory. Again, no direct experimental evidence was found to demonstrate peroxides formed in the cell while oxygen was being reduced. The strongest argument in favor of this mechanism was that the potential of their unimpregnated sinter became more positive when the oxygen pressure was increased, as happens with the fuel cell oxygen electrode.

Baars separated the function of the Cd metal and the nickel sinter in an ingeniously simple manner. He merely immersed Cd under electrolyte and "floated" a sintered nickel mass on top of the electrolyte. These two electrodes were connected through an ammeter. When oxygen was reaching the nickel mass, current flowed. In another experiment, having two unimpregnated nickel sinters closely spaced but separated by an electrolyte moistened separator, conducted in an atmosphere of oxygen, he was able to show that current could be passed without a change in oxygen pressure. Baars concluded that the reaction was electrochemical in nature, and that the reaction took place on metallic nickel sites.

Dehmelt and von Dohren[14] ran experiments with unimpregnated cathodes. They too observed the reaction occurring at nickel sites. A cell was constructed in these laboratories consisting of nickel oxide electrodes and unimpregnated cathodes. During overcharging a substantially steady pressure was reached, indicating and agreeing with the previous investigators, that metallic Cd is not needed in a certain instance to effect oxygen reduction. The instance is overcharge. As will be seen later, however, metallic Cd is needed for the bulk of the pressure decay during open circuit.

Quintin and Viltange[15] conducted experiments with electropolished Ni immersed in electrolyte. Currents up to certain values for each interelectrode spacing could be passed without altering the oxygen pressure within the cell. They found two distinct regions which they feel correspond to a rapid diffusion of oxygen from the anode to cathode at small interelectrode spacings, region II. The other region, occurs when the electrodes are widely spaced so that the oxygen becomes gaseous, enters the gas phase and then redissolves in order to reach the cathode.

It is fairly difficult, in practice if not in principle, to run investigations on the oxygen reduction reaction in cells. The difficulty is due to the self-discharge of the positive electrodes which occurs at a substantial rate for approximately one-half to several hours (depending upon charge rate and temperature) following charge interruption. In spite of this inherent difficulty, some information on the reaction was obtained in cells,[16] and were later confirmed by other workers in these laboratories.[17]

It was shown that at oxygen pressures greater than about 2/3 atmosphere the oxygen decay with time is semi-logarithmic. This indicates that the reaction is first order with respect to oxygen and zero order with respect to Cd. These observations were confirmed by even more direct eperimentation. In some even more recent work, it was found that the region below 2/3 atmosphere is also semi-logarithmic, but additional efforts are needed to interpret the meaning of this finding.

Data were also obtained indicating that the specific heterogeneous rate constants during overcharge are greater than the specific heterogeneous rate constants during open circuit.

Preliminary current-voltage studies indicate an absence of an oxygen wave at the cathodic nickel electrode.[18] Confirming this lack of a diffusion wave is the fact that the activation energy for the process is virtually independent of temperature.[17] Its value is 5.07 kcal per mole over the range of 25 to 40°C.

The theories extant in the literature do not satisfactorily explain experimental observations made on cells and on negative electrodes. Let us first discuss the theory concerning short circuits. It would, indeed, be fortuitous for a "high resistance" short circuit to occur that will just compensate for the self-discharge of the positive electrodes, the voltage of the cells, and the gas pressure. More likely shorts may form that are intermittent. When the voltage starts to fall, the short will break. Under these circumstances one should be able to see the noise on an oscilloscope. Such noise was not observed. It should be noted that noise would not be caused uniquely by shorts. Bubbles of gases forming on, and leaving

the electrode would also cause noise. Consequently, the evidence does not indicate intermittent shorts, nor does it indicate gas bubble formation.

The peroxide theory, when set into the form of the Nernst equation, indicates a reaction that should be (1) first order with respect to oxygen, (2) zero order with respect to cadmium (3) and at a constant current, make the electrode more positive when the oxygen pressure is increased. This theory does not of itself explain the apparent increased specific rate constant during overcharge, although it does predict the open circuit reaction at the cadmium electrode. Thus there are only two points which cause doubt to be established about this theory. One is the fact that peroxide was not found, and the second is that the polarization of the negative electrode is small[19] and in the wrong direction to account for a faster oxygen consumption during overcharge. If the earlier data are further substantiated, the lack of a peroxyl wave can not be explained in these terms.

Since the evidence is mounting[20] that the reduction of oxygen is indirect and activation controlled, the present theories are inadequate. A new theory has been promulgated and is presented next. An unpoised nickel electrode can cause the discharge of ions in solution when the potential is fixed. These discharged ions will be adsorbed on the surface of the electrode. Since an equilibrium is not set up with gases, the equilibrium is probably set up between the surface concentration of adsorbed gas and the concentration of the undischarged ions in solution or of water. In this way the current associated with the change of potential is explained. If the applied potential is greater than the decomposition potential the surface will become saturated and gases will be evolved from the electrode.

The fact that the negative electrode is a bi-electrode may now be used:

$$\overline{\text{Cd, Cd(OH)}_2\text{/KOH aq (H}^+\text{, K}^+\text{, OH}^-\text{)/ H - Ni}}$$

The line connecting the Cd to the Ni represents a short circuit as it exists in the system. That is, a mixture of Cd and $Cd(OH)_2$ is contained in the pores of the electrode which is sintered nickel. The electrolyte, aqueous KOH, covers both the Cd, $Cd(OH)_2$ mixture and the exposed nickel.

Oxygen reaching the nickel surface at any point where nickel is covered by electrolyte reacts with the adsorbed hydrogen and thereby upsets the equilibrium between the surface coverage and the solution. But the Cd, $Cd(OH)_2$ electrode buffers the voltage, in a sense, and additional Cd is converted into $Cd(OH)_2$ while depositing H atoms on the nickel surface:

1) $Cd + H_2O \longrightarrow Cd(OH)_2 + 2H^+ + 2e^-$

2) $2H_2O + 2e^-(Ni) \longrightarrow 2H\text{-}Ni + 2OH^-$

The reaction between oxygen and the adsorbed hydrogen is not represented since we have no concept, except a negative one, about the mechanism involved. Breiter[7] has shown that an electrochemical reaction between adsorbed oxygen and hydrogen exhibits a maximum rate at an intermediate potential. If the rate of this reaction is proportional to the surface area covered by oxygen, θ, and to the surface area covered by hydrogen, $1-\theta$, a maximum reaction rate would be observed when $\theta = 0.5$. This has not been observed on Ni, although it was found on a gold electrode in 7.2N KOH. Therefore, there is still a lack of evidence concerning the mechanism of the reaction between hydrogen and oxygen at the surface.

Thus oxygen can be reduced at any place where the conditions are appropriate. During open circuit the reaction sites are elemental nickel which are at the potential of the Cd, Cd $(OH)_2$ electrode and also covered with a film of electrolyte. If we consider that the electrodes are closely spaced and the separator and electrodes are essentially saturated with electrolyte then the reaction sites are limited to the edge of the electrodes, the backs of the end electrodes and the tabs and terminals. The electrode faces covered by separator will represent a long path through which the oxygen must travel. It is much more likely for the reaction to occur through the shortest path[21] which is the film.

When a cell is placed on overcharge, oxygen can continue through the gas phase. In addition, with interelectrode distances of 0.2 mm, or less,[15] oxygen can travel directly from the anode to the cathode, effectively increasing the number of reaction sites.

This theory will account for the observations made on sealed cells, on negative electrodes, and on unimpregnated electrodes.

At the pressures to which this theory is applicable it is readily understood why the rate is independent of the amount (or state-of-charge) of the negative electrode whether the electrode state-of-charge is altered by discharge or by reaction with oxygen. The reaction will occur at a rate proportional to the amount of oxygen at the metal/solution interface. The Cd, Cd $(OH)_2$ electrode, which does not significantly polarize under these conditions, will merely replace the hydrogen removed.

The rate of the reaction will be dependent upon the number of sites, or electrode area, at which the reaction will occur. Thus it will

be sensitive to the amount of electrolyte within the cell; more electrolyte will leave fewer film paths. Also, additional reaction sites will be available during overcharge if the interelectrode distance is small.

A low activation energy merely means that the reaction can occur at a significantly rapid rate at low temperatures. The constancy of the activation energy over the 25 to 40°C range is not inconsistant with a chemical process, also its low value is consisted with an atomic hydrogen process.

While the theory proposed above does fit the observations drawn from many sources, certain proofs must be obtained. These proofs must be obtained under unquestionable and rigorous experimental conditions. Perhaps one of the most important of these proofs is a continued study of the current-voltage and current-time characteristics of nickel wire and porous nickel electrodes. These studies are to be made to study the effects of convection (natural convection is absent in zero G environment), the effects of porosity, and the effects of several oxygen partial pressures on these characteristics. These experiments were started during the past quarter and shall constitute the experimental section on this reaction.

Let us set up the chemical equations that correspond to the reactions of this theory;

$$(2)\quad H_2O + e^- (Ni) \xrightarrow{r} H\text{-}Ni + OH^-$$

$$(3)\quad O_2 + 4H(M) \xrightarrow{r} 2H_2O.*$$

Equation 2 is merely the electrochemical process of discharging a proton from water which is then either absorbed on the electrode or forms an interstitial compound with Ni. The rate at which this process proceeds

*Equation 3 does not purpose to represent a mechanism, but merely gives the overall process. Equation 2 is mechanistic.

is given by the current H. This process will occur only with current, that is, it commences with current flow and ceases with interruption as in any electrochemical process. Equation 3 is a chemical process that will proceed at a rate dependent only upon the surface concentration of adsorbed atoms and the partial pressure of oxygen. If the rate at which the process represented by equation 3 proceeds is slower than the rate at which that represented by equation 2 proceeds, then two predictions can be made. The first prediction is that there will be a lag in oxygen consumption before the steady oxygen consumption rate is reached. This corresponds to the deposition of H atoms on the nickel surface. The second prediction is that oxygen will continue to be consumed after current interruption. This corresponds to a depletion of the hydrogen already on the Ni. These predictions of transients constitute an especially pertinent test of the theory.

Another test of the theory is the relationship between the pressure of the electrode and the potential. Because of the potential buffering by Cd/Cd $(OH)_2$, this too must be done at the blank electrode (a porous Ni body). Using the Nernst equation one expects a logarithmic relationship between pressure and voltage corresponding to 15 MV for a peroxyl electrode. For a depolarization mechanism as postulated herein, this slope is expected to be much greater indicating that use of the Nernst relationship is improper. During the course of this investigation, deficiencies in the use of reference electrodes in the presence of oxygen became apparent, and necessitated an investigation of reference electrodes in the presence of oxygen. This work is applied in the sense that a useable electrode was sought, rather

than basic where an understanding of the cause of potential changes by oxygen was sought.

Another attempt was made to find peroxide in the cell. Conditions were set up to have a large concentration of H_2O_2, if it did form. A preliminary measurement of the rate of decomposition of H_2O_2 in electrolyte was made in order to estimate the amount lost between cessation of charge and neutralization of the electrolyte in a negative electrode.

Polarographic investigation of oxygen reduction at nickel electrodes was also performed.

A. EXPERIMENTAL

1. Polarographic Study of Oxygen Reduction at Nickel.

The polarization circuit consisted of a transformer which steps up the AC to 350 volts. This was rectified through a 6 X 4 vacuum tube, filtered and regulated to 105 volts with an OB2 mercury vapor voltage regulator. The output was then stepped down through a resistor and a Zener diode (Motorola Catalogue No. ½M2.4AZ) which supplied a regulated 1.5 volts. A Spectral Model 810 ten turn precision linear potentiometer having a resistance of 100 ohms was connected across the Zener diode. A 1 rpm synchronis motor was used to drive the potentiometer through a 1:1 gear train.

A shunt was placed in the positive leg of the circuit. This shunt was a General Radio Decade Resistance Box. The current was read on the Y coordinate of a Mosely Model 2A X-Y recorder. The recorder was always set on its most sensitive range (5MV full scale) so that the

potentiometric feature of the instrument could be used.

The positive electrode, the counter electrode, was a 0.005 inch platinum foil having a relatively large geometric surface area, 63.0 cm^2.

The negative terminal of the power supply was connected to the test electrode.

A mercury, mercuric oxide/KOH half-cell was used to determine the cathode potential. The potential was recorded on the X coordinate of the X-Y recorder. The reference electrode was connected to the system using a Luggin capillary.

The electrolyte used was identical with that employed in the hermetically sealed nickel-cadmium cell, 34% aqueous potassium hydroxide.

Grade B nickel wire of 0.0589 cm. diameter was sealed into a soft glass tube. The exposed length of wire was cut to 1 cm. leaving a geometric surface of 0.19 cm^2.

The electrode was mechanically cleaned to remove the blackened oxides caused by heat sealing into glass. It was degreased in acetone and air dried. Nitric acid cleansing did not permit the current-voltage curves to be reproducible, and this treatment was abandoned.

The initial runs, cathodic polarizations were not reproducible. After two runs, the subsequent cathodic polarizations are very reproducible. Between runs, the electrode is kept on open circuit until it reaches the potential that it had in the previous run.

The porous electrode was cut from an unimpregnated sinter. The dimensions were 1 cm. by 1/2cm. The termination was the nickel plated steel tab. The edges of the electrode were coated with polystyrene

dissolved in methyl ethyl ketone in order to stop-off the exposed steel grid edges. This electrode was degreased in acetone prior to application of this stop-off lacquer. This edge-coating process is identical with that used in cells. The sintered electrode also requires one or two preliminary cathodic polarizations before subsequent runs are reproducible. However, the sintered electrode does not require a waiting period before the next run is made.

The nickel wire electrode was rotated at 600 rpm in several experiments using a Sargeant Synchronous Rotator.

To sweep out all gas which may interfere, tank nitrogen was used as a purge. The end of the tubulation contained a sintered glass gas dispersion tube. Experiments with air (P_{O_2} = 0.2 atm.) were done by attaching a compressed air line to the gas dispersion tube. Experiments with oxygen were carried out using tank oxygen gas. All experiments were done at room temperature (27° to 28°C).

The current-voltage curves (polarograms) of Ni wire microelectrode obtained in a relatively oxygen-free electrolyte are shown in Figure 45. The electrolyte was purged with N_2 for 15 minutes prior to each run, but the purging was stopped just before the run was started. This particular run was reproducible and the figure is only one example of the data obtained. Other examples, in which the voltage was not driven above 1.0 volt are shown in Figure 46.

At the potential of the Cd, Cd $(OH)_2$ electrode, -0.90 volts (obtained by a direct measurement), the average current at the unstirred electrode is 39.5 $\pm$ 1.3 uA/cm^2. When the electrode is rotated at 600 rpm,

the current at the same potential increases to 43.3 $\pm$ 2.6 uA/cm^2.

In Figure 47 the current-voltage curves for the sintered nickel electrode are shown. The upper and lower curves indicate the reproducibility obtained. Qualitatively, these polarograms for the sintered electrode are similar to those obtained at the solid wire electrode. That is, they do show a typical activation controlled type process. Quantitatively there are differences between the two kinds of electrodes. At -0.90 volts, the current through the electrode is 406 $\pm$ 31 uA/cm^2. This area is based on geometric area. This is 9.4 times greater than on the wire electrode. At -0.8 V the current at the sinter is 188 $\pm$ 25 uA/cm^2. The ratio in this case is 38. These differences may merely be due to the fact that the data is obtained in a transitory manner, polarographically.

The effect of oxygen on the stationary microelectrode was determined with the results shown in Figure 48. In the earlier runs stirring was achieved with a motor, while in this run agitation was achieved by vigorously bubbling nitrogen through the solution with the aid of a gas dispersion tube. Note that the current at -0.90 volts are in good agreement.

The run in which the partial pressure of oxygen is at 0.2 atmospheres was obtained by introducing compressed air into the solution. The current density increased, at the potential of interest, from 47 to 50 uA/cm^2.

When the solution is saturated with oxygen at a partial pressure of one atmosphere, the current is increased to 60 uA/cm^2.

2. TRANSIENTS

In contrast to the log P versus E work, the time lag study is difinitive in several respects. First, there is no doubt about the experimental data, and second, it provides a unique differentiation between a chemical and electrochemical mechanism.

The theory which is to be substantiated states that oxygen is reduced by atomic hydrogen in the nickel grid, or on it. A recent paper provides proof of interstitial hydrogen in Ni.[22] If oxygen is added to a cell that contains porous Ni bodies as cathodes, and the hydrogen atoms are removed from the Ni by waiting until the pressure no longer drops, it is reasonable to assume that the Ni is clear of H atoms.

When oxygen is present over clean nickel, and current is passed through to make the nickel cathodic, several cases may occur. If the O_2 is reduced electrochemically, then one expects the pressure decay to be instantaneous with current. Also, when the current is interrupted, the oxygen pressure should no longer decay. On the other hand, the chemical theory advanced here requires that hydrogen atoms first be put into the nickel, and the oxygen consumption rate is dependent upon the degree to which the atoms are in the nickel. Since the surface is originally clean, then the instantaneous rate should be zero and slowly build up to some steady rate of consumption. A time lag is therefore predicted by the theory.

Continuing this argument, when the current is interrupted there will be some concentration of H atoms in the Ni corresponding to the steady state coverage. It is therefore predicted by this theory that

even after current interruption, oxygen will be consumed at a decreasing rate until the Ni is again free of H atoms.

The experiment consisted of reducing the oxygen pressure in the cell to barometric pressure and attaching a 1 ml graduated pipet. The pipet had a drop of water in it to serve as an indicator. The pipet was kept horizontal.

When the current was started, approximately 10 to 20 seconds elapsed before the water column started to move. The current was interrupted when the water column was near the end of the graduations (0.9 ml). The water column continued to move off scale, and definite motion was perceptible for about 90 seconds after current interruption.

3. PEROXIDE TEST

This test selected is very sensitive and involves the oxidation of Ti^{+4} by hydrogen peroxide, which is thought to yield peroxytitanic acid by some workers. The peroxy-acid imparts a yellow to red color in the presence of peroxide, depending upon the concentration of Ti^{+4}. The test reaction proceeds in acid or even neutral solution. From data given by Wells,[23] the sensitivity of the test was calculated to be 0.4 ppm which corresponds to 1.25×10^{-5}M H_2O_2.

A VO-6 hermetically sealed Ni-Cd cell was pressurized to 50 psig with oxygen and placed on 5A charge for 1 hour. The cell was taken off charge, and within the next 3 minutes, the cell was opened, a negative electrode was stripped from the cell stack and plunged into a solution containing twice the amount of acid needed to neutralize the KOH on the electrode. Within four minutes, 10 ml of titanium sulfate

test solution were added.

Under these conditions, peroxide should have been formed and detected, if the necessary reaction with Ti^{+4} occurred. The peroxide test was negative. This test could detect 0.4 ppm H_2O_2. Upon dilution by neutralization, the concentration of H_2O_2 should be about 0.0007 molar or 3ppm.

4. REFERENCE ELECTRODE

A mercury, mercuric oxide electrode pasted upon an amalgamated silver sinter subjected to a hydraulic pressure of 15 tons per cm^2 gave reproducible results in the presence of oxygen. The response data for two such electrodes for atmospheres containing oxygen at 0.2 atm. and 1.0 atm. are given in Figure 49. The slope of the Nernst equation for these electrodes are 15.4 MV (V-7) and 15.5 MV (V-8). The potentials versus a customary Hg/HgO, KOH electrodes are extrapolated from the following Nernst relations.

4. (Electrode V-7) $E = 3.6 + \frac{15.4}{1} \log P_{O_2}$

5. (Electrode V-8) $E = -0.4 + \frac{15.5}{1} \log P_{O_2}$

5. Slope of log P versus E for the Cathodic Reduction of Oxygen at Nickel

Early measurements of potential of the oxygen consuming electrode were taken versus the anode of the system. Where Mi $(OH)_2$ blank cells were used the potential of the anode was that of the polarized Ni $(OH)_2$, Ni OOH electrode. Where Ag-blank cells were used the potential was that of the Ag, Ag_2O electrode. The fact that these anodes were polarized implies, that at least for some time,

their potentials were not constant. Further, in the case of the silver the literature reveals a dependence on oxygen pressure. Earlier work in these laboratories also indicates that a nickel oxide electrode may undergo potential changes in the presence of oxygen.

The work on the hydraulically compressed Hg/HgO electrode was to find a reference electrode suitable for use. Because of the success at the range of oxygen pressures of 0.2 and 1.0 atmospheres a cell was built using one such Hg/HgO as an unpolarized reference electrode. The cell contained Ni $(OH)_2$ as anodes with porous Ni bodies as cathodes. This cell was pressured to 4.3 atmospheres with oxygen and then current passed through to charge the anodes and reduce oxygen at the cathodes. The oxygen pressure and the potential of the Ni bodies with respect to the Hg/HgO electrodes were determined. These potential measurements were corrected on the basis of the work previously described. The derived data are shown in Figures 50 and 51.

It is assumed that at constant current polarization effects are neglibible. It can be shown theoretically that the slope of the log pressure - voltage relationship should be affected by not more than a factor of 2. This assumption was substantiated by measurements of hydrogen evolution at porous Ni electrodes.

The initial portion of these curves are ignored since polarizations are being set up. The duration of the experiments were approximately 90 minutes. The slopes range from about 350 MV to about 400 MV.

B. DISCUSSION

The polarographic data confirms previous work that there is an absence of an oxygen diffusion wave. This, of course, implies that the reaction is irreversible. Use of the rotating electrode indicates that connective processes have but a small influence on the rate at which oxygen is reduced. Oxygen pressure does affect the potential of the porous nickel body at a given current. The effect is to make the potential more anodic.

The theory proposed predicted certain transients attending the consumption of oxygen at a porous Ni body. Such transients were experimentally observed.

Since a negative result was found for H_2O_2 with the titanate test, it is postulated that either the amount of peroxide found is below a detectable limit, or it is not found at all. Peroxide does decompose readily in strongly alkaline, but does not instantaneously. It is estimated that in the absence of specific catalytic effects the test would detect H_2O_2 if it were formed. Therefore, it is concluded that H_2O_2 is not formed by the reduction of oxygen at the negative electrode.

The finding that the slope of the Nernst equation which ranges about 350 MV is much greater than expected for a peroxide mechanism. A similarly large slope is implicit in the data of Dehmelt and von Dohren.[14] This value of 233 MV is taken versus a Cd electrode. But the Cd electrode also becomes more anodic in the presence of oxygen[21] so that an appropriate connection would cause the va lue of the slope to increase. The presence

of oxygen is expected to stabilize the hydrogen on or in the Ni body. The potential of this Ni body should therefore not be very dependent on oxygen pressure. The erratic behavior observed is not surprising, nor is the large value of the slope calculated from the "best" parts of the log P vs. E relation.

There are several key points that the present theory fits which the electrochemical theory does not fit. In addition, no disagreement has been found between the results of investigations by various workers in the field, including the work this laboratory has done, and the theory.

The key points are:

1. While the negative electrode becomes more anodic with an increase of oxygen pressure, the consumption rate does not decrease.

2. The small activation energy of 5 kcal/mole is consistent with a reaction involving atoms.

3. The polarographic curves at Ni do not exhibit an oxygen wave.

4. Peroxide is not found.

5. Oxygen consumption lags are observed at initiation of current and after cessation of current.

Other poins that are fitted equally well by both theories are:

1. Pressure versus current curves are straight lines over wide regions.

2. There is an anodic shift of potential with increased oxygen pressure.

3. The Kinetics are zero order in Cd and first order in oxygen.

4. Consumption of oxygen proceeds on open circuit at the cadmium electrode.

5. Decreased oxygen consumption rate is observed in flooded cells.

6. Faster consumption of oxygen is observed on overcharge than on open circuit.

Thus there are eleven experimental facts, six of which can be equally satisfied by both theories, but the other five are satisfied by the chemical theory given in the previous report.

XI. CONCLUSIONS

Hermetically sealed nickel-cadmium cells with ceramic-to-metal seals have been successfully fabricated, and a pilot line has been established to produce these cells.

The VO-6 HS cell has been perfected in a deep drawn cell container, and its life characteristics have been shown to be at least 1500 cycles at 70% depth and 4900 cycles at 50% depth.

To meet the growing needs for large size sealed cells, a VO-50 HS, a fifty-ampere hour hermetically sealed cell, has been designed, fabricated and tested. This large cell has been optimized to allow for waste heat rejection. It has an output capability of 18.4 watt-hours per pound -- the highest capability ever achieved in a hermetically sealed nickel-cadmium cell.

Thin plate cells were investigated and found to have enhanced overcharge voltage and pressure capabilities due to the larger surface area available as compared to a thicker plate cell of equivalent capacity. No significant improvement in the watt-hour per pound capability was evidenced, however.

Thermal studies have yielded data which is useful both for cell designers and users. Since waste heat rejection in space applications is a major consideration these studies represent a significant engineering contribution.

Electrode fabrication studies have shown that more active material can be loaded into sintered nickel plates without decreasing the coefficient of utilization of the active materials. Extended cycle life studies are now needed to determine if these electrodes can match the

established life of currently produced plates.

Charge efficiency studies of sealed nickel-cadmium cells have shown that at low rates of constant current charge the positive electrode is less efficient than at high rates. The behavior of the negative is just opposite, i.e., at low charge rates the negative electrode is more efficient than at high rates. The behavior of these electrodes during a controlled potential charge appears to be explicable in terms of a variable current charge. During the limiting constant current portion, when current is high, the electrodes exhibit a behavior similar to that at a high rate charge. The region during which the current falls off rapidly is complicated. Finally a plateau of low current is reached, and the electrodes exhibit characteristics observed during low rate constant current charge.

A fundamental study of the mechanism of oxygen reduction at the negative electrode has led to a theory recognizing the negative electrode to be a corrosion bielectrode:

$$\underline{Cd,\ Cd(OH)_2/KOH\ aq/H\text{-}Ni}.$$

As long as the potential at the Ni sites does not exceed -1.08V (vs. Hg/HgO) H_2 will not be evolved. Oxygen, dissolved in the electrolyte film covering the Ni reaction site, reacts chemically with the H atoms on the Ni:

$$O_2 + 4\ H\text{-}Ni \longrightarrow 2H_2O.$$

During open circuit stand Cd is oxidized while water is reduced. The resultant H atoms are then oxidized by O_2. On overcharge Cd is not pertinent except to act in the $Cd/Cd(OH)_2$ electrode as a potential buffer.

XII. ACKNOWLEDGEMENTS

Gulton Industries greatfully acknowledges the support it has received for the work described in this report. The work was performed in the Research Department of the Alkaline Battery Division at Metuchen, New Jersey during the period from January 1961 through June 1963.

It is our pleasure to acknowledge the assistance and support of the following personnel of NASA Goddard Space Flight Center: Tom Hennigan, Paul Donnelly and Gene Stroup, also, Fred Yagerhoffer and William Cherry. The interest and encouragement from Walter Scott and Ernst Cohen of NASA Headquarters is also appreciated.

Many people at Gulton Industries contributed to this effort. The major technical contributors are listed as coauthors; each of the supporting contributors will recognize his own efforts and take pride in the thought that this effort has made a significant contribution to the state-of-the-art of hermetically sealed batteries for space application.

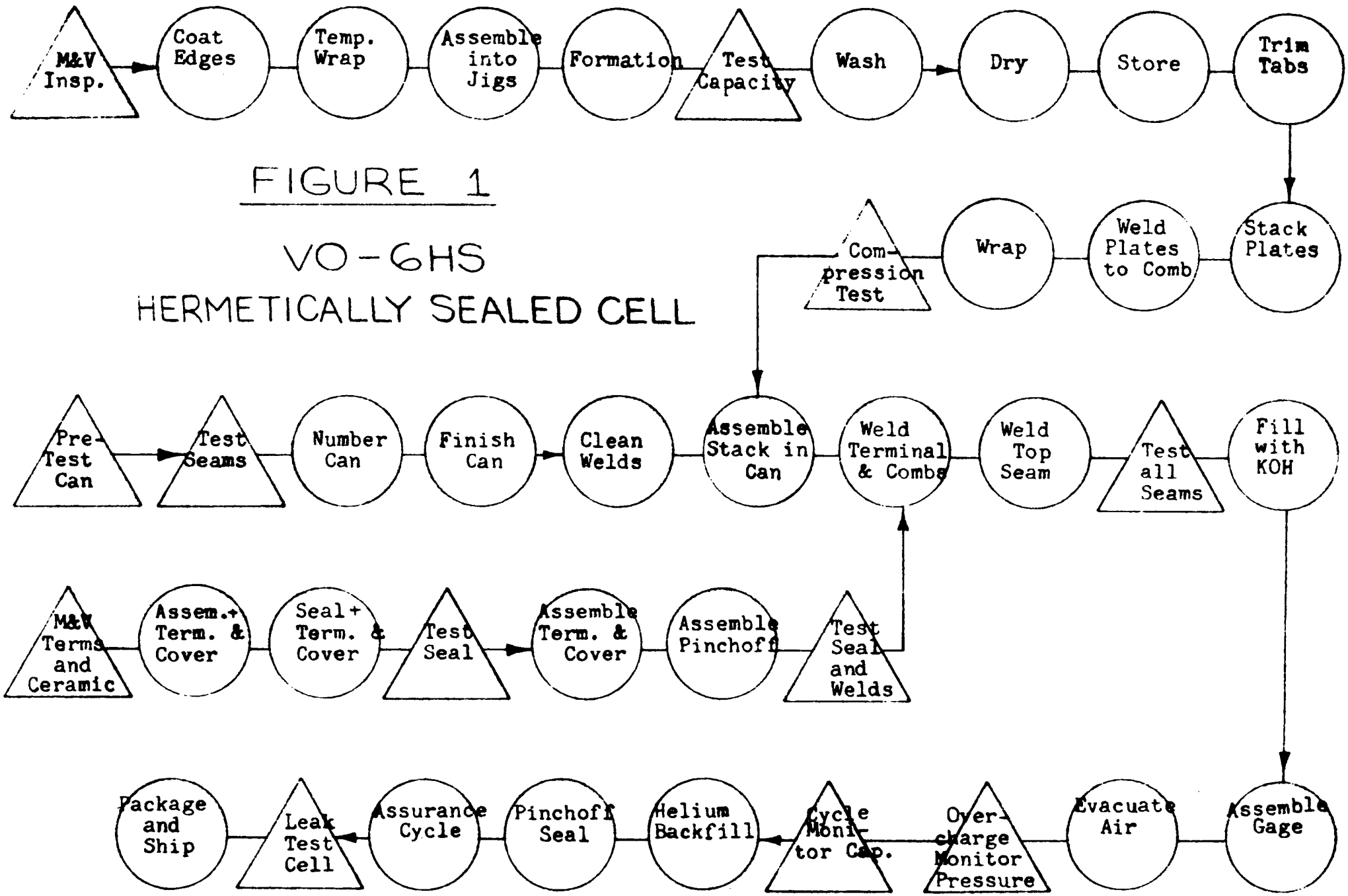

FIGURE 1

VO-6HS

HERMETICALLY SEALED CELL

M0388

GULTON INDUSTRIES, INC.
Alkaline Battery Division
Metuchen, New Jersey

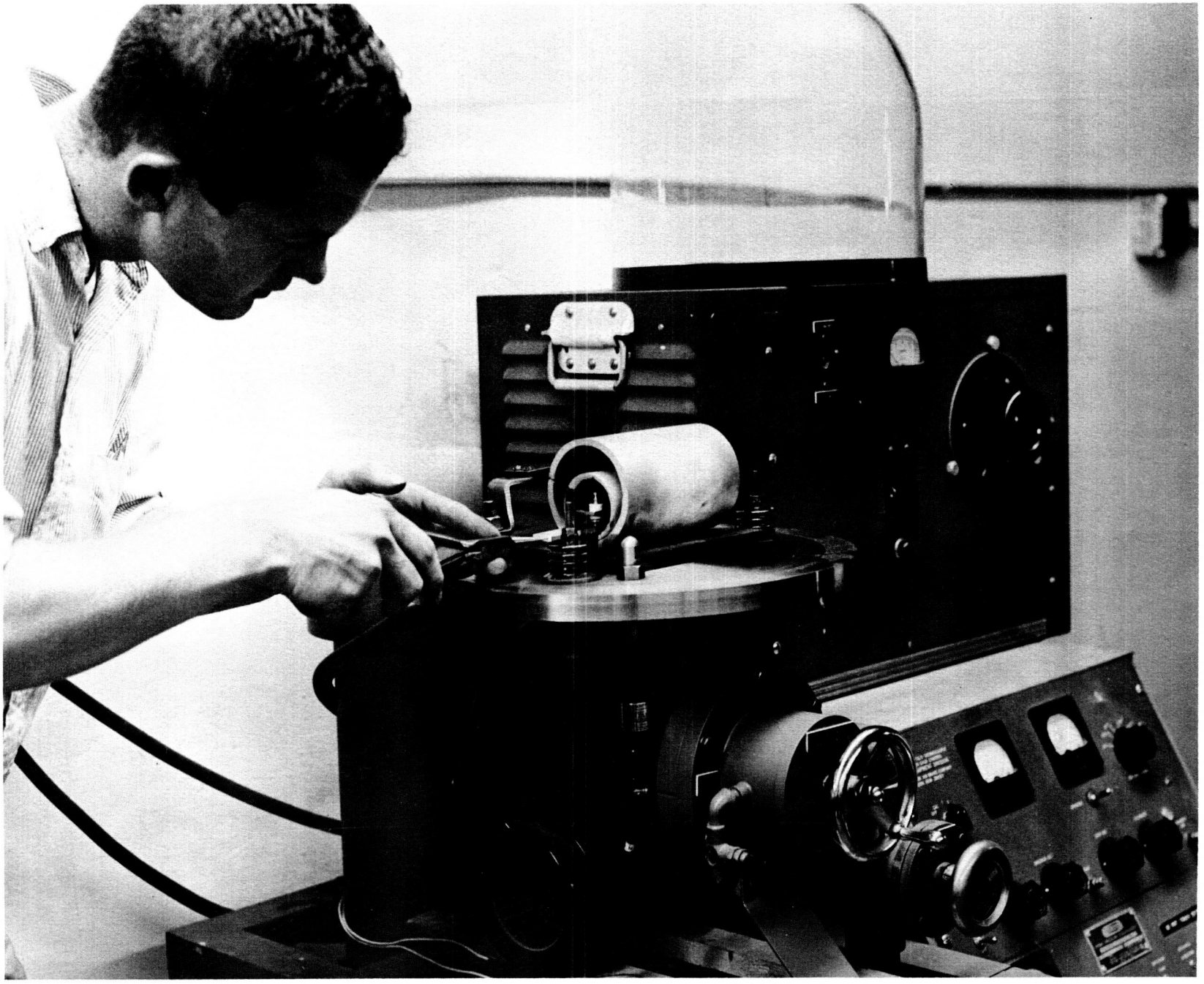

Figure 2

Vacuum Pumping Station and Resistance Furnace
For Experimental Fabrication of Ceramic-to-Metal Seal

GULTON INDUSTRIES, INC.
Alkaline Battery Division
Metuchen, New Jersey

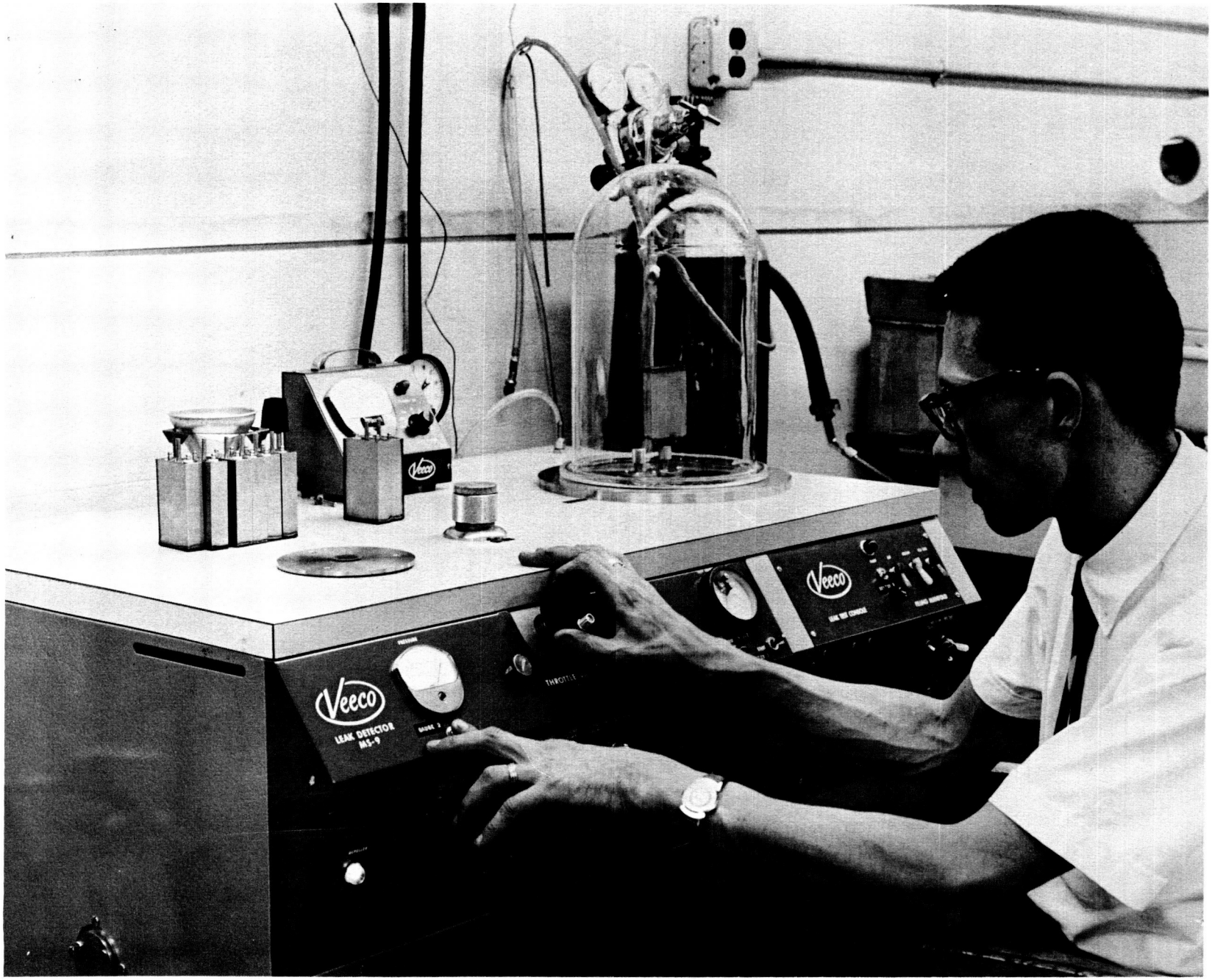

Figure 3

Helium Leak Detector

GULTON INDUSTRIES, INC.
Alkaline Battery Division
Metuchen, New Jersey

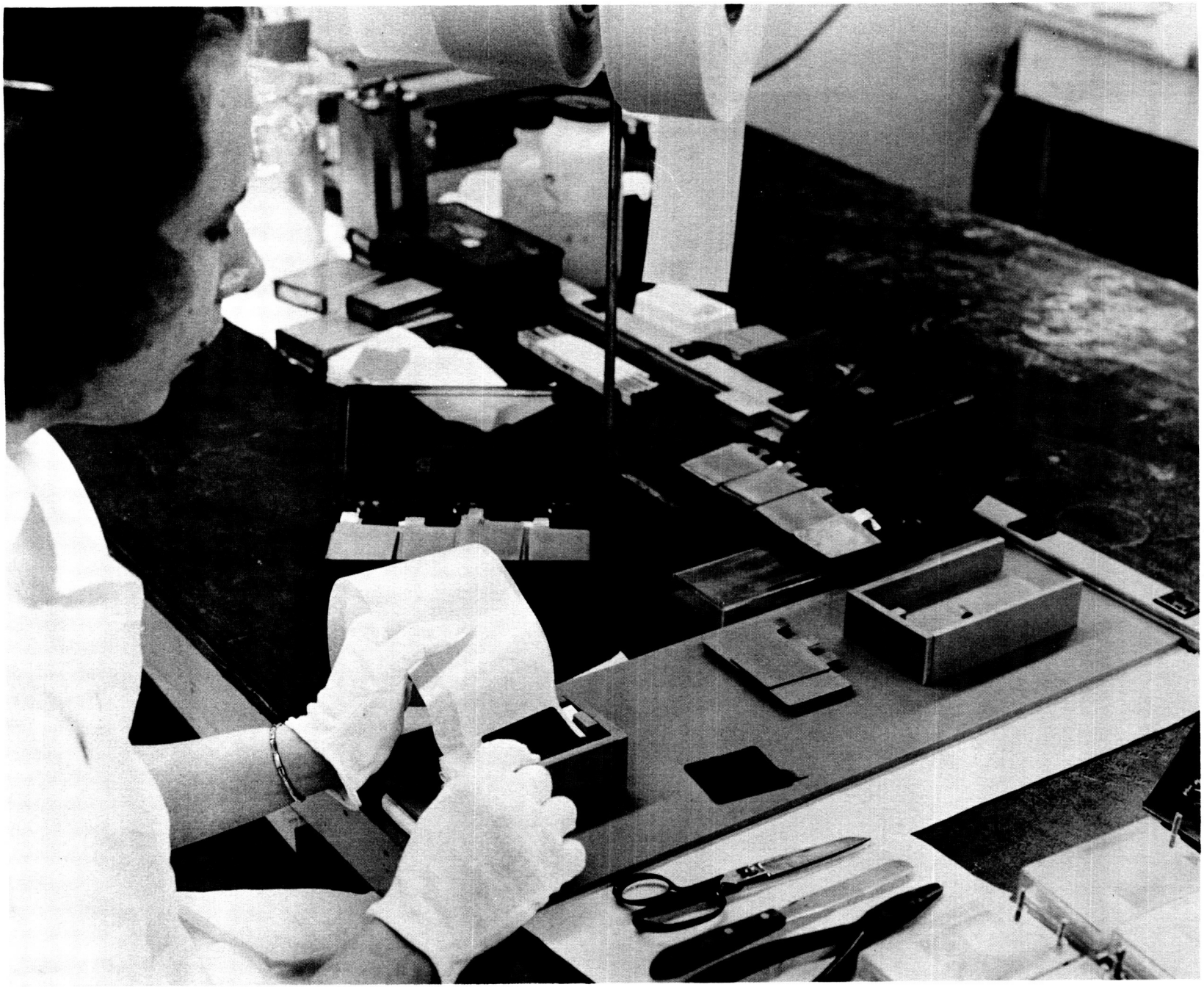

Figure 4

Preliminary Wrapping of Electrode Stacks Prior to Formation

GULTON INDUSTRIES, INC.
Alkaline Battery Division
Metuchen, New Jersey

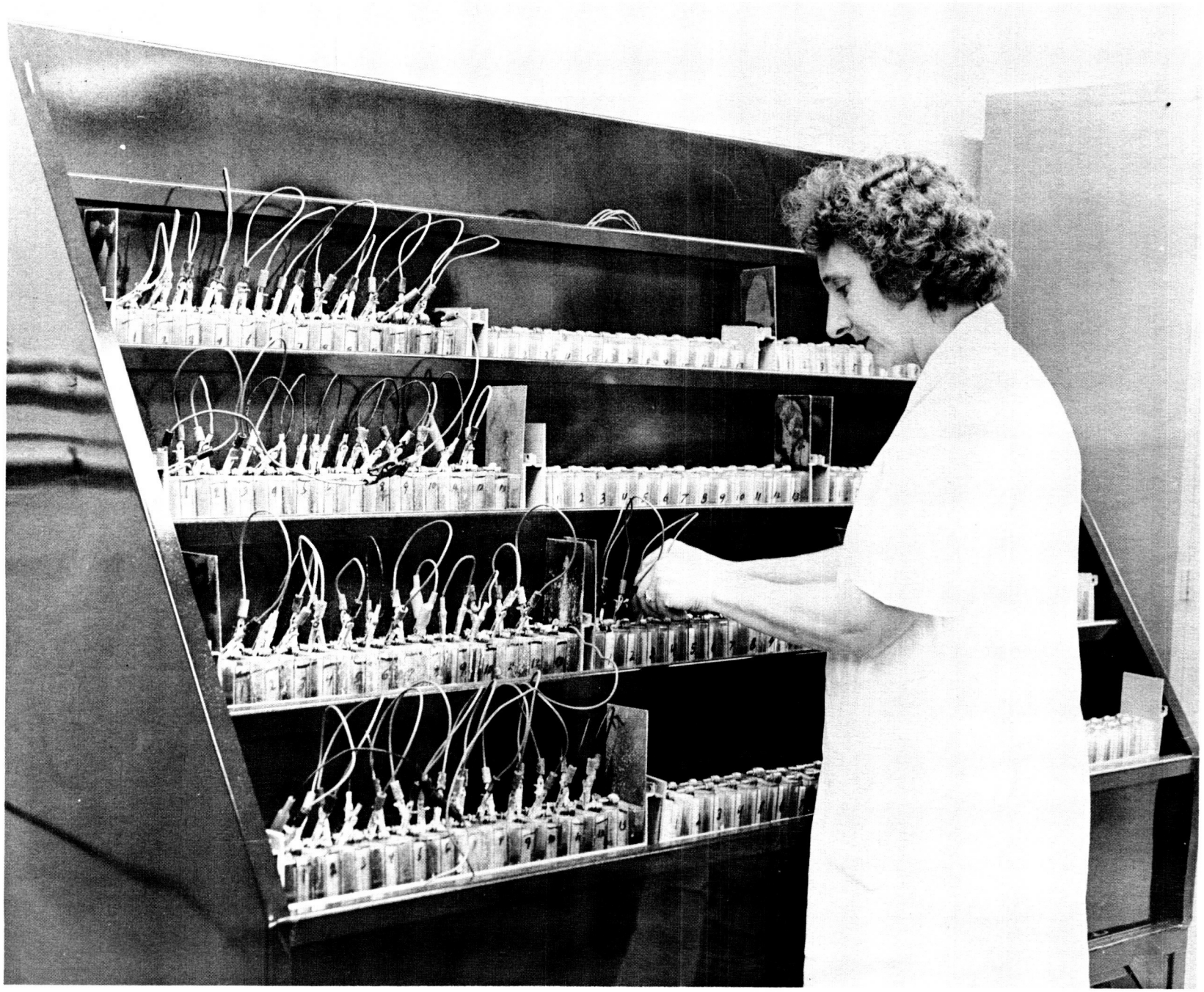

Figure 5

Formation Rack For Electrodes

Figure 6

Connection of Electrode Assembly to Cell Cover

GULTON INDUSTRIES, INC.
Alkaline Battery Division
Metuchen, New Jersey

Figure 7

Final Wrapping of Electrode Assembly With Separator

GULTON INDUSTRIES, INC.
Alkaline Battery Division
Metuchen, New Jersey

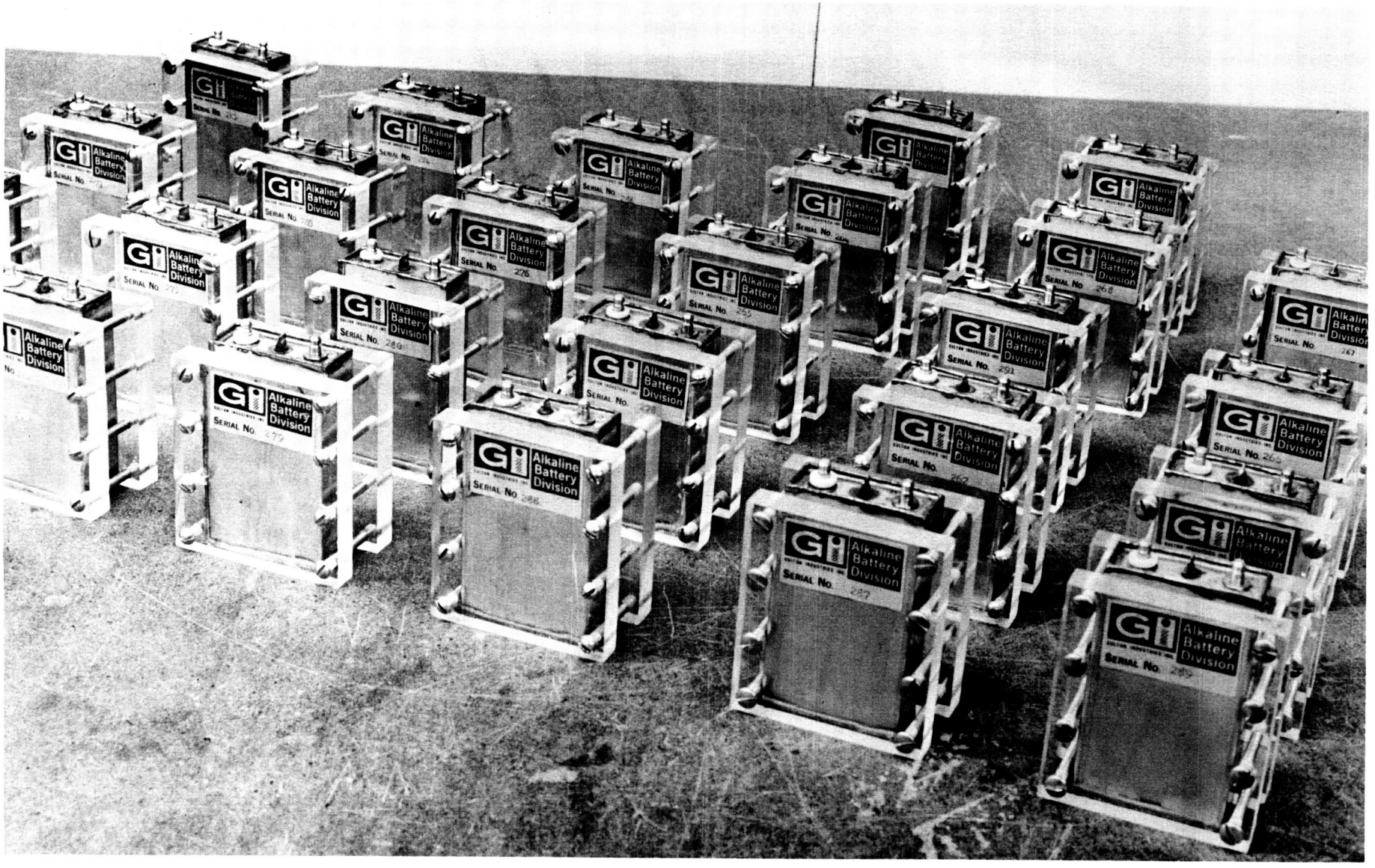

Figure 8

Hermetically Sealed VO-6 HS Cells

APPLICATION		REVISIONS				
NEXT ASSY	USED ON	CHG NO.	SYM	DESCRIPTION	DATE	APPROVAL
		63-96	A	DWG NO WAS M1518	3/29/63	JB

A

7026

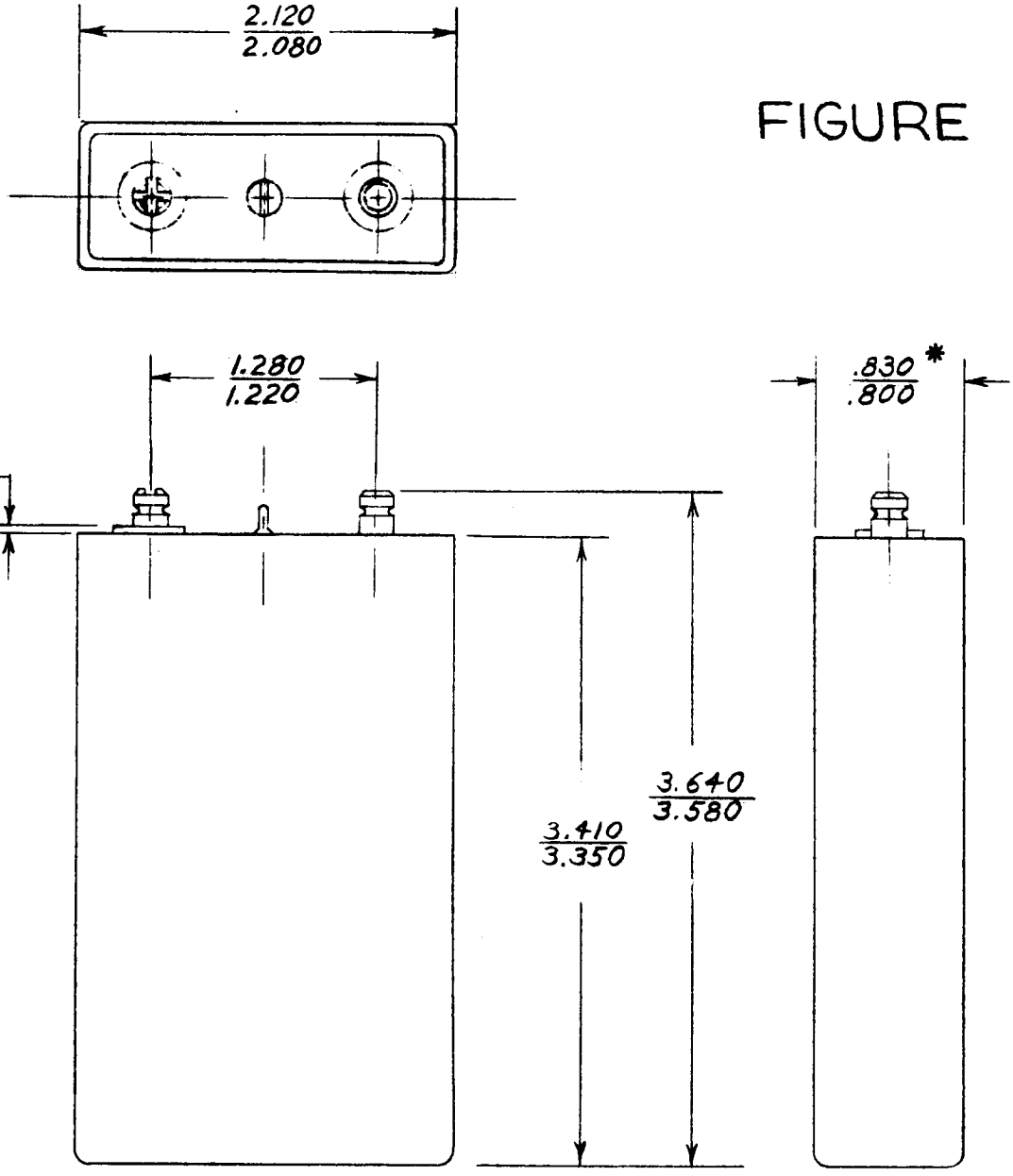

FIGURE 9

NOTES: 1. TERMINALS TO BE 90° ±3° TO THE HEADER
2. DIMENSION DENOTED * MEASURED WHILE CELL IS RESTRAINED
3. CELL WEIGHT .62 LBS.

UNLESS OTHERWISE SPECIFIED	SIGNATURES	DATE
DIMENSIONS ARE IN INCHES TOLERANCES ON FRACTIONS DECIMALS ANGLES ± XX ± ± XXX ±	DR JPB	3/20/63
	DSGN	
MATERIAL	PROJ ENGR RJD	3-20-63
	CHKD	
	APPD	
FINISH		

HERMETICALLY SEALED CELL TYPE VO6-HS

GULTON INDUSTRIES, INC.
METUCHEN
NEW JERSEY

SCALE 1:1

DRAWING NO. (A) 7026

REV A

MODEL A

AB3000-F

GULTON INDUSTRIES, INC.
Alkaline Battery Division
Metuchen, New Jersey

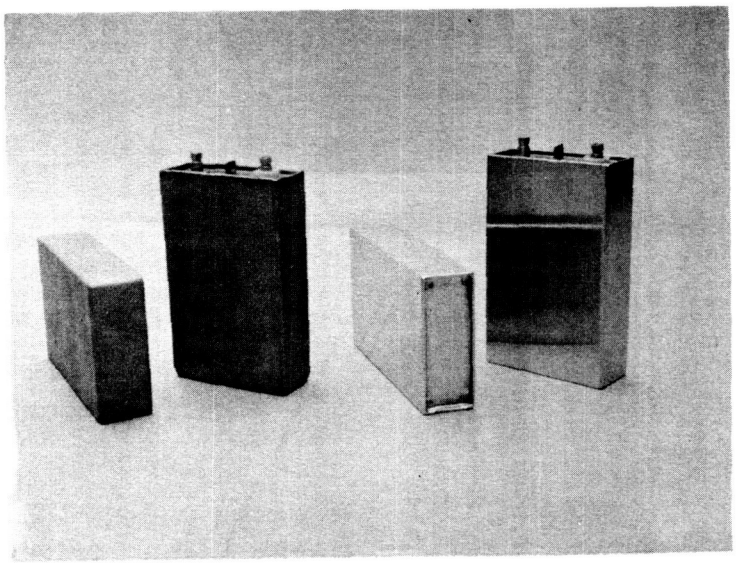

Figure 10
DRAWN AND WELDED CAN VO-6HS CELLS

FIGURE 11

VO-6 HS
C/2 CAPACITY

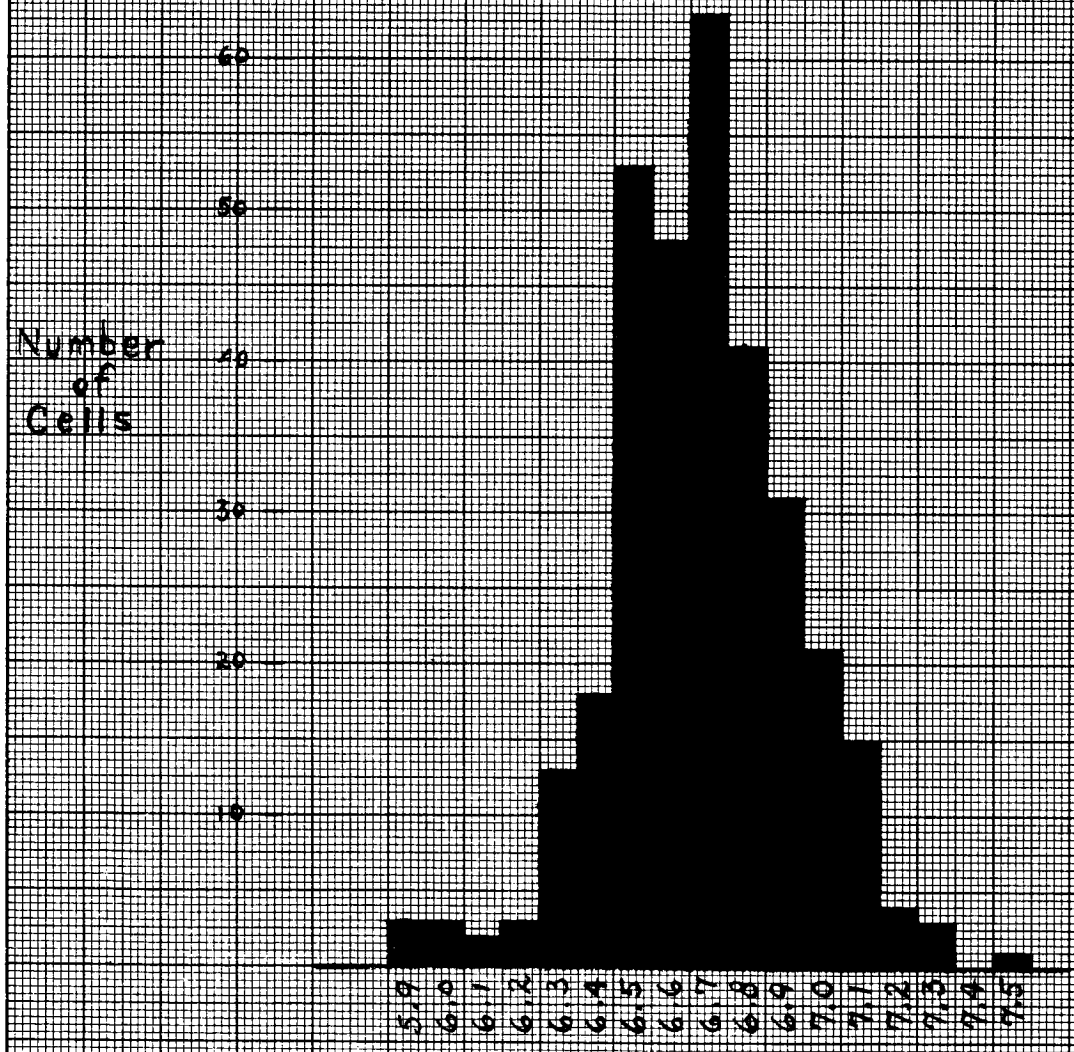

PRODUCTION PERIOD
11/4/62 thru 2/6/63

M1461
AB3000-F

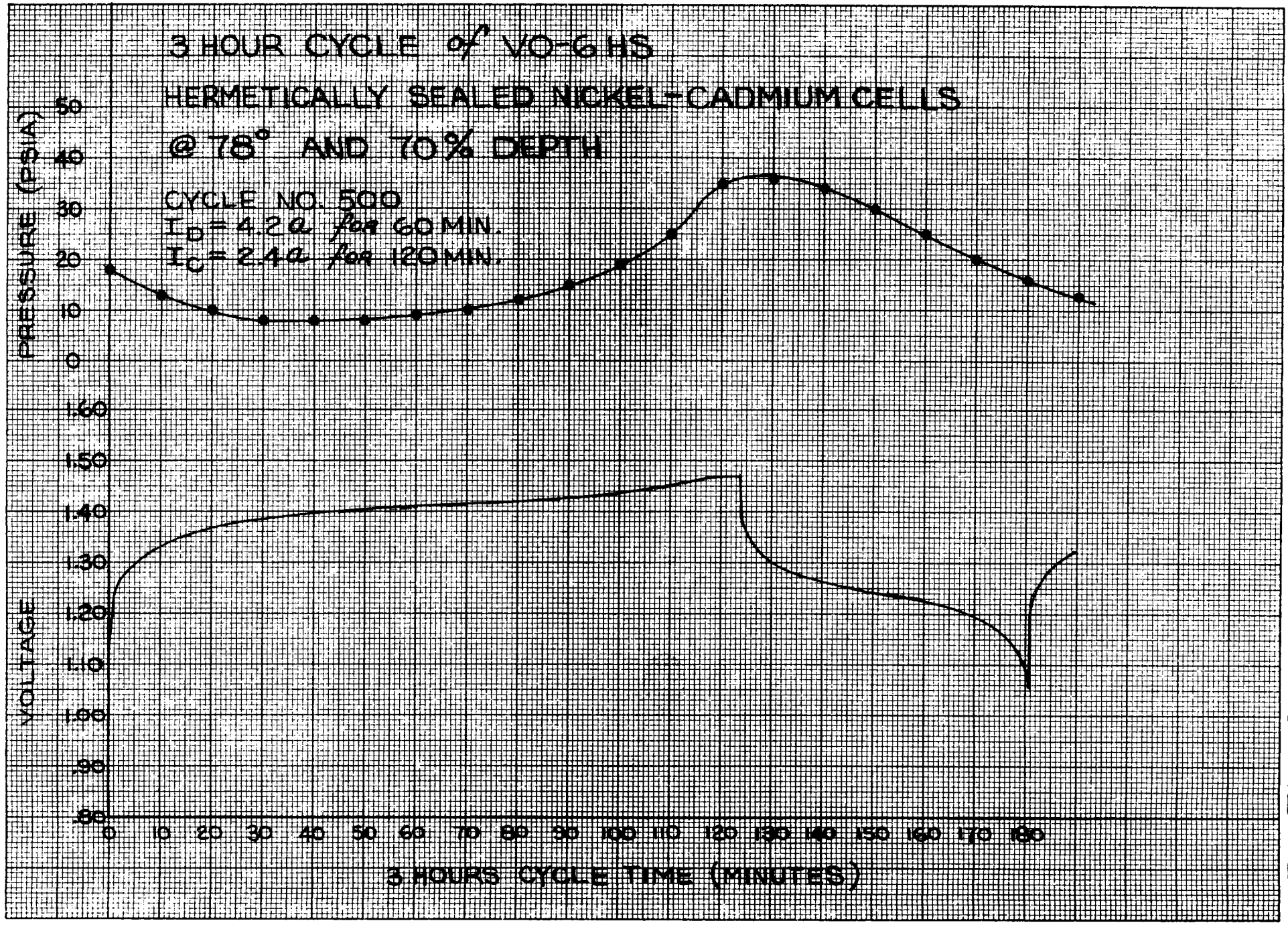

FIGURE 12

M1114
AD3000-5

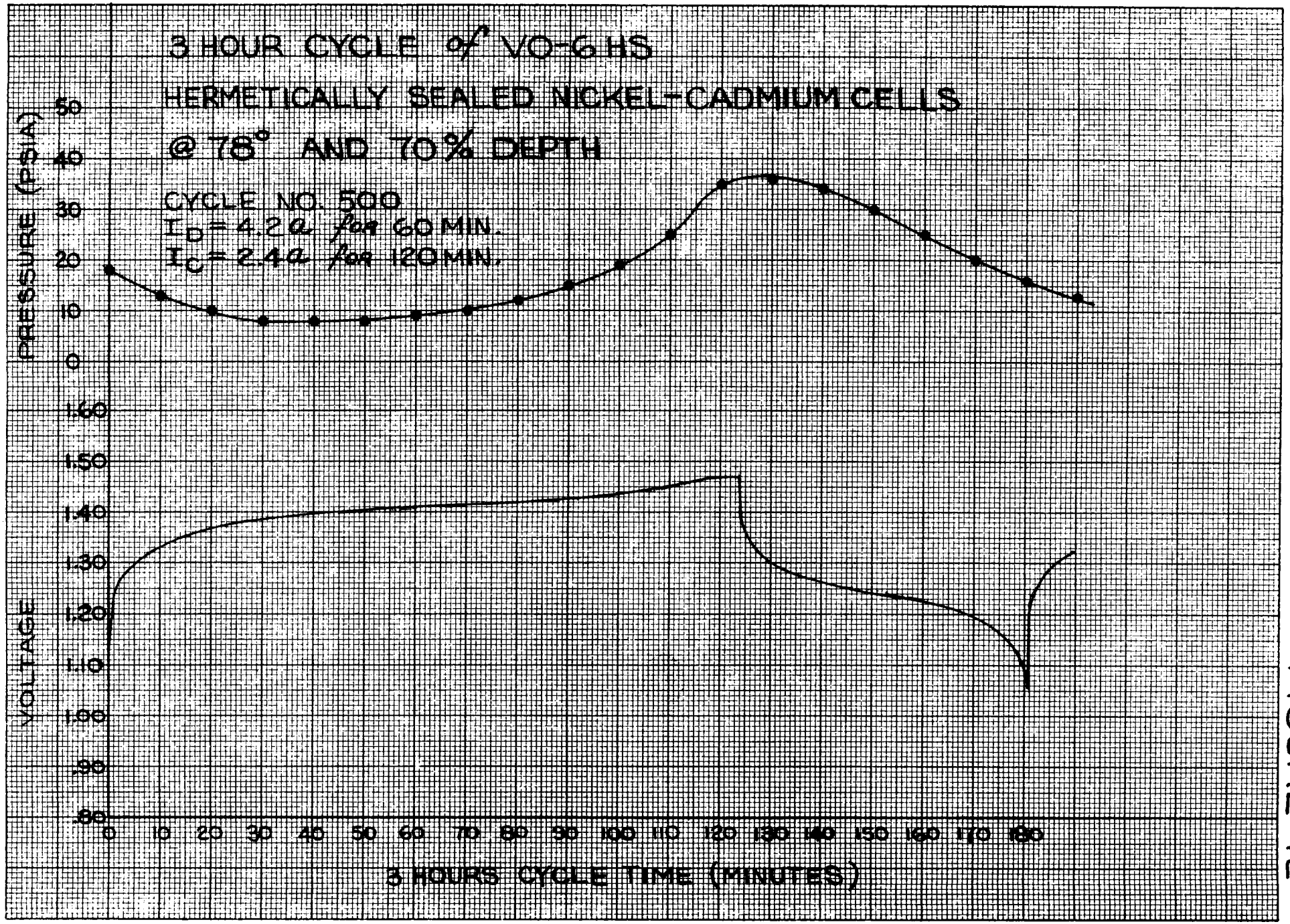

FIGURE 12

M1114
AB3099-F

FIGURE 13

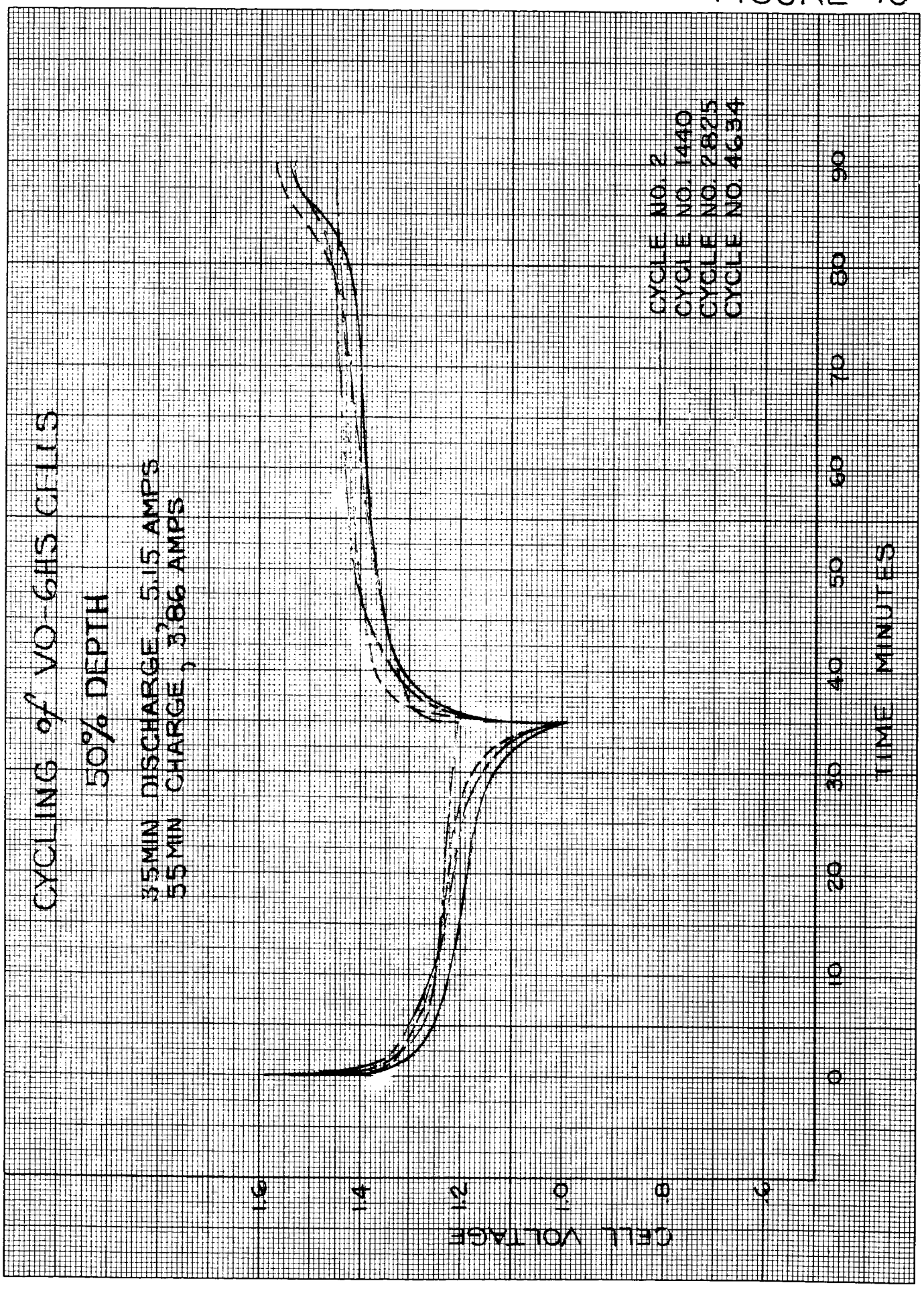

M1658
AB3000-F

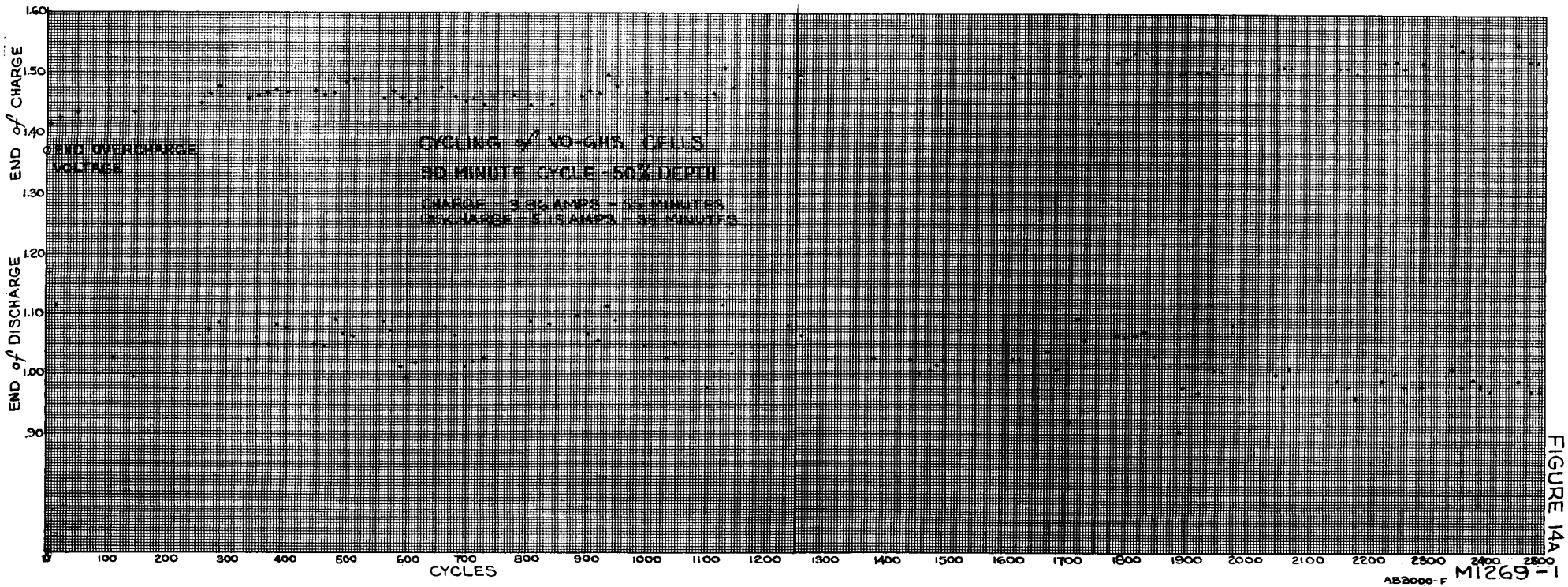

FIGURE 14A

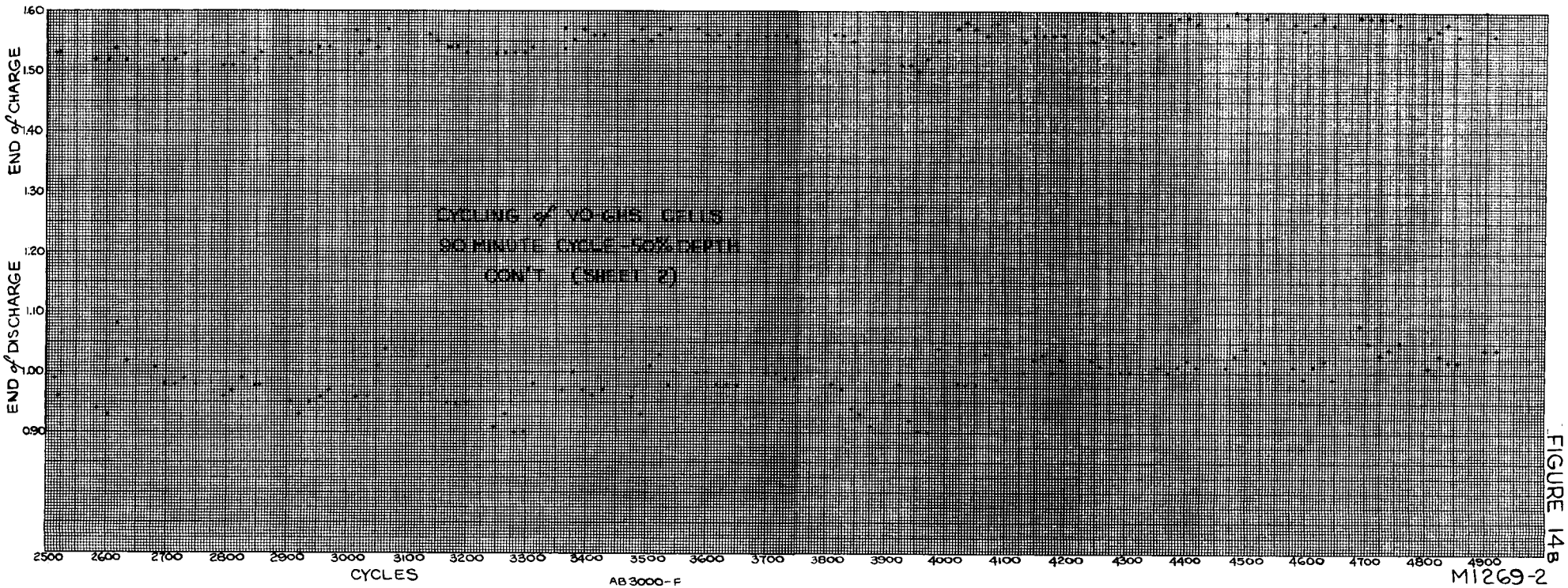

FIGURE 14B

FIGURE 15

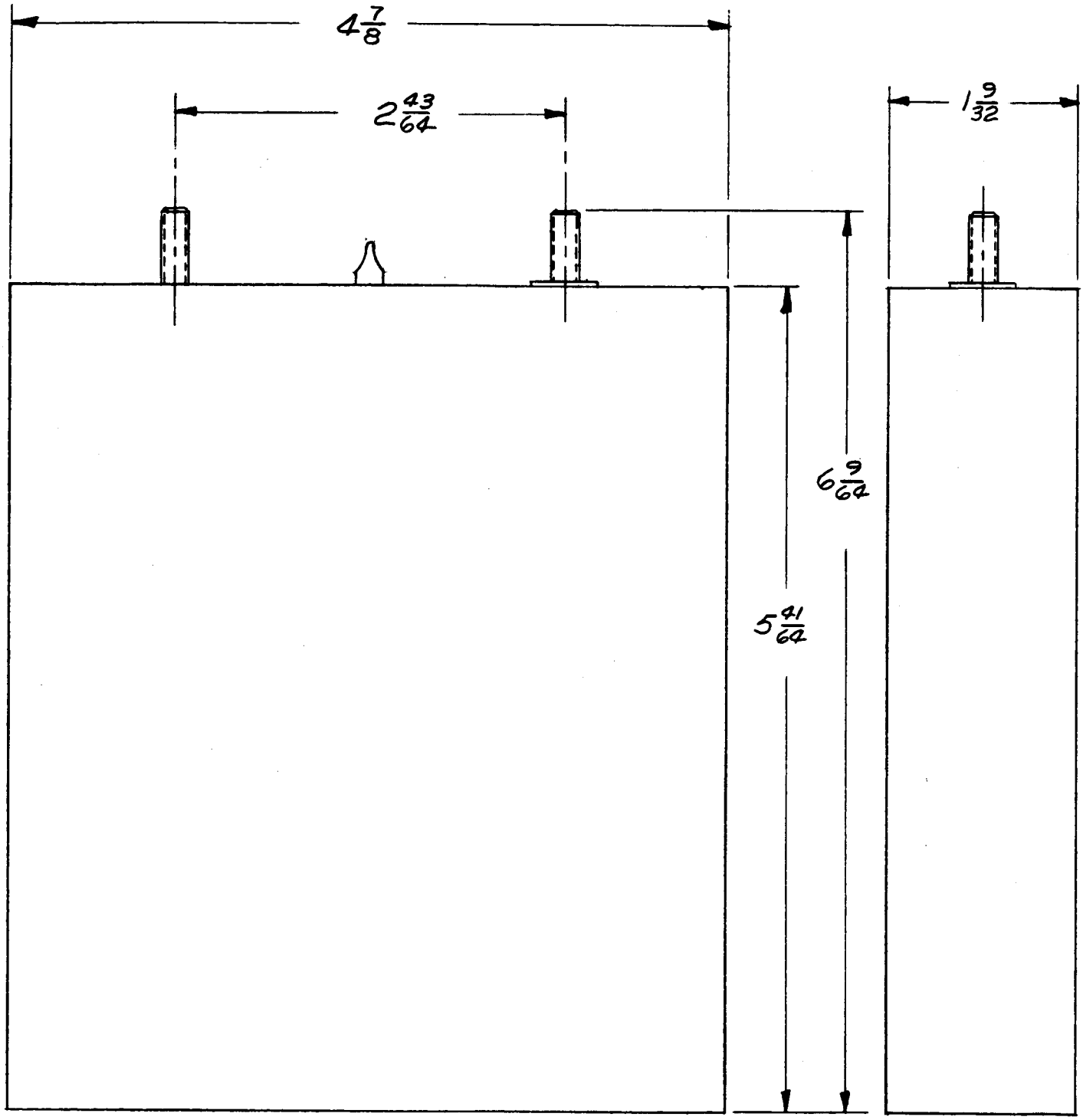

VO-50HS
HERMETICALLY SEALED
NICKEL CADMIUM CELL

M0950
AB3000-E

GULTON INDUSTRIES, INC.
Alkaline Battery Division
Metuchen, New Jersey

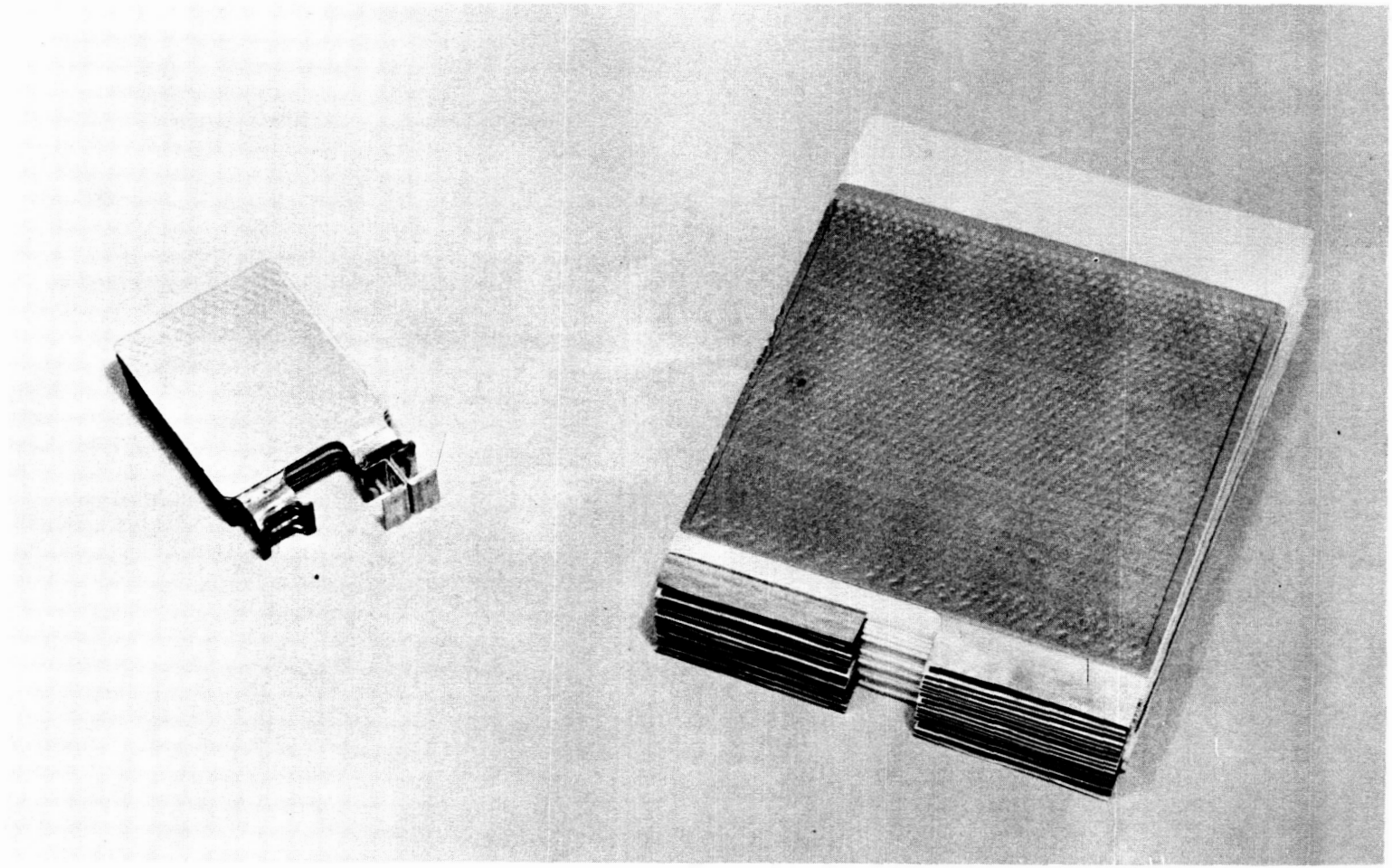

Figure 16

50 AH SEALED NICKEL-CADMIUM ELECTRODE ASSEMBLY
(6 AH ASSEMBLY AT LEFT FOR COMPARISON)

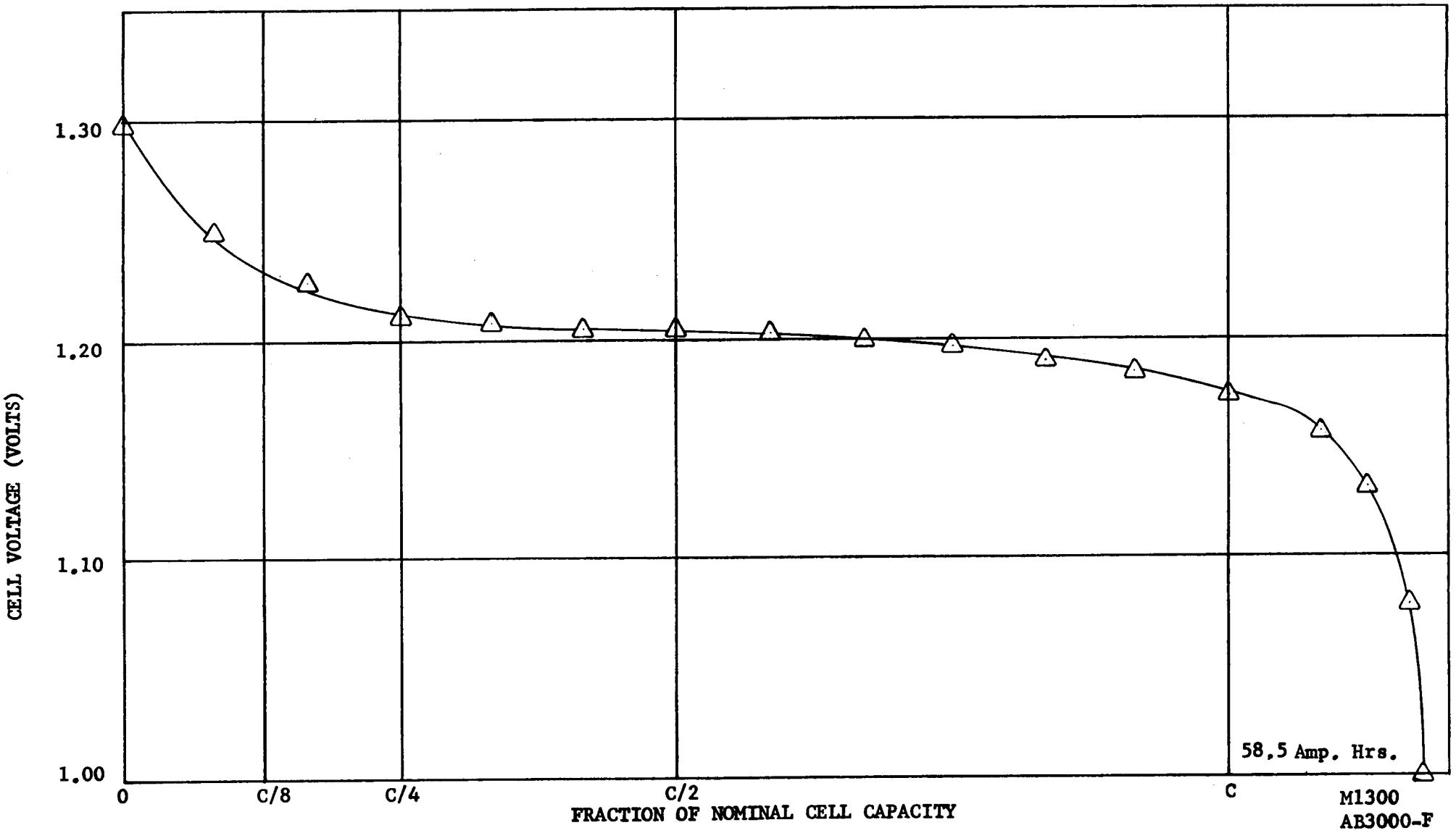

Figure 17 VO-50 HS Hermetically Sealed Nickel-Cadmium Cell Discharge Characteristic at 77°F

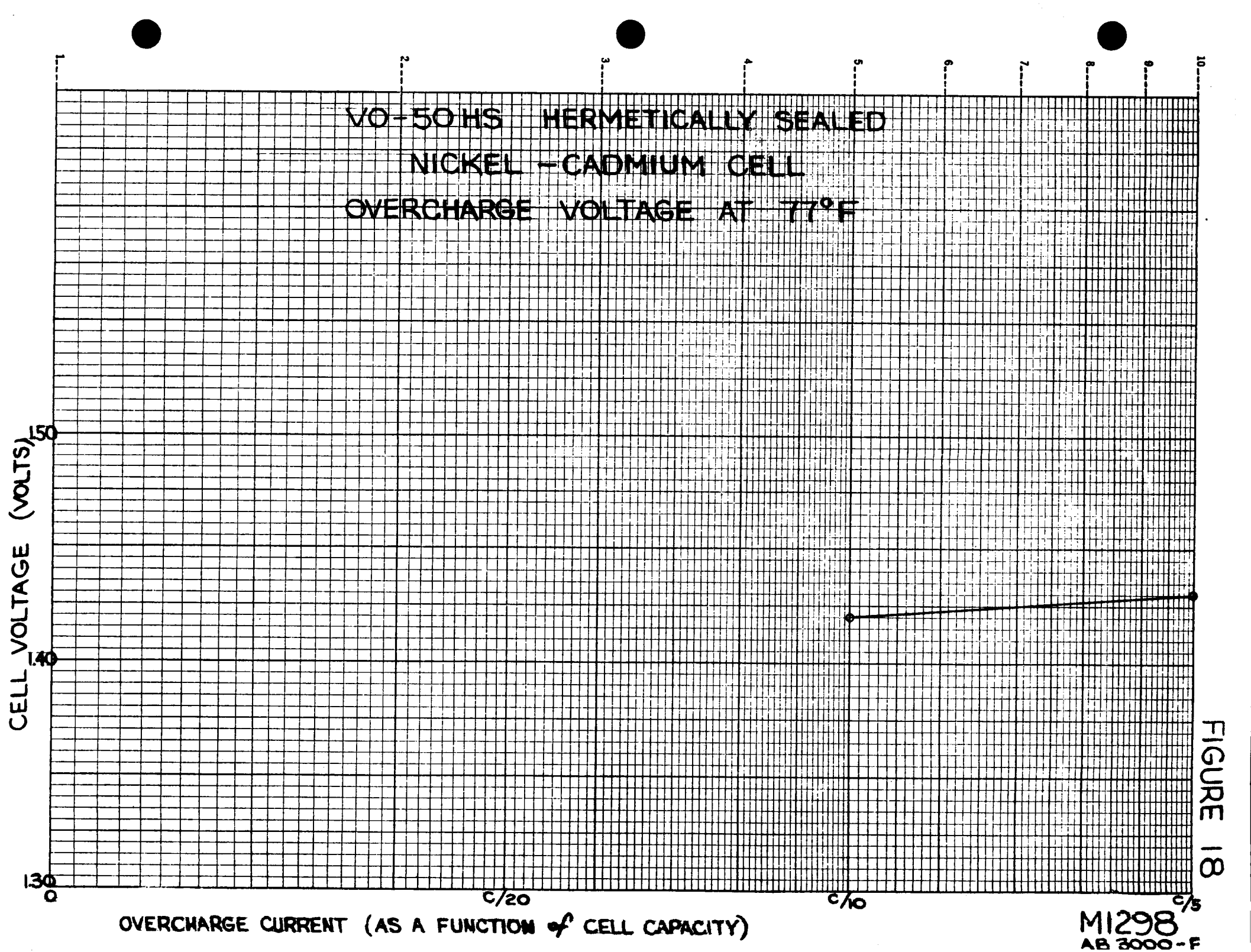

FIGURE 18

M1298
AB 3000-F

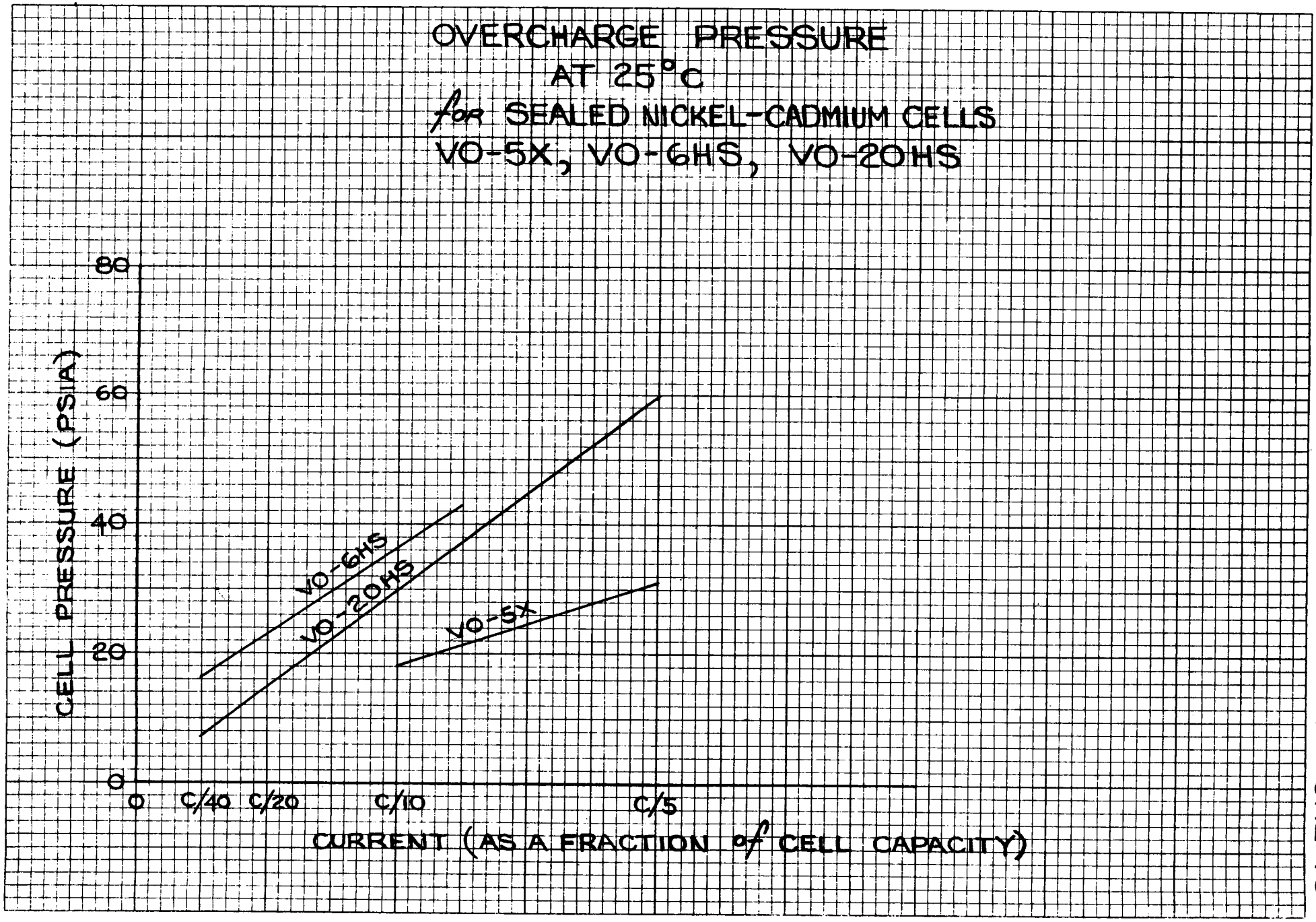

FIGURE 19

M1111
AB3000-F

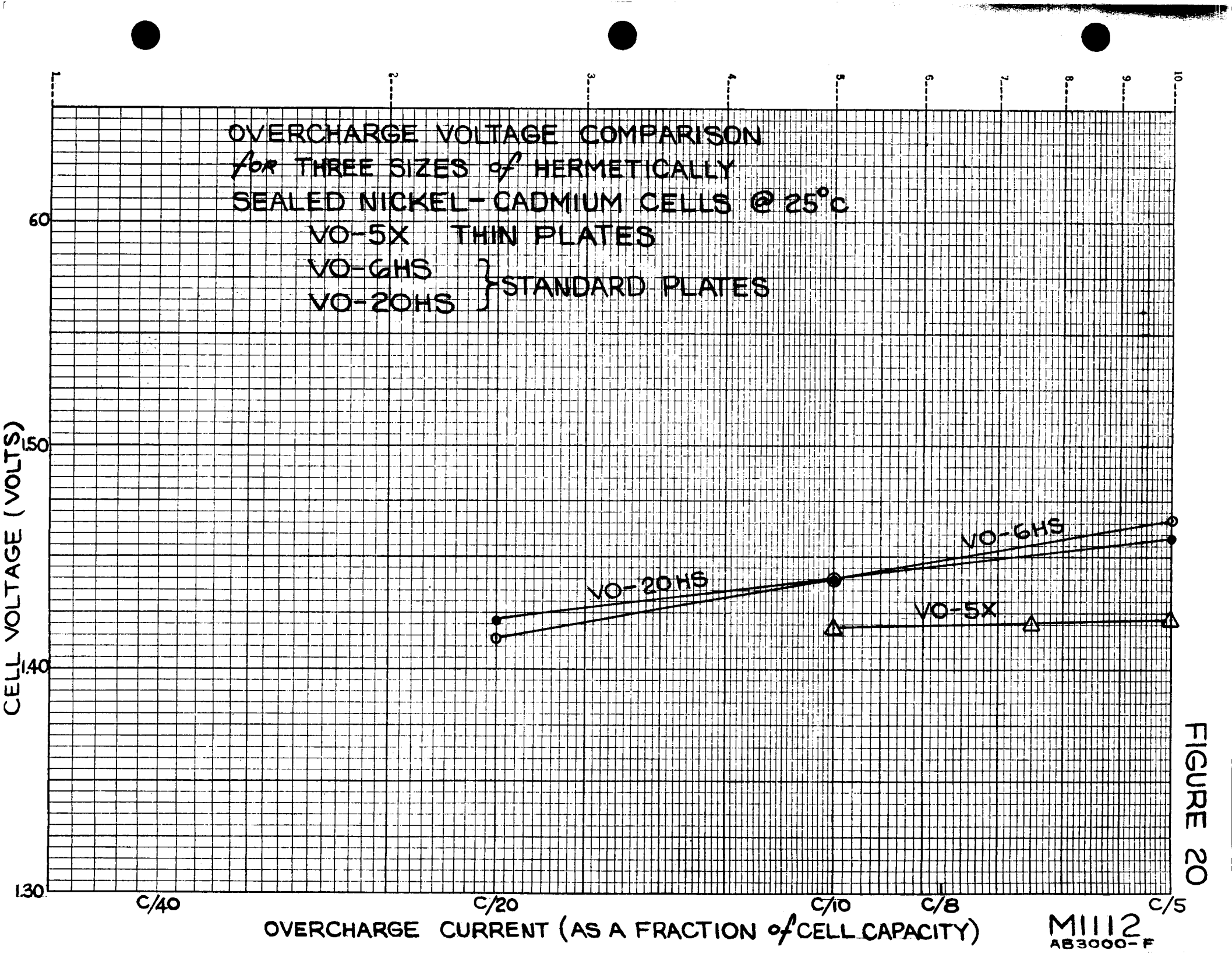
OVERCHARGE VOLTAGE COMPARISON
for THREE SIZES of HERMETICALLY
SEALED NICKEL-CADMIUM CELLS @ 25°C
VO-5X THIN PLATES
VO-6HS } STANDARD PLATES
VO-20HS }
CELL VOLTAGE (VOLTS)
1.60
1.50
1.40
1.30
VO-6HS
VO-20HS
VO-5X
C/40
C/20
C/10
C/8
C/5
OVERCHARGE CURRENT (AS A FRACTION of CELL CAPACITY)
M1112
AB3000-F

FIGURE 20

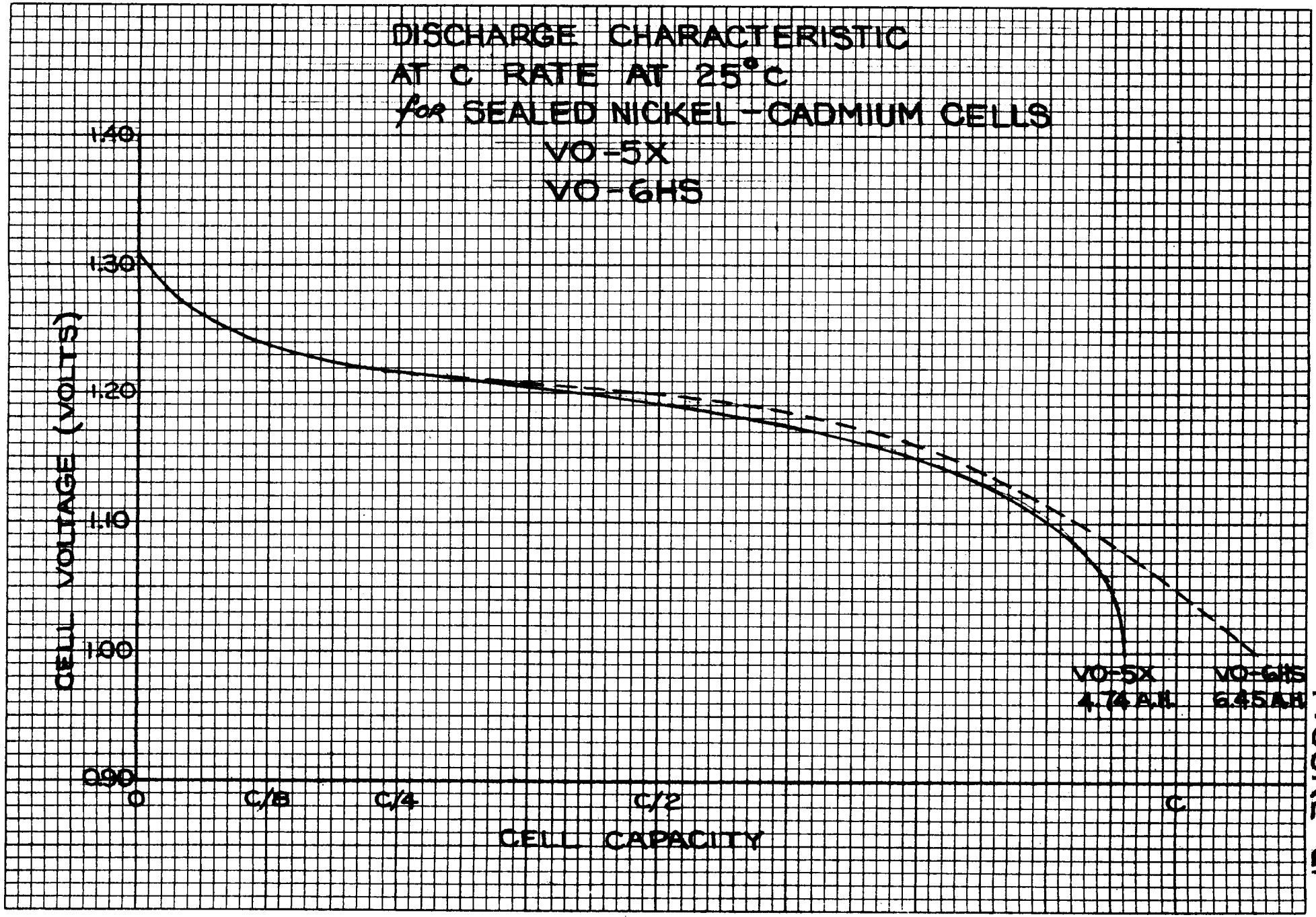

FIGURE 21

M1113
AB3000-F

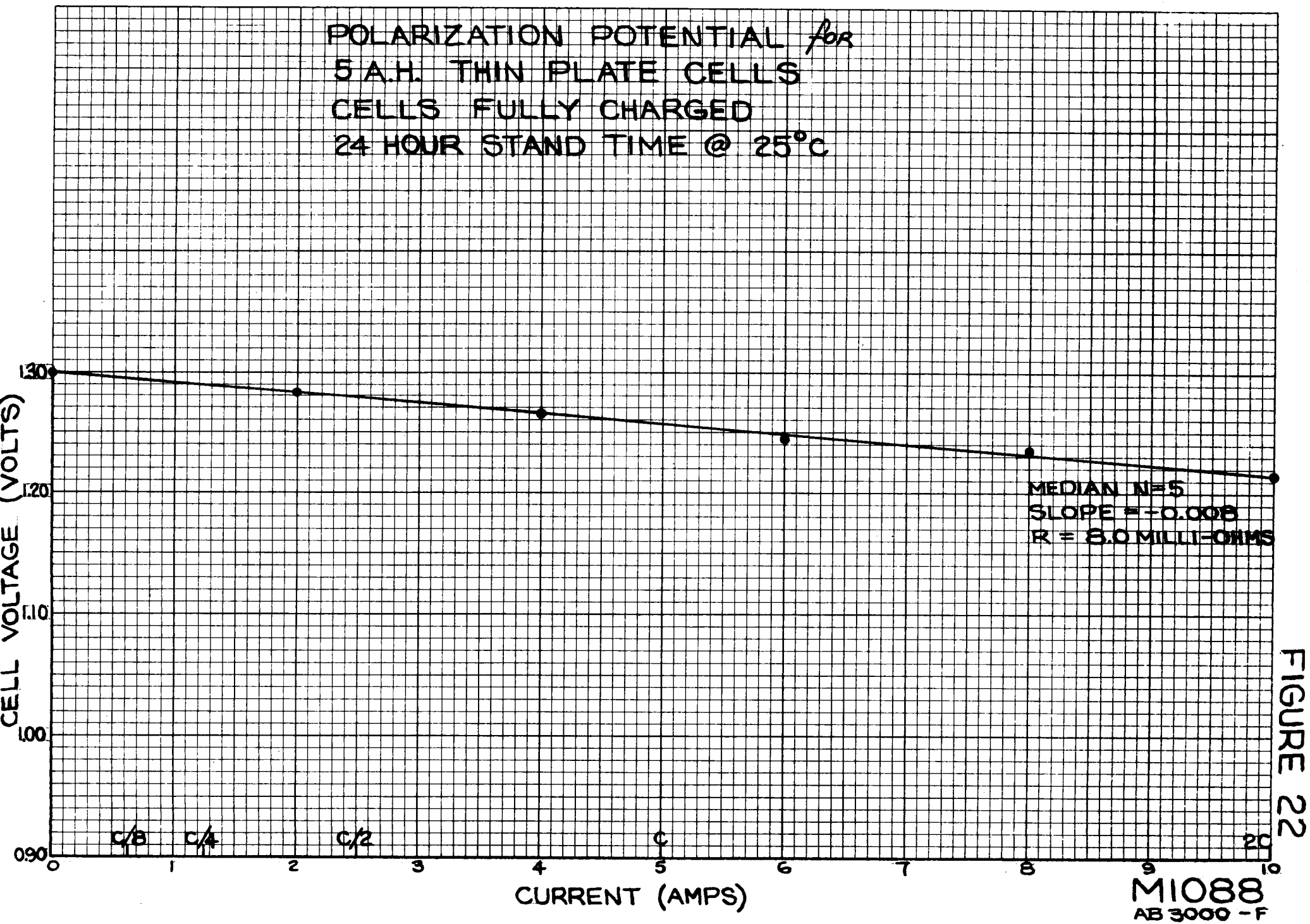

FIGURE 22

M1088
AB 3000 - F

FIGURE 23

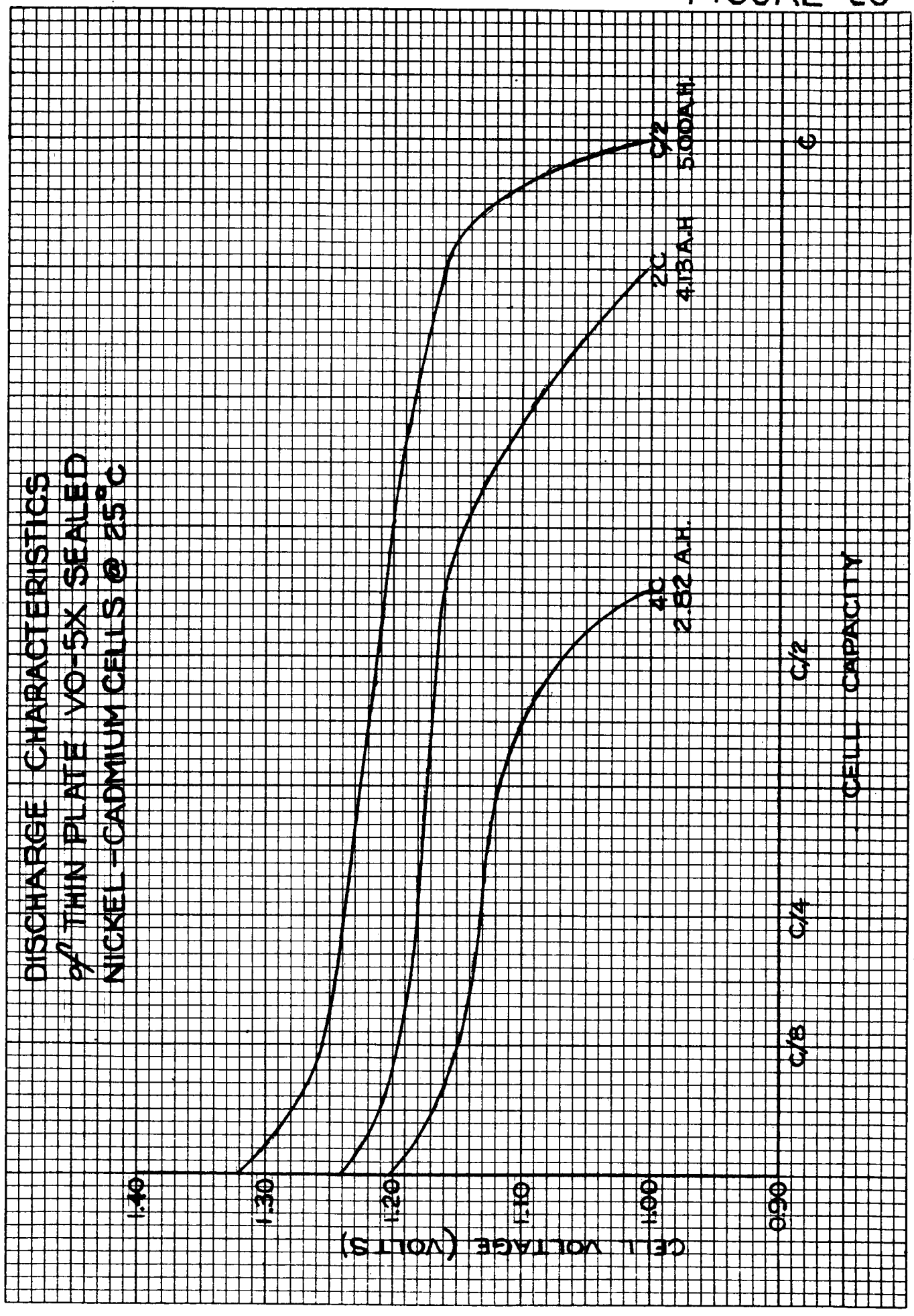

M1099
AB3000-F

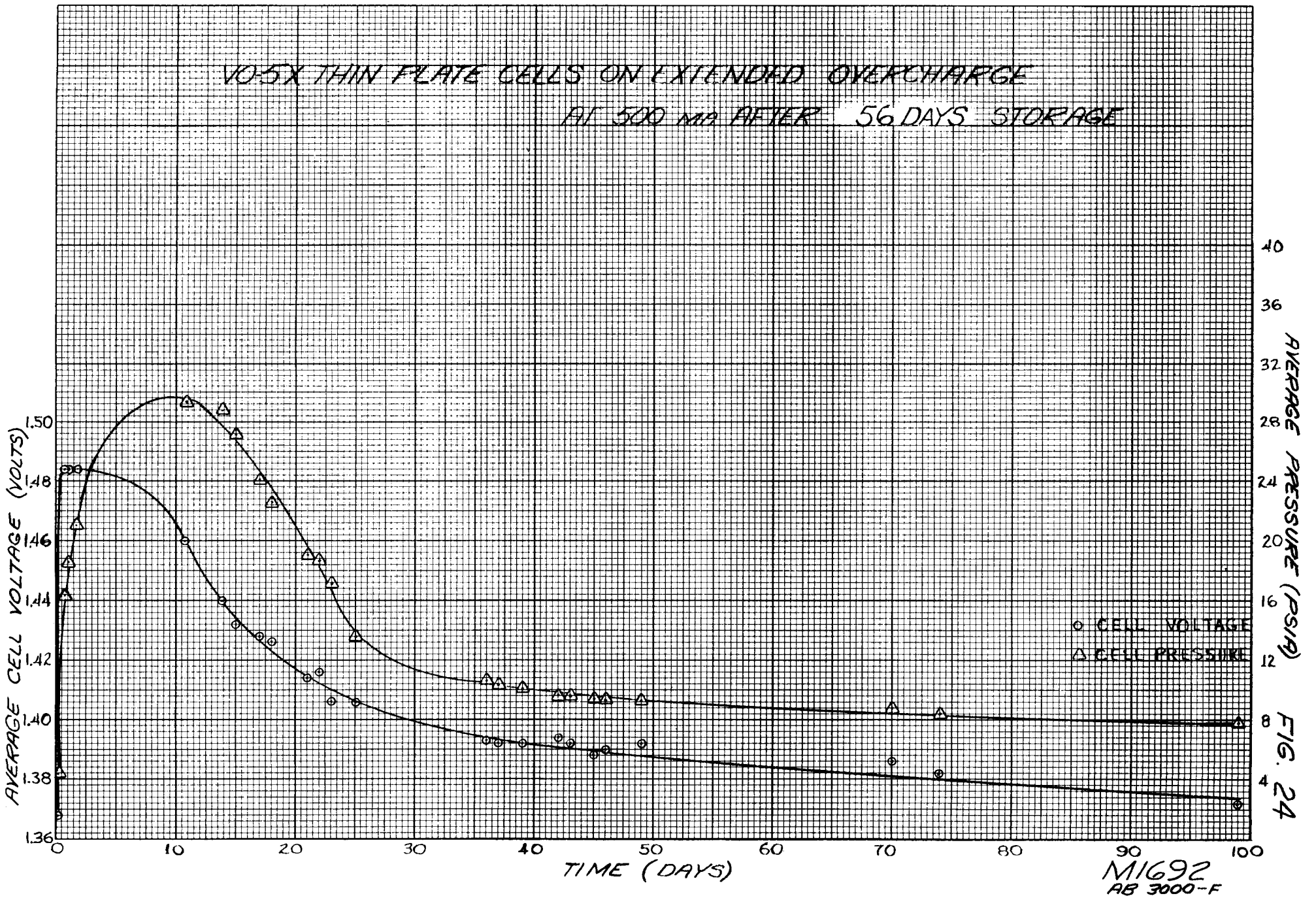
VO-5X THIN PLATE CELLS ON EXTENDED OVERCHARGE
AT 500 MA AFTER 56 DAYS STORAGE
AVERAGE CELL VOLTAGE (VOLTS)
1.50
1.48
1.46
1.44
1.42
1.40
1.38
1.36
0
10
20
30
40
50
60
70
80
90
100
TIME (DAYS)
AVERAGE PRESSURE (PSIA)
40
36
32
28
24
20
16
12
8
4
CELL VOLTAGE
CELL PRESSURE
M1692
AB 3000-F

FIG. 24

FIGURE 25

VO-6HS CELL

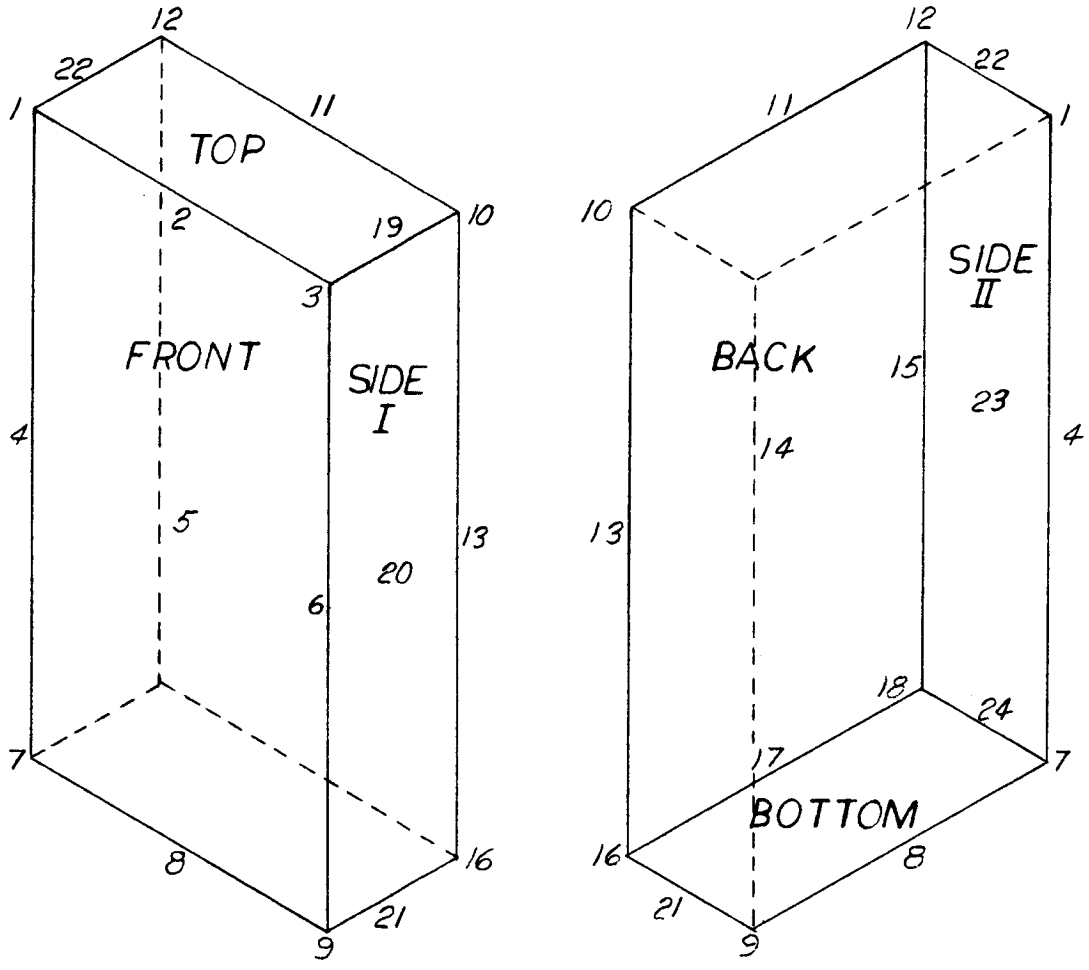

TEMPERATURE MEASUREMENT POINTS

M0685
AB 3000-F

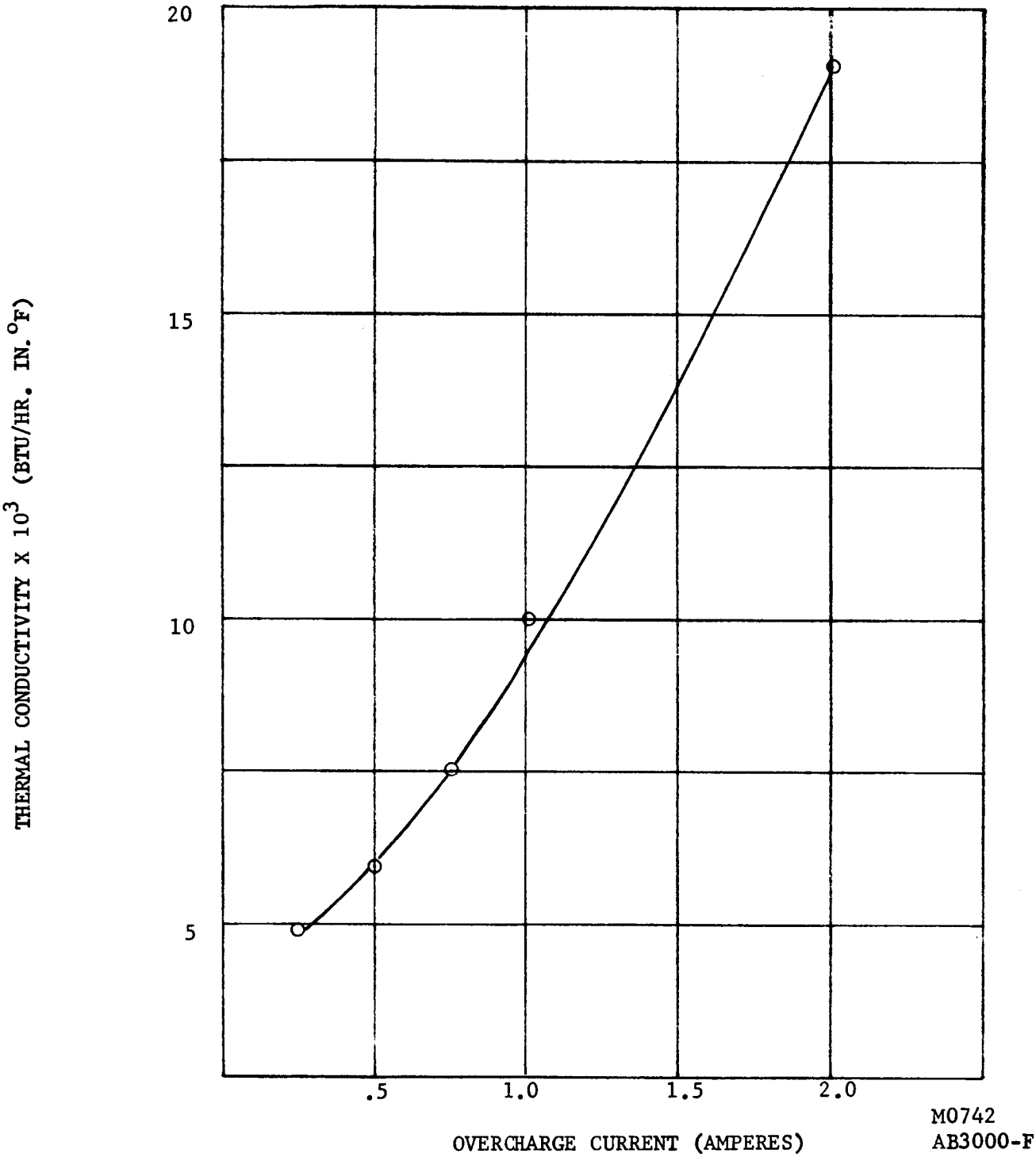

Figure 26 Thermal Conductivity Vs. Overcharge Current for a VO-6-HS Cell at an Ambient Temperature of 80°F

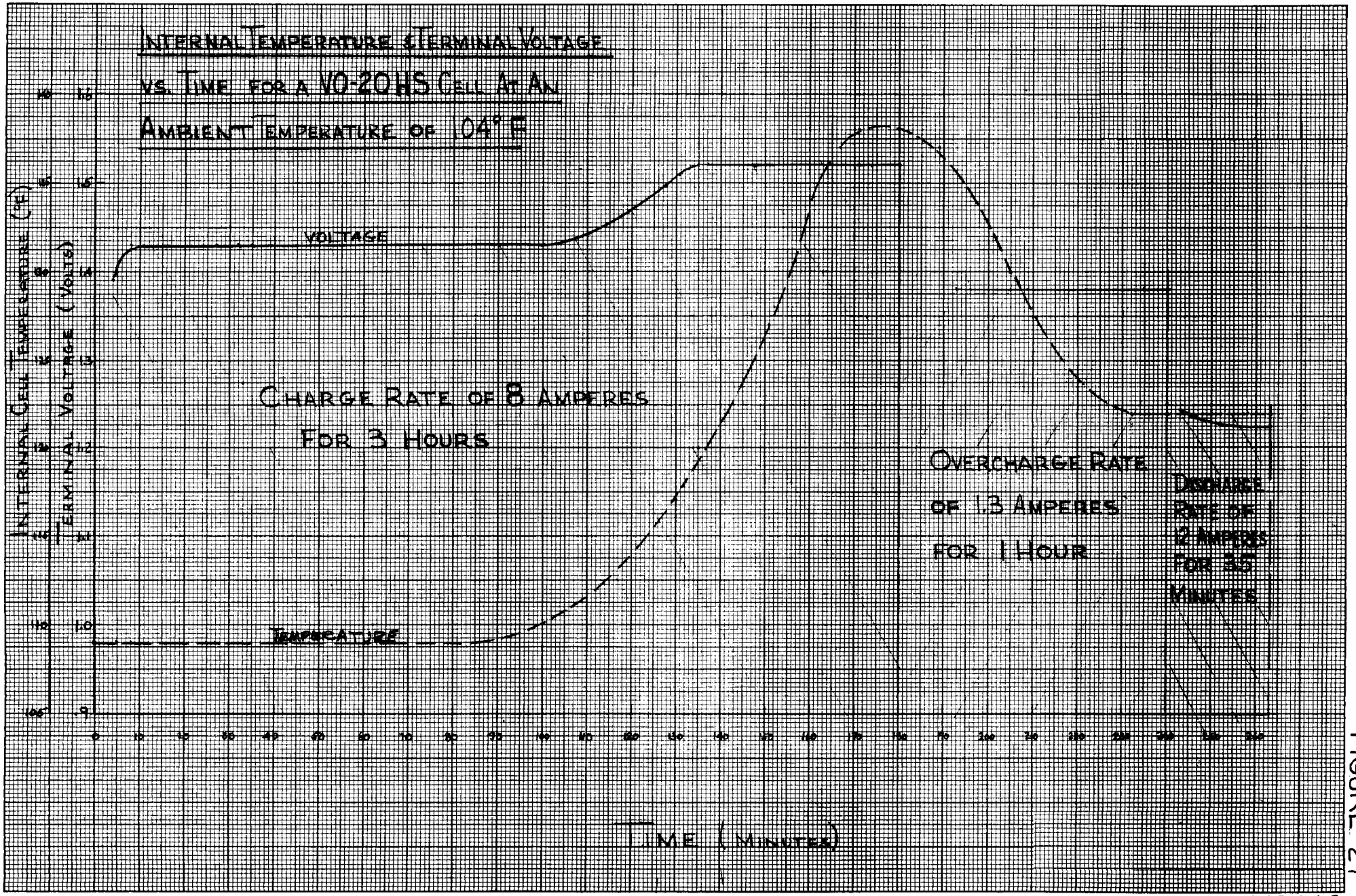

FIGURE 27

M0446
AB 3000 - F

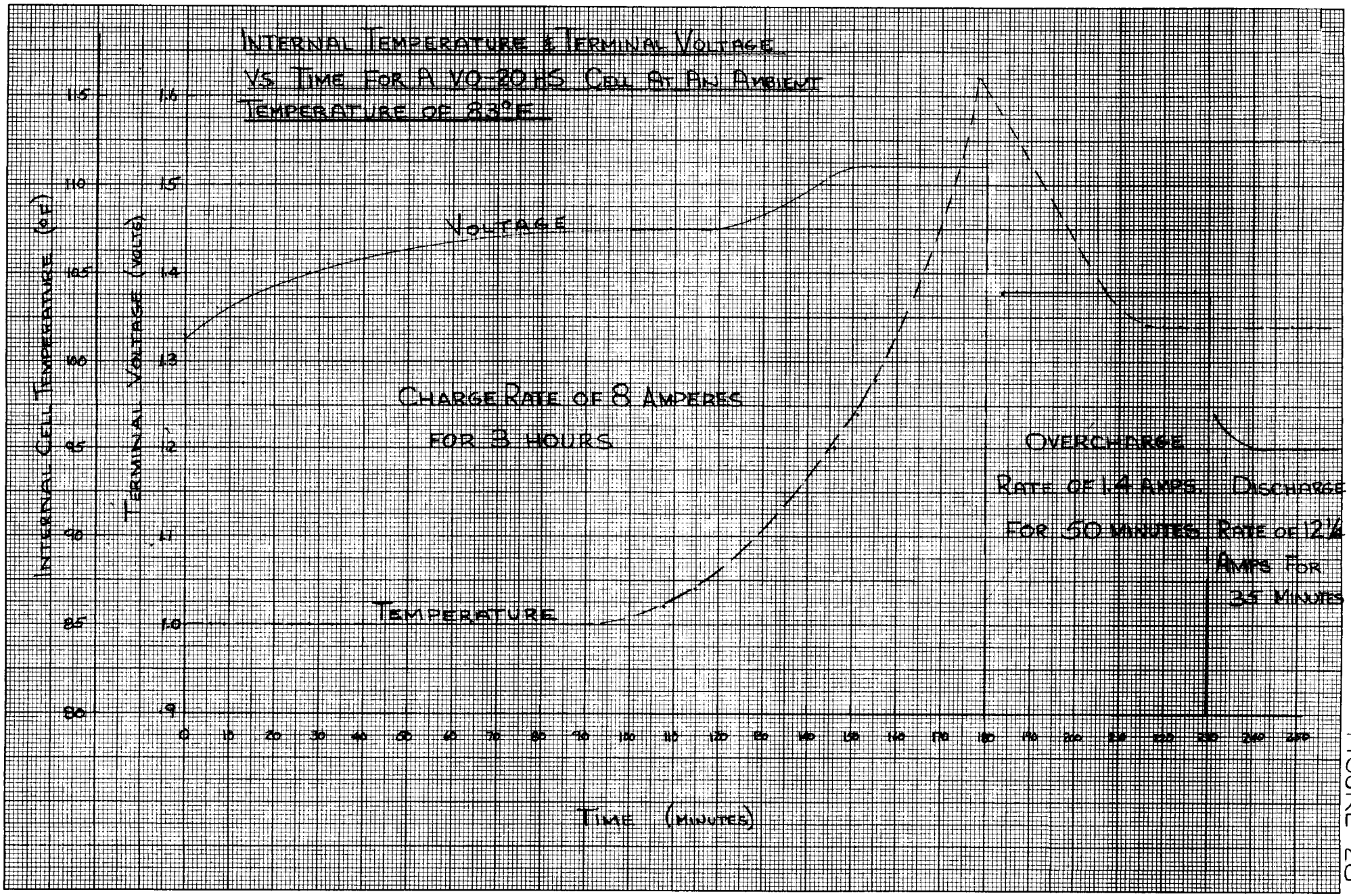

FIGURE 28

M0447
AB 3000-F

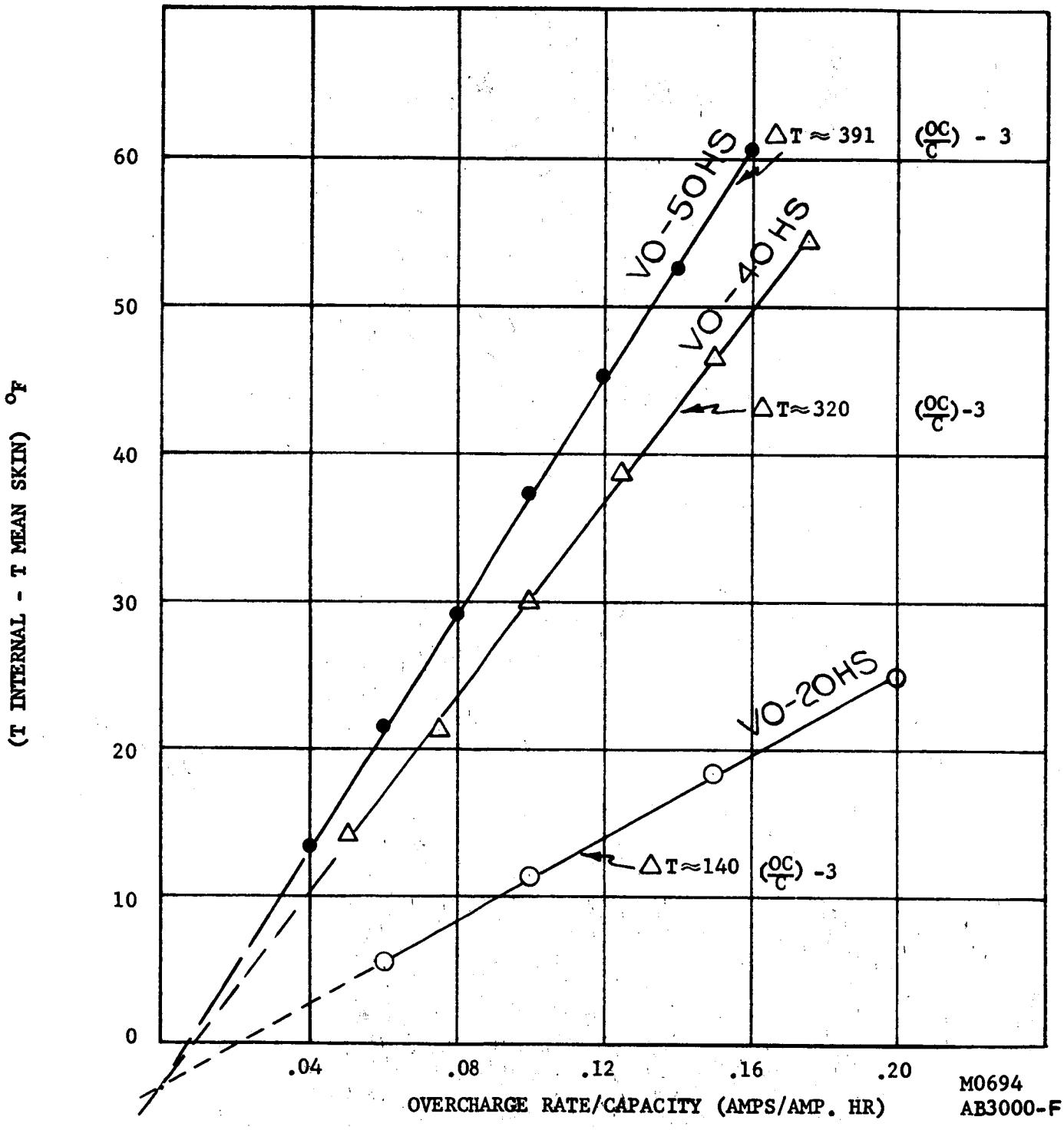

Figure 29 ΔT Versus OC Rate for a VO-20-HS, VO-40-HS, and VO-50-HS, Cell at an Ambient Temperature of 77°F

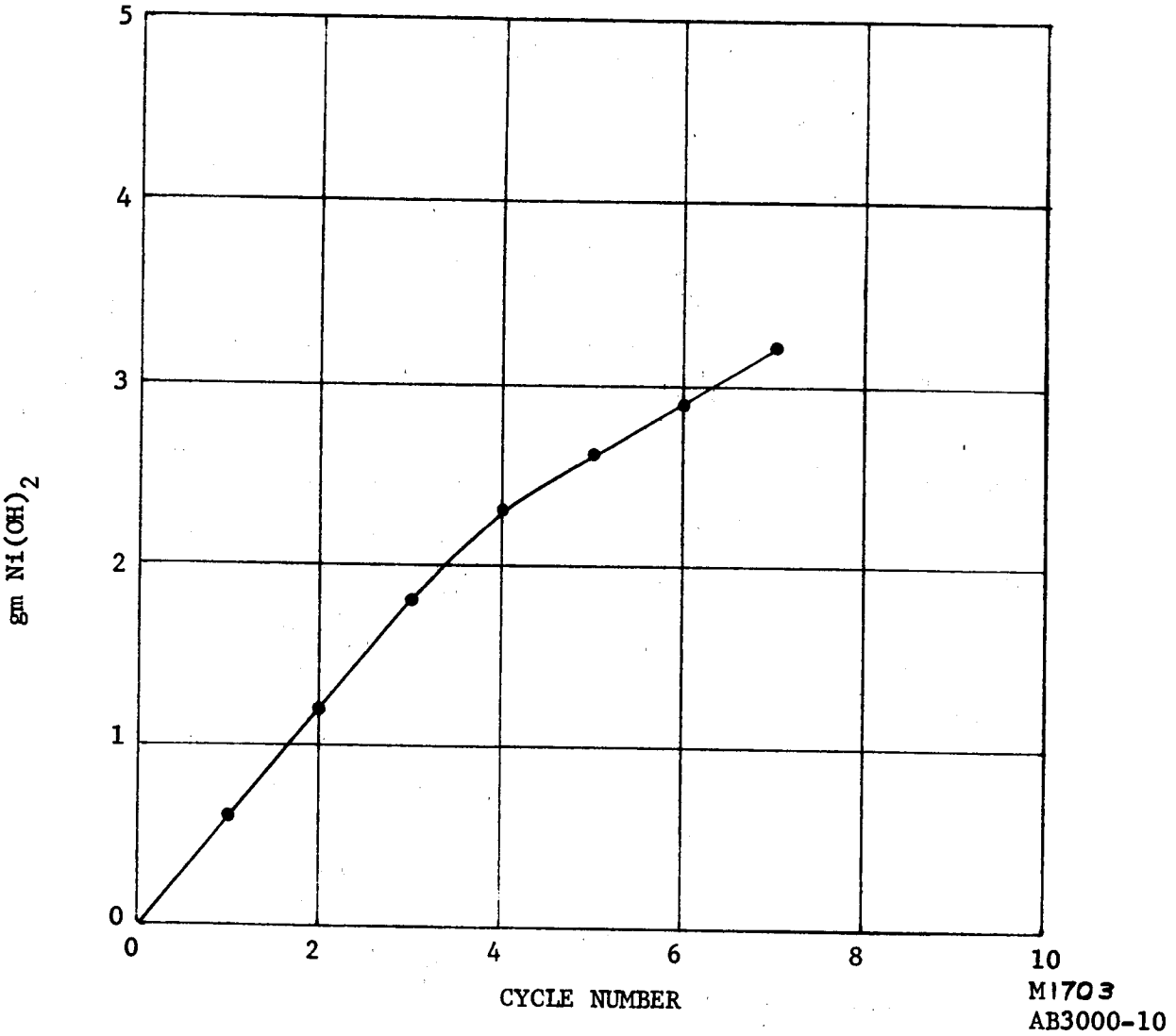

Figure 30 Weight Gains of Positive Plates

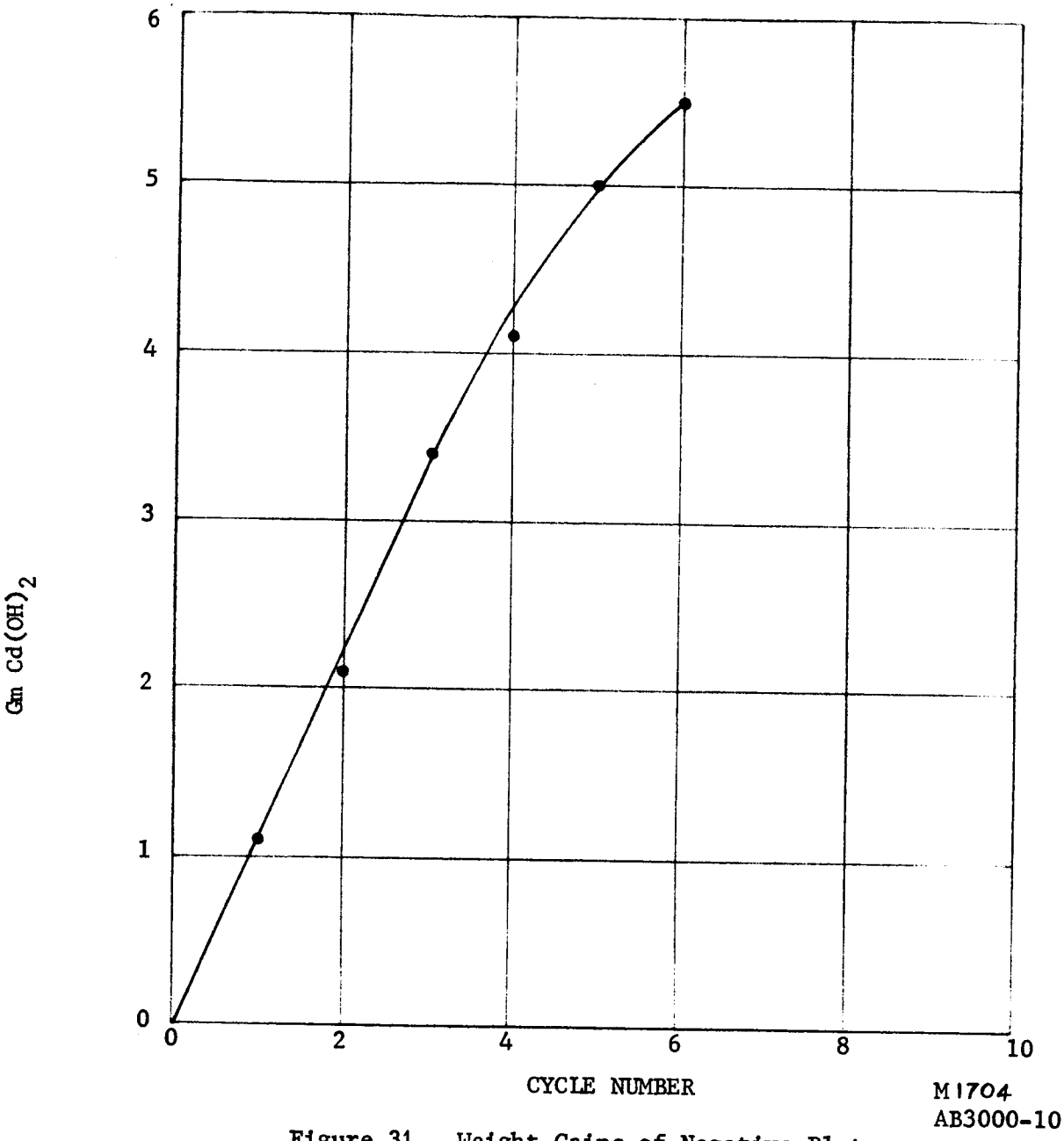

Figure 31 Weight Gains of Negative Plates

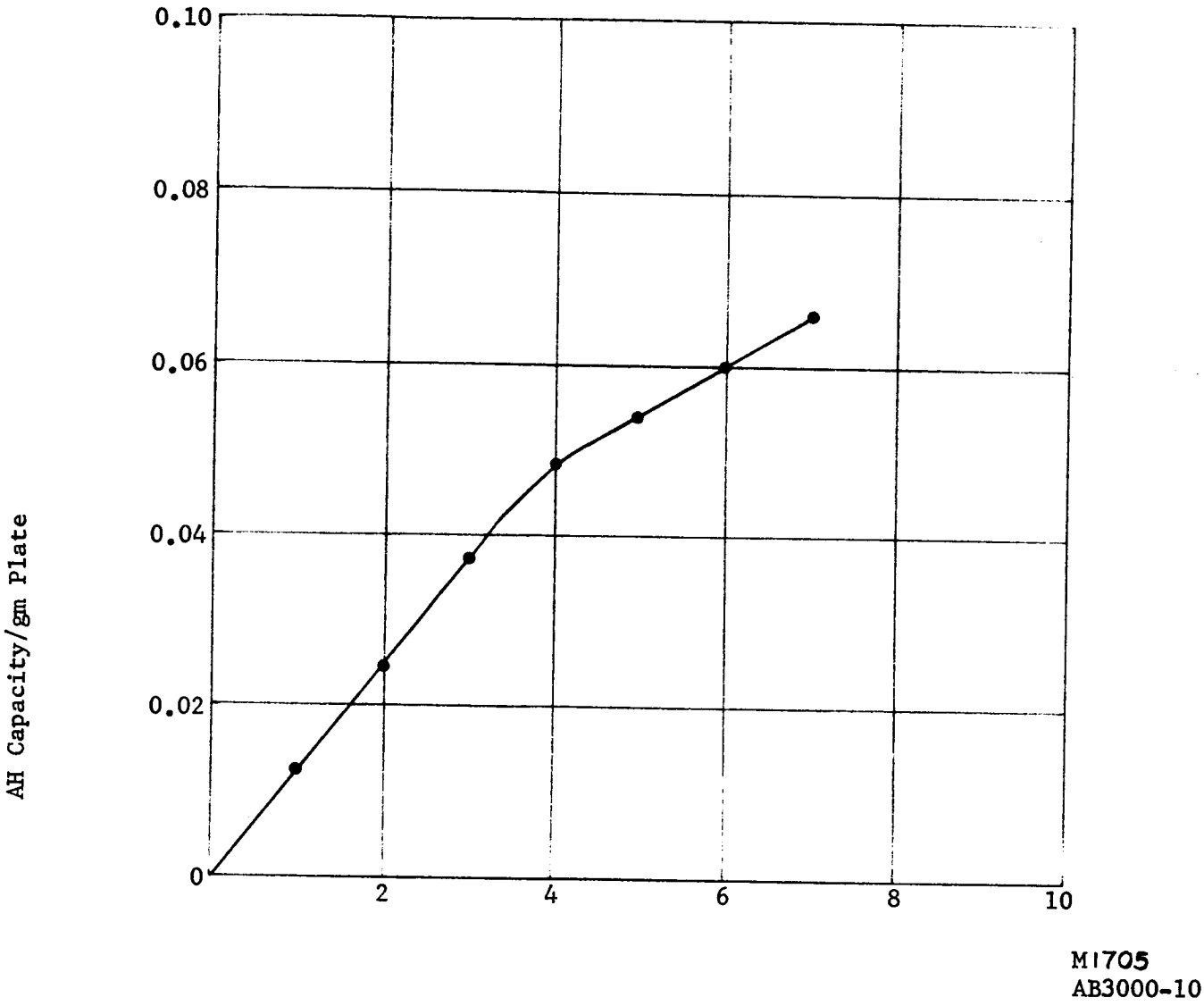

Figure 32 Ampere-Hour Capacity Gains as a Function of Impregnation Cycles

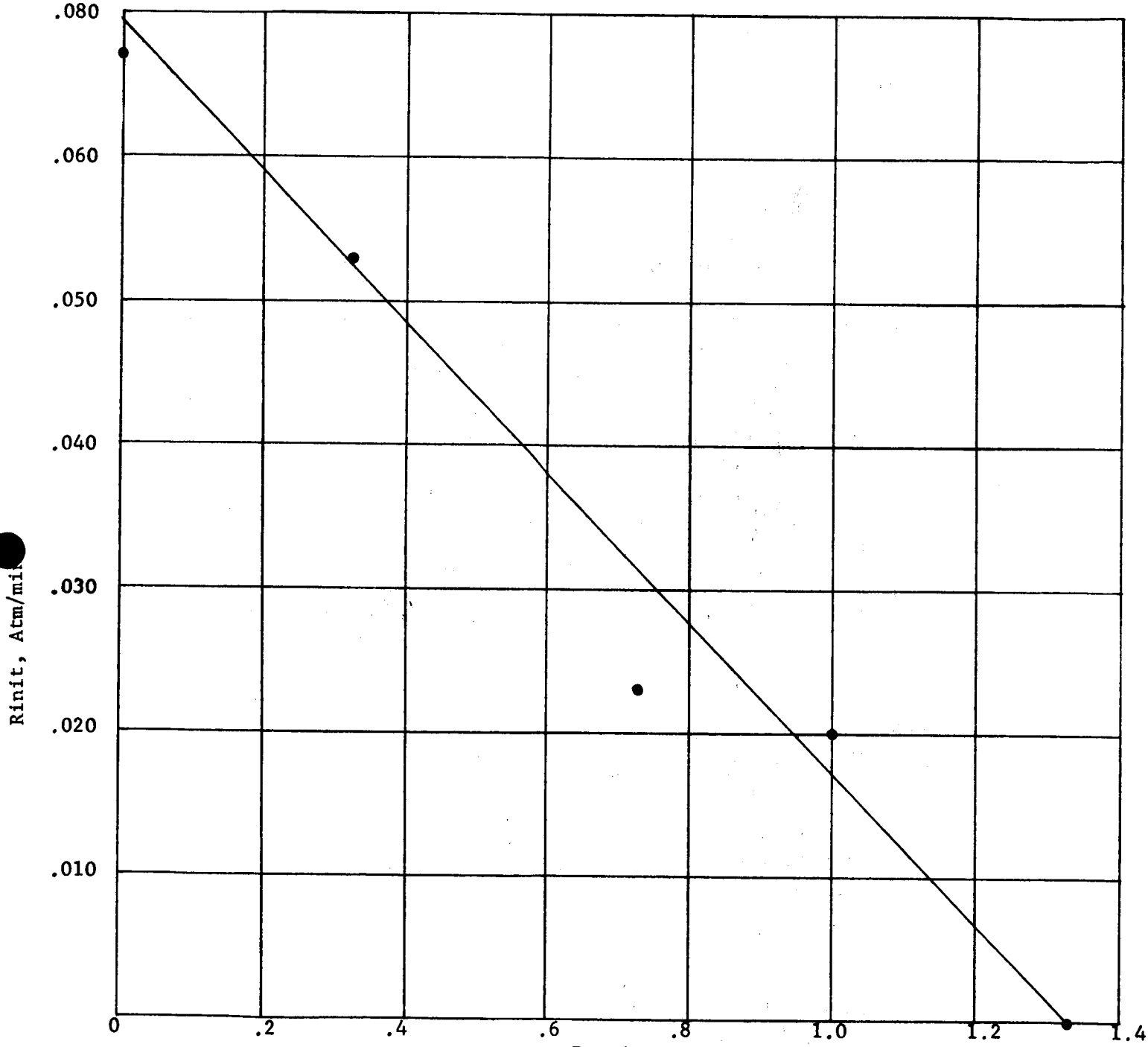

Figure 33 Initial Pressure Rise Vs. Initial Pressure in Non-flooded Sealed Nickel-Cadmium Cell at 77°F

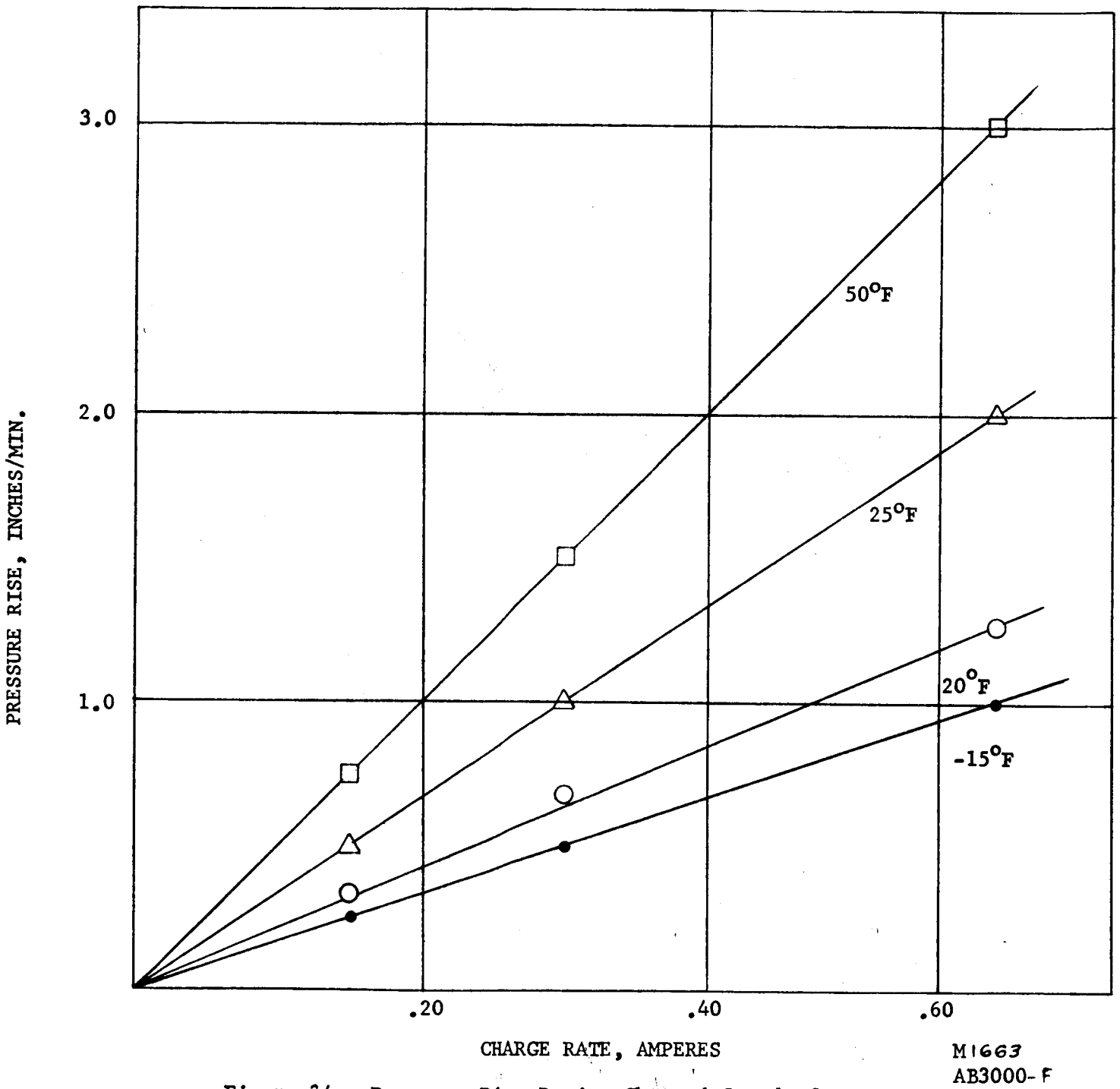

Figure 34 Pressure Rise During Charged Stand of a Non-flooded Sealed Nickel-Cadmium Cell

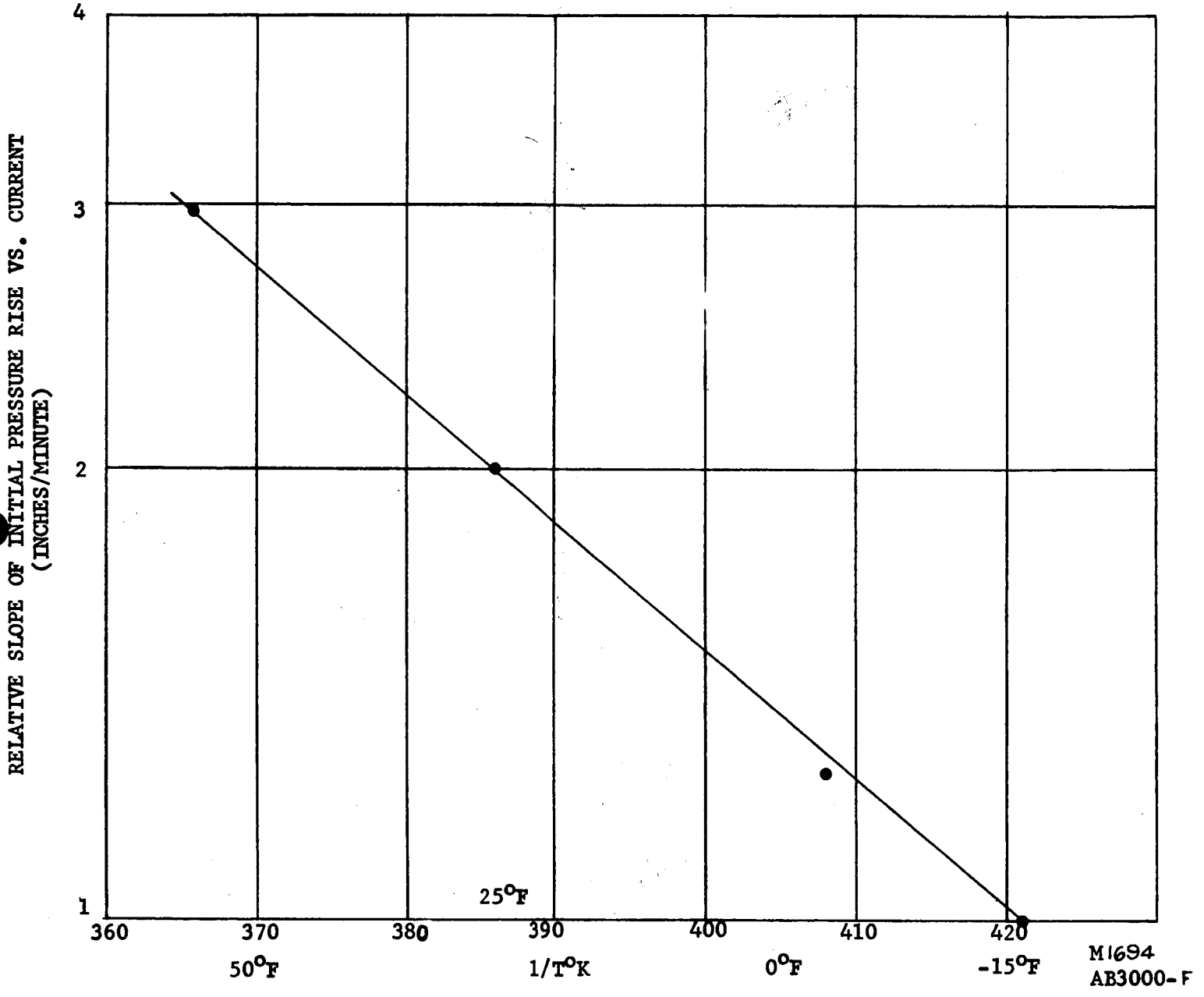

Figure 35 Slope of Decay Rate Vs. Current as a Function of Temperature in a Non-flooded Sealed Nickel-Cadmium Cell

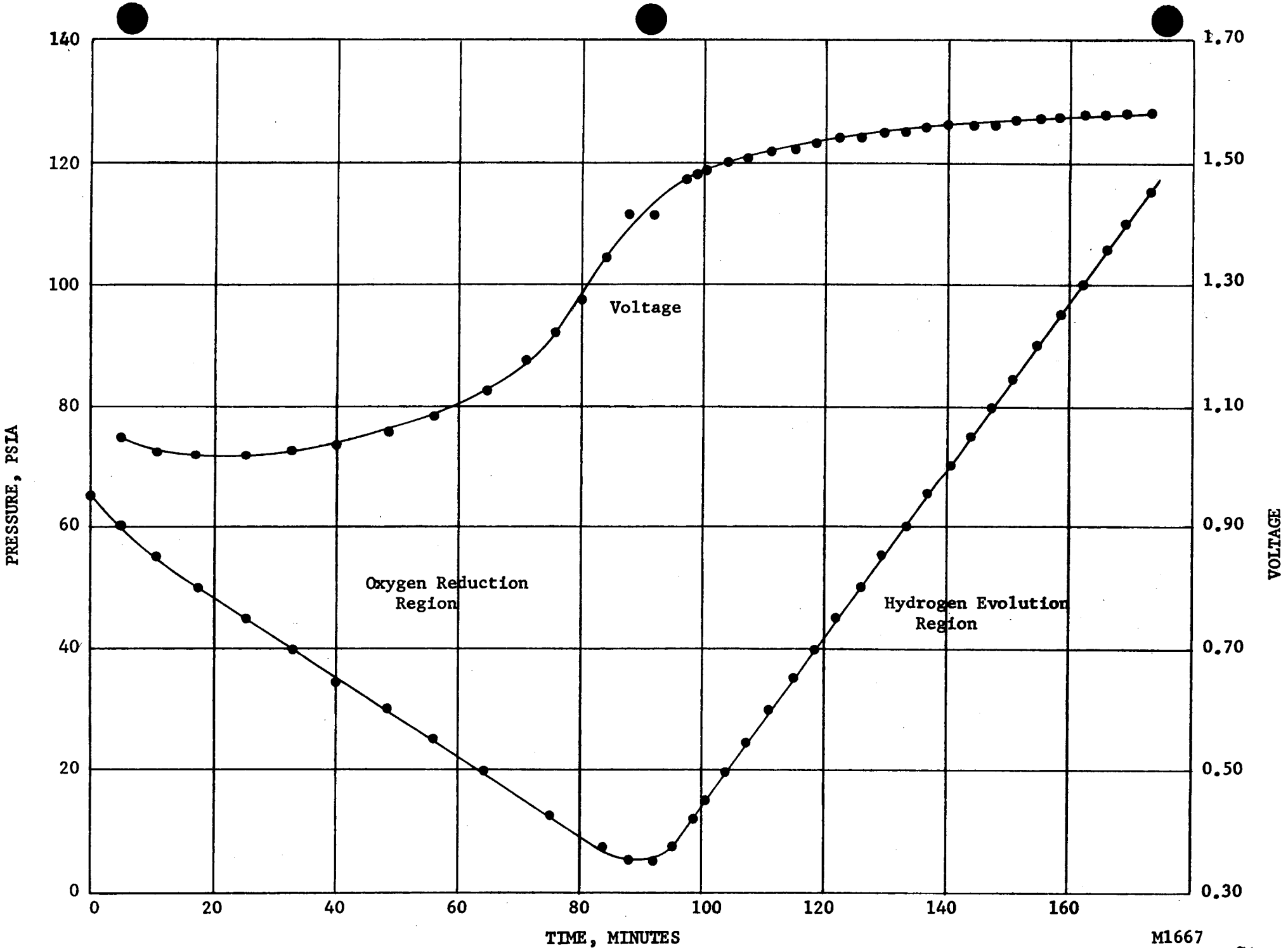

M1667
AB3000-F

Figure 36 Pressure and Voltage Changes in a Sealed Nickel-Blank Cell During Charge at 0.6A After Pressurization with 50 psig Oxygen

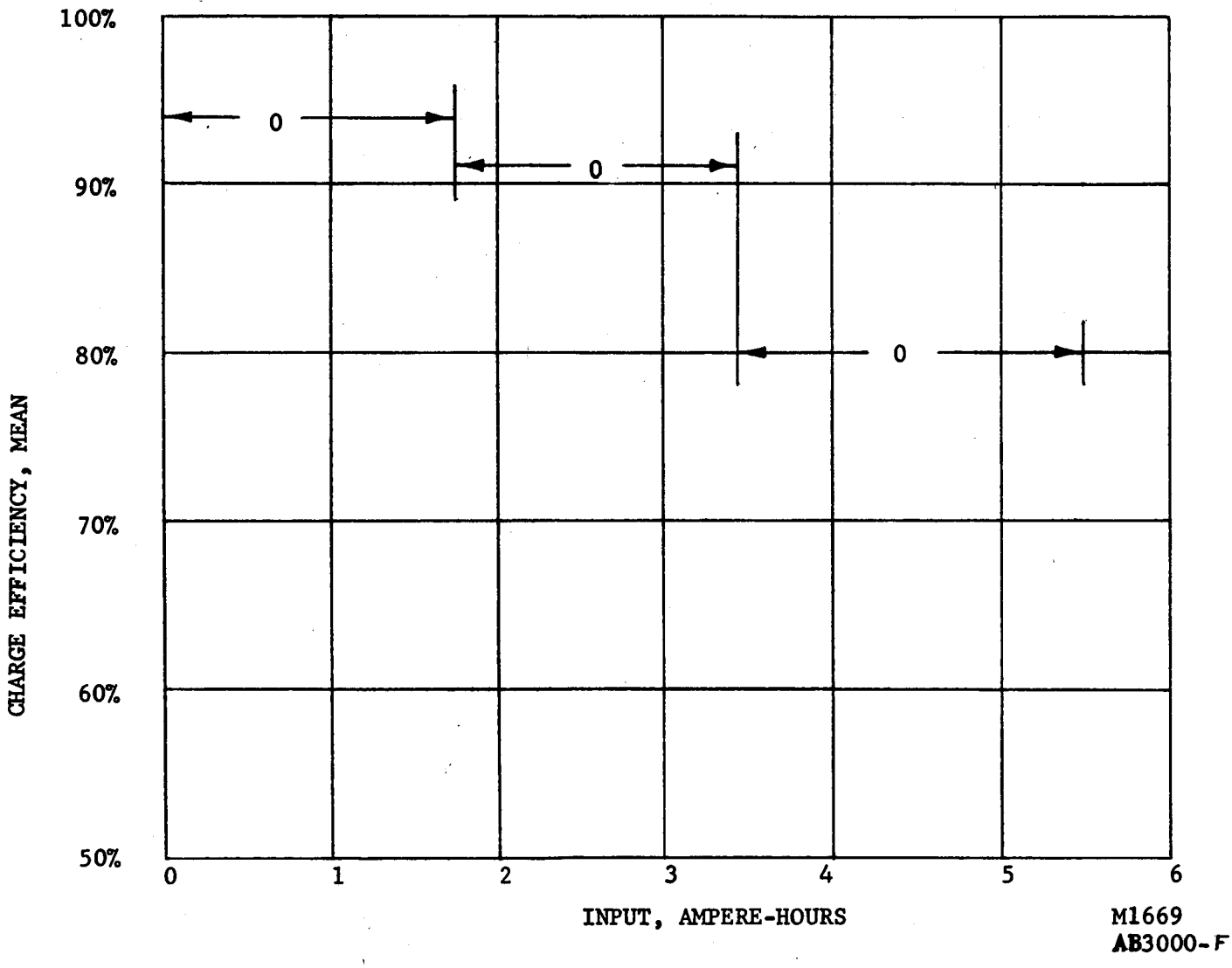

Figure 38 Mean Charge Efficiency of VO-6 HS Cells as a Function of Charge Input

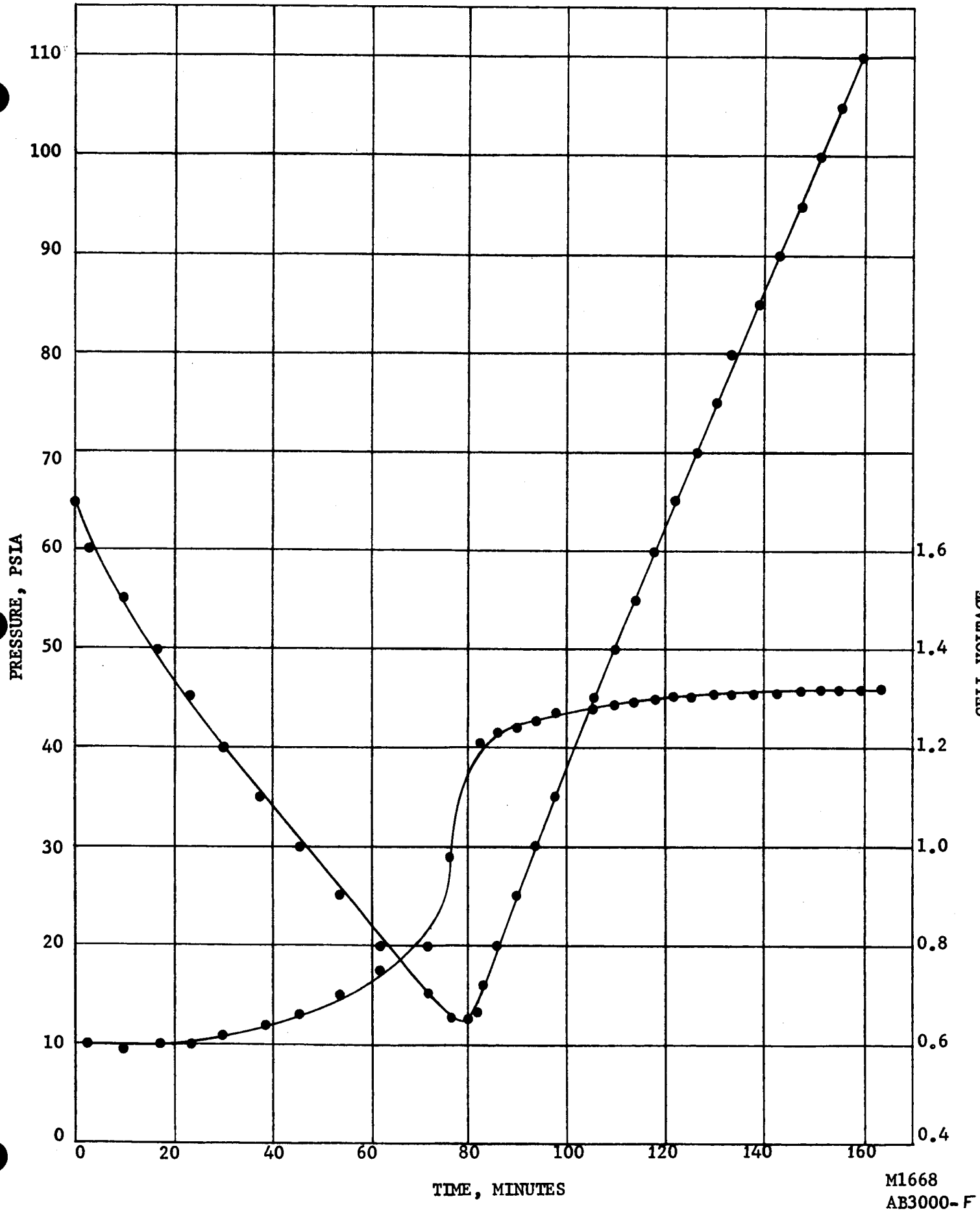

Figure 37 Pressure and Voltage Changes in a Sealed Silver-Blank Cell During Charge at 0.6A After Pressurization with 50 psig Oxygen

FIG. 39

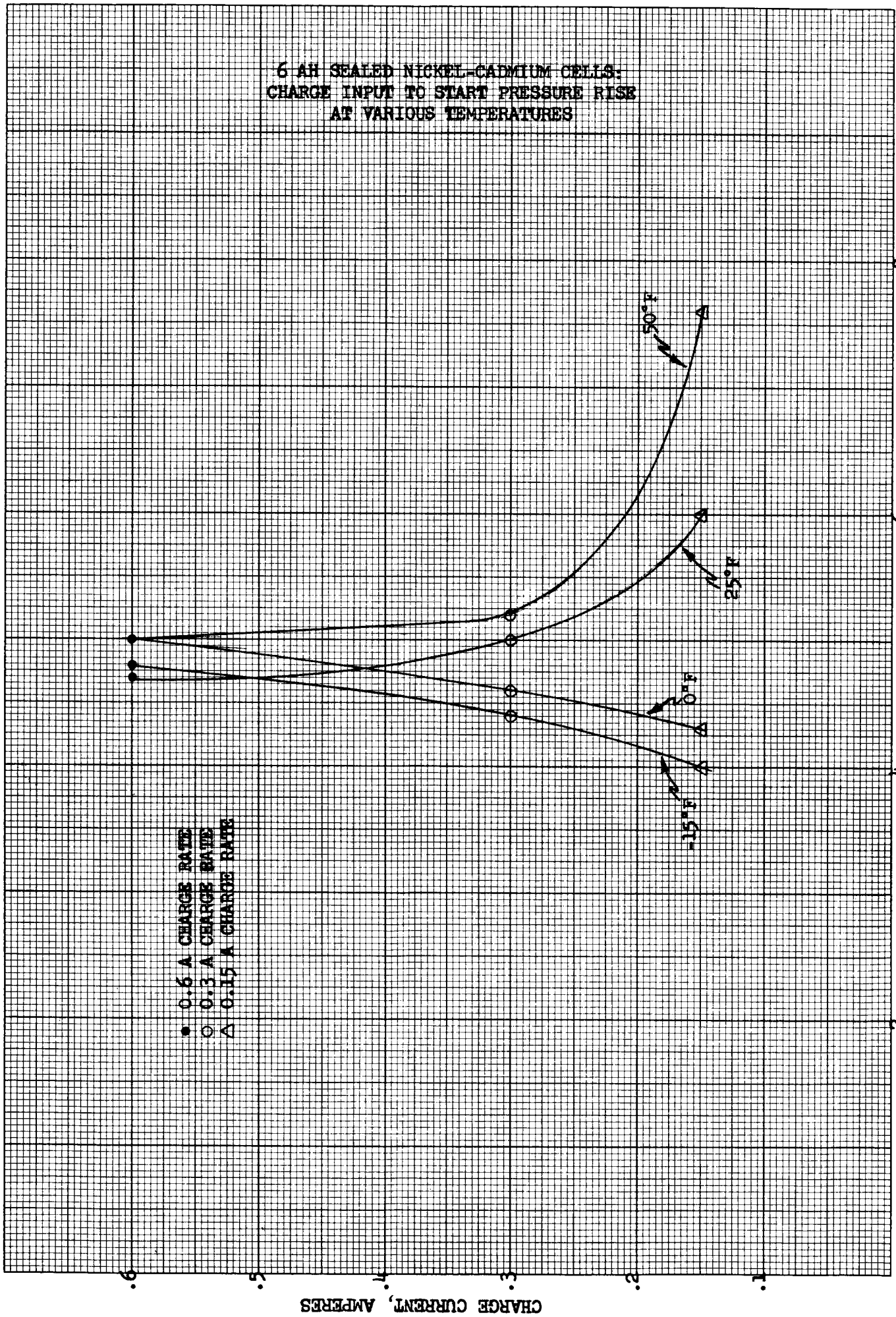

M1510
AB 3000-F

FIG. 40

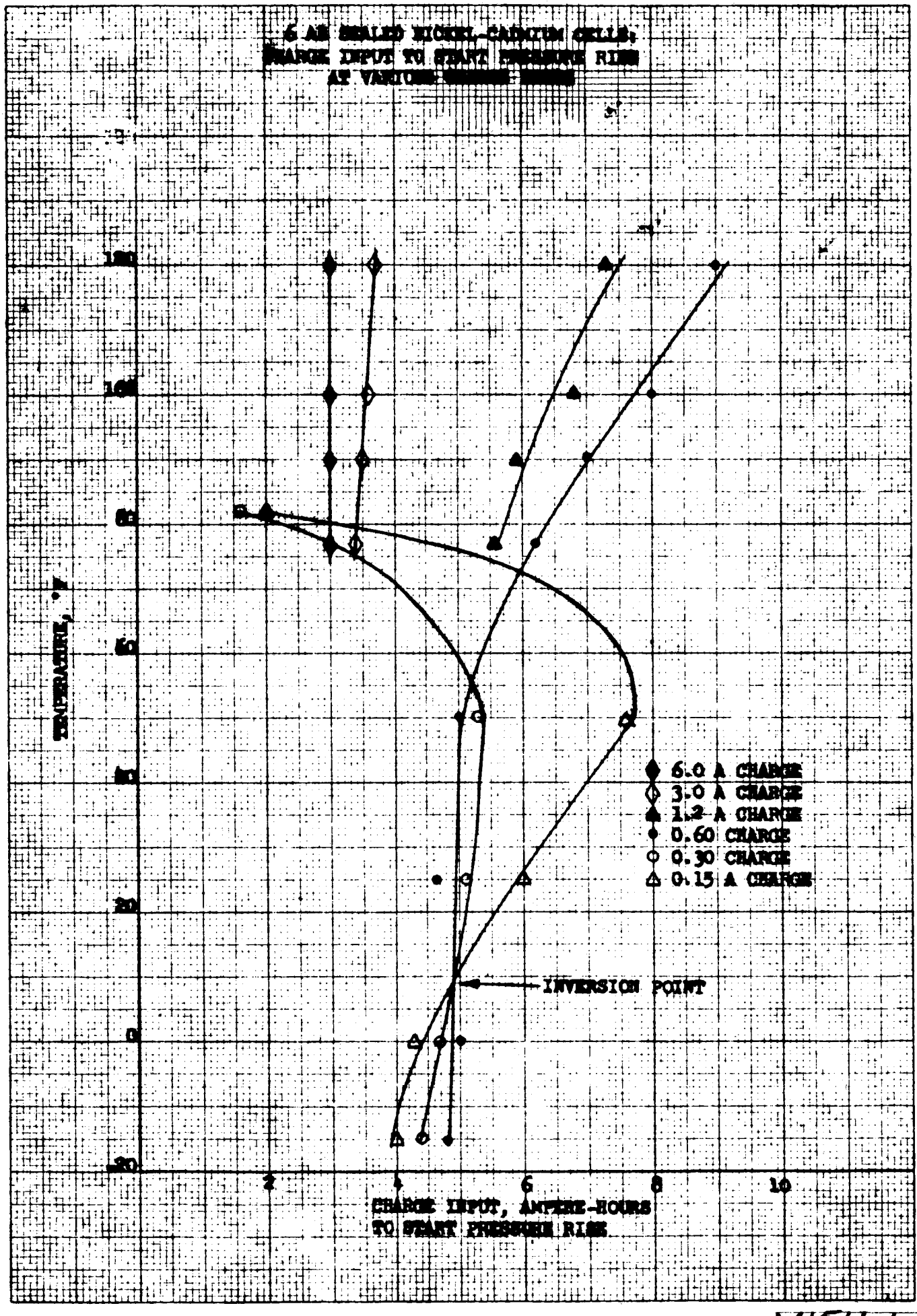
6 AH SEALED NICKEL-CADMIUM CELLS:
CHARGE INPUT TO START PRESSURE RISE
AT VARIOUS CHARGE RATES
TEMPERATURE, °F
100
80
60
40
20
0
-20
2
4
6
8
10
CHARGE INPUT, AMPERE-HOURS
TO START PRESSURE RISE
6.0 A CHARGE
3.0 A CHARGE
1.2 A CHARGE
0.60 CHARGE
0.30 CHARGE
0.15 A CHARGE
INVERSION POINT

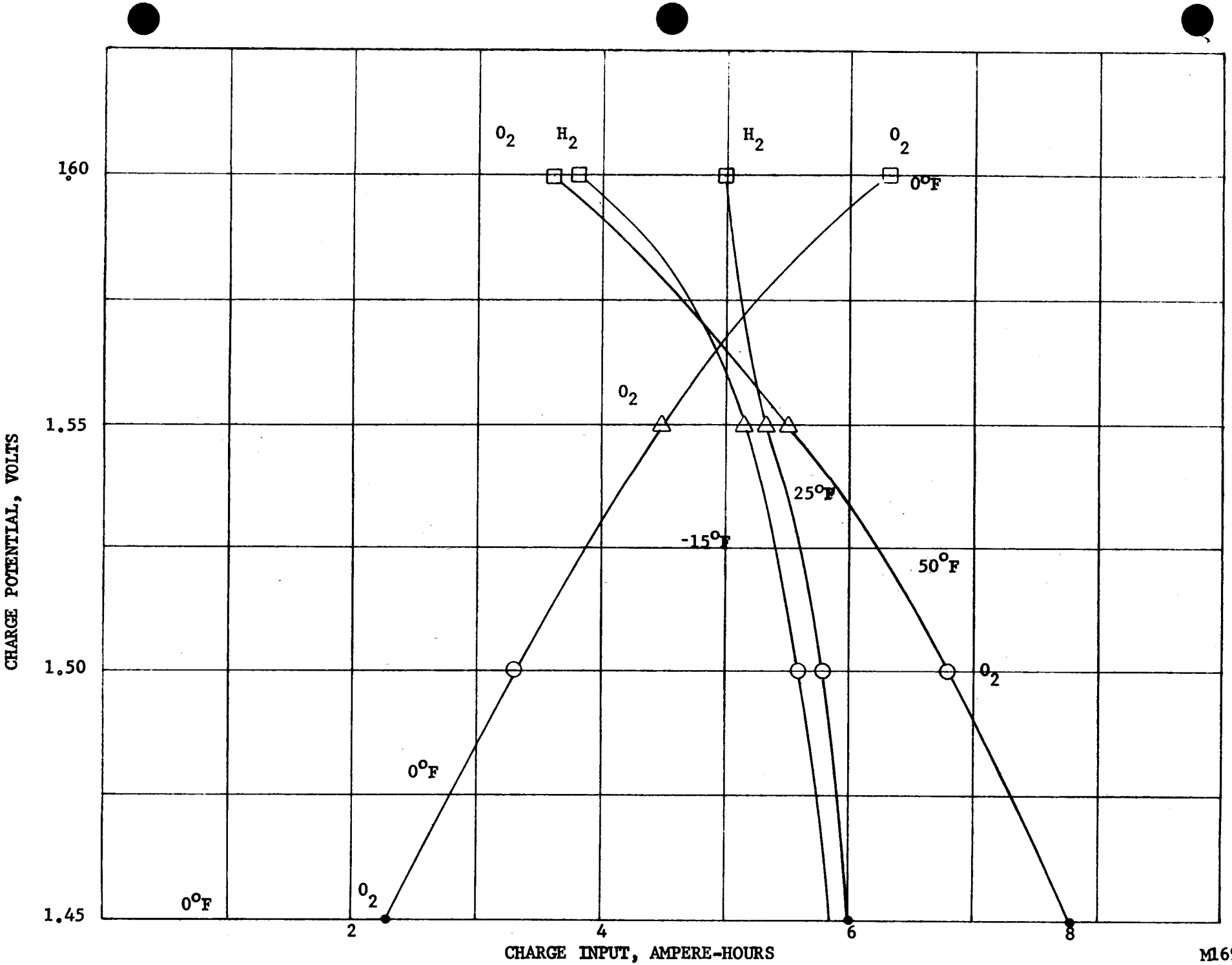

Figure 41 Charge Input to Start Pressure Rise in VO-6 HS Cells at Various Temperatures

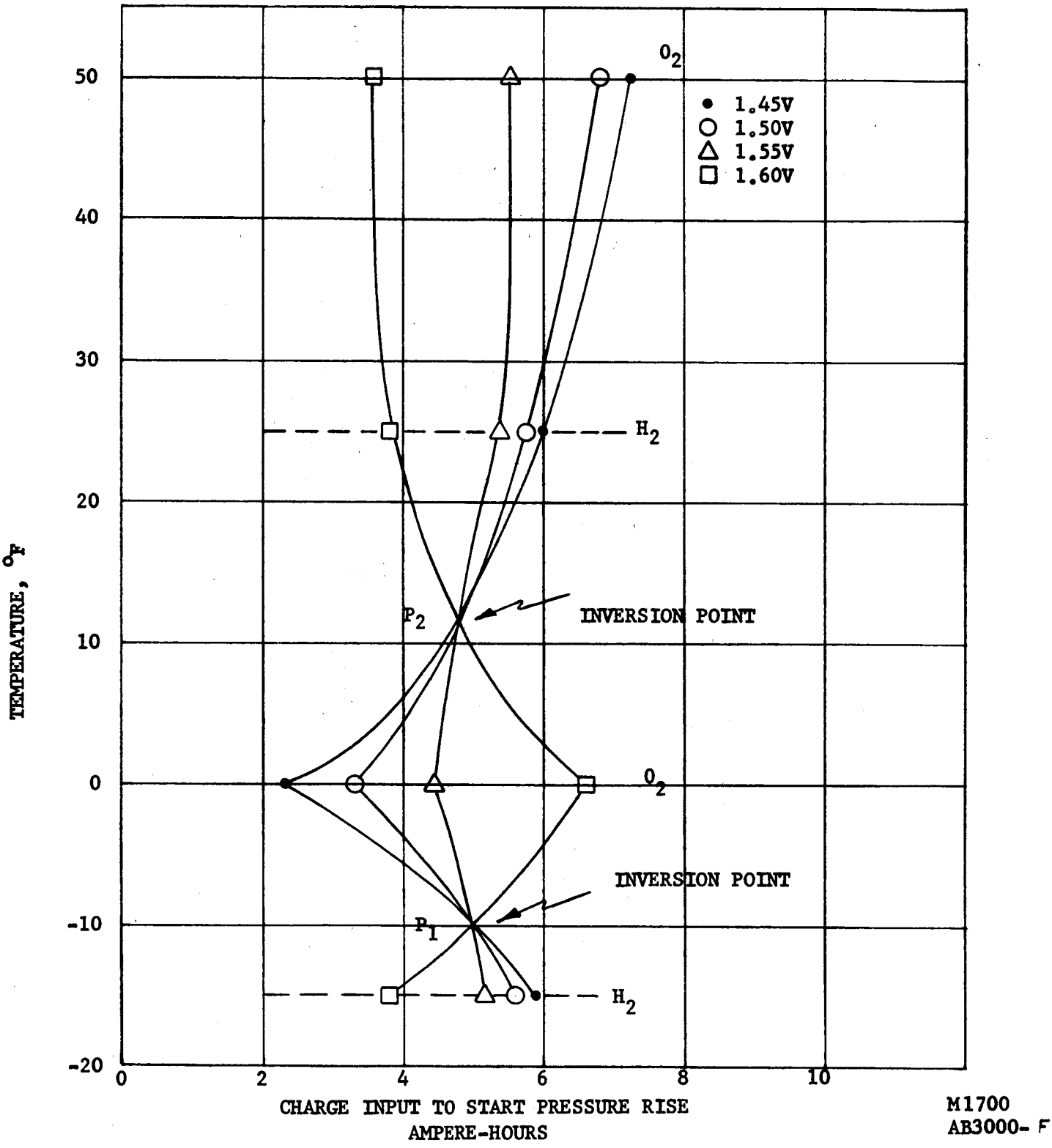

Figure 42 Charge Input to Start Pressure Rise in VO-6 HS Cells at Various Potentials

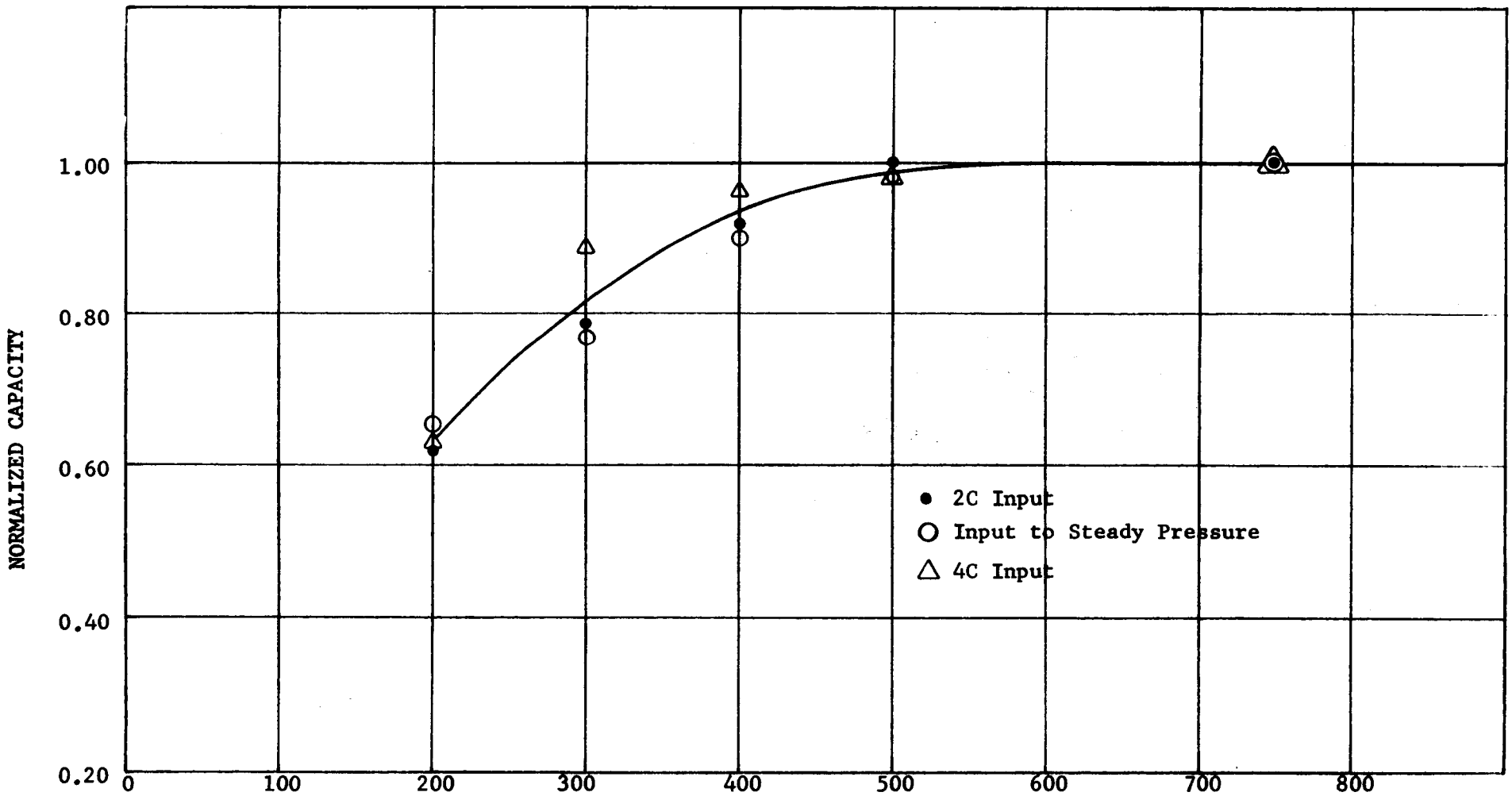

M1670
AB3000- F

Figure 43 Normalized Capacity of VO-6 HS Cells Following Charge at Various Rates

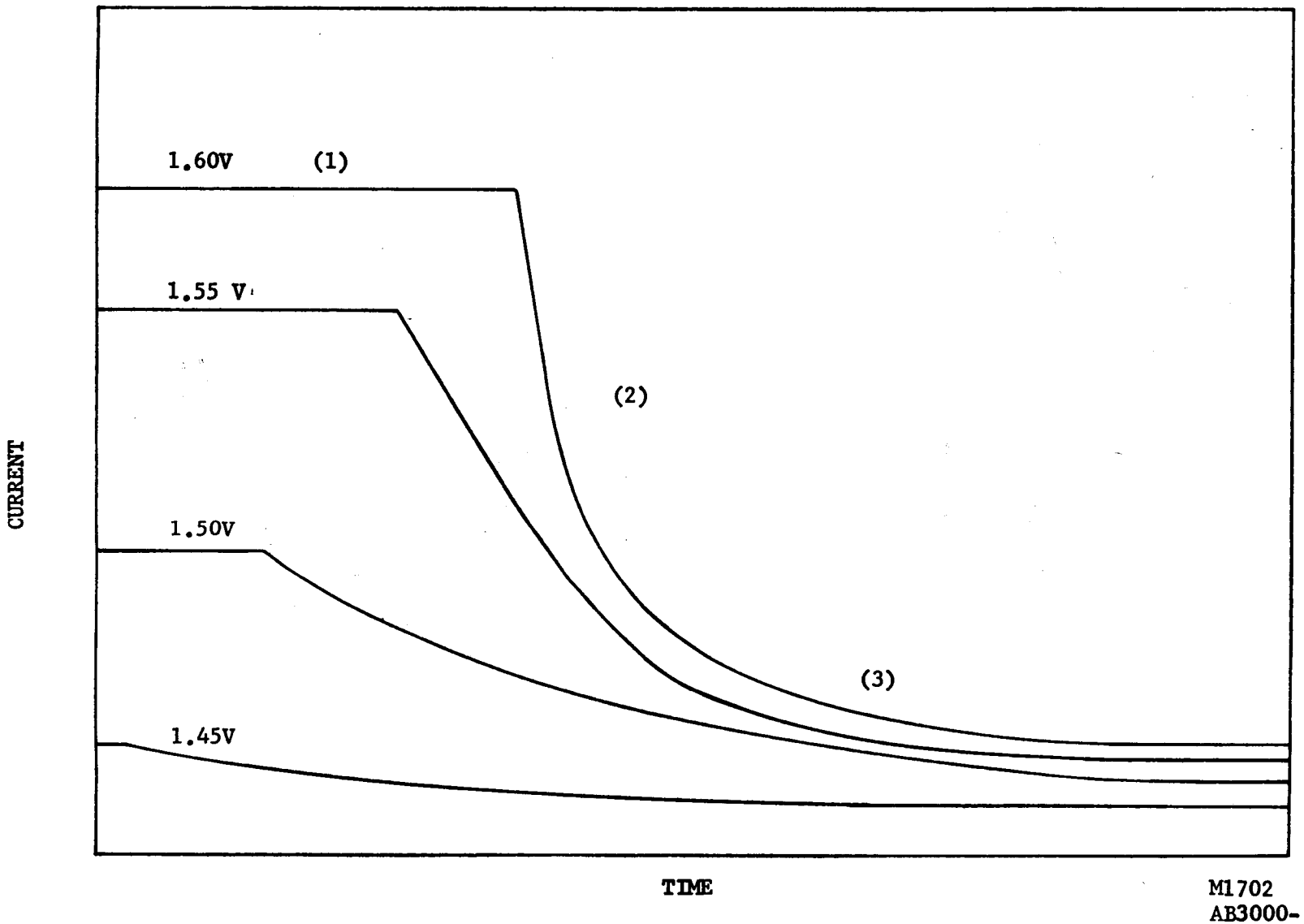

Figure 44 Typical Set of Current Vs. Time Curves Obtained During Constant Potential Charges at any Temperature

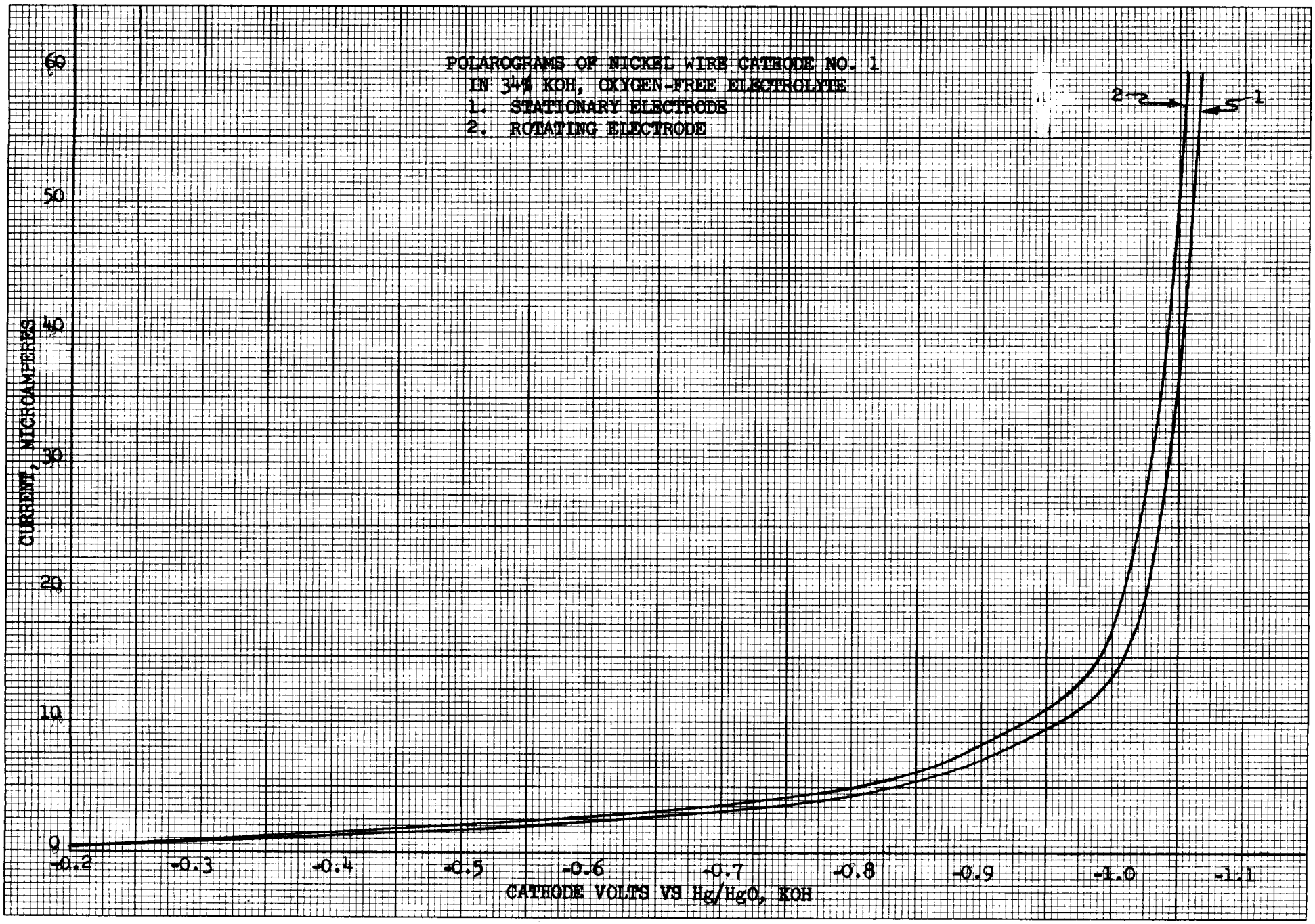

FIG. 45

M1500
AB 3000-F

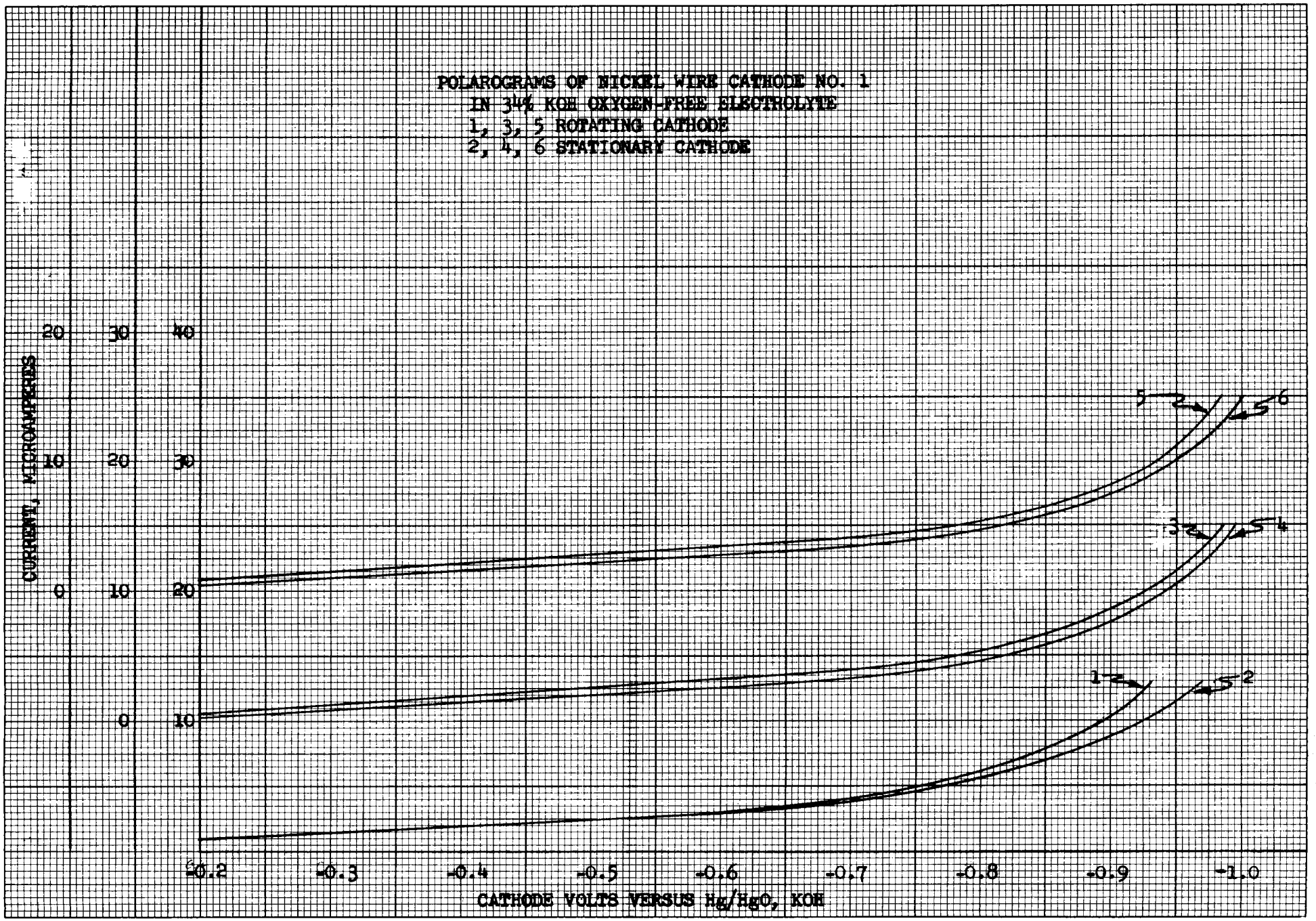

FIG. 46

M1501
AB 3000-F

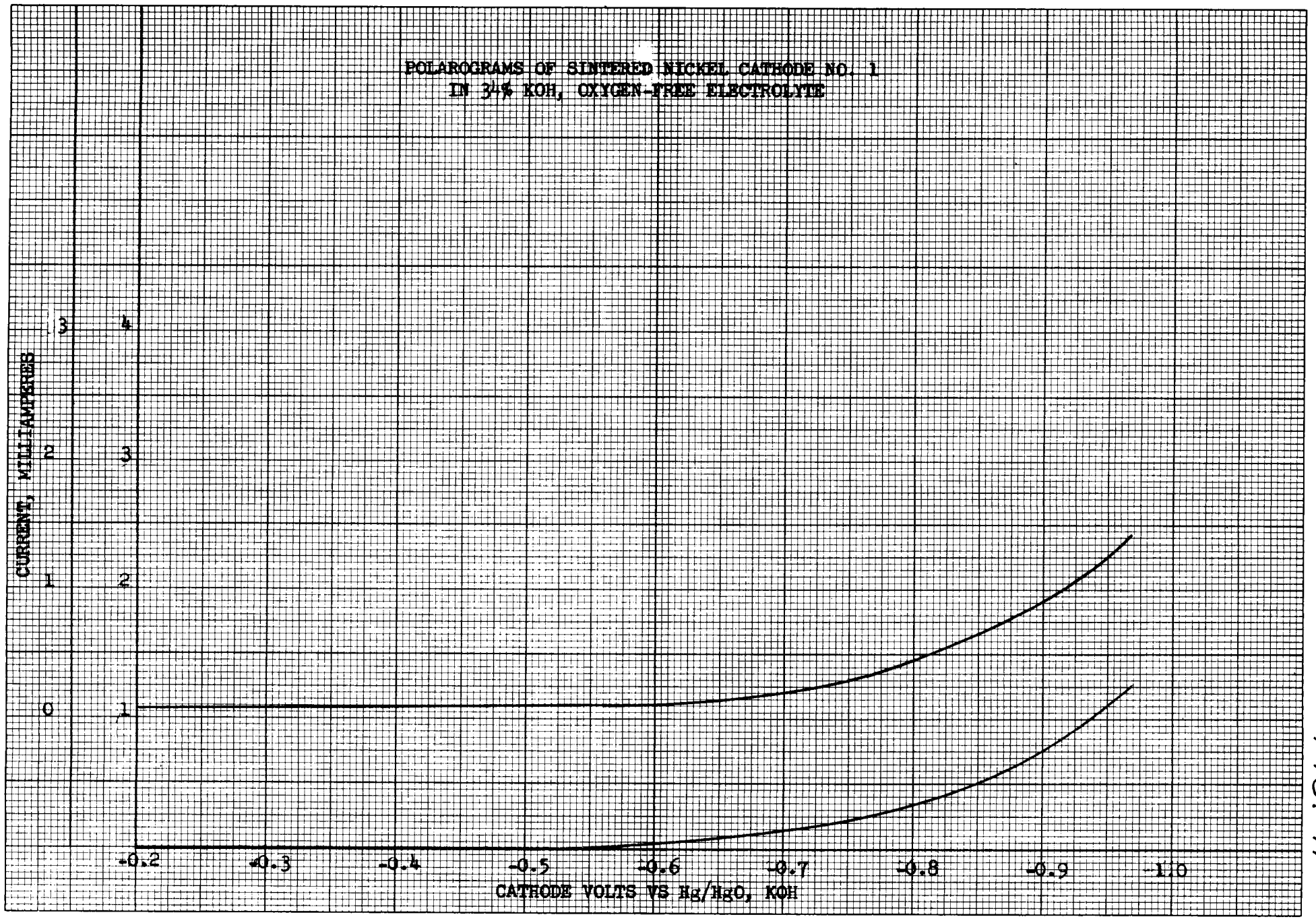

FIG. 47

M1502
AB 3000-F

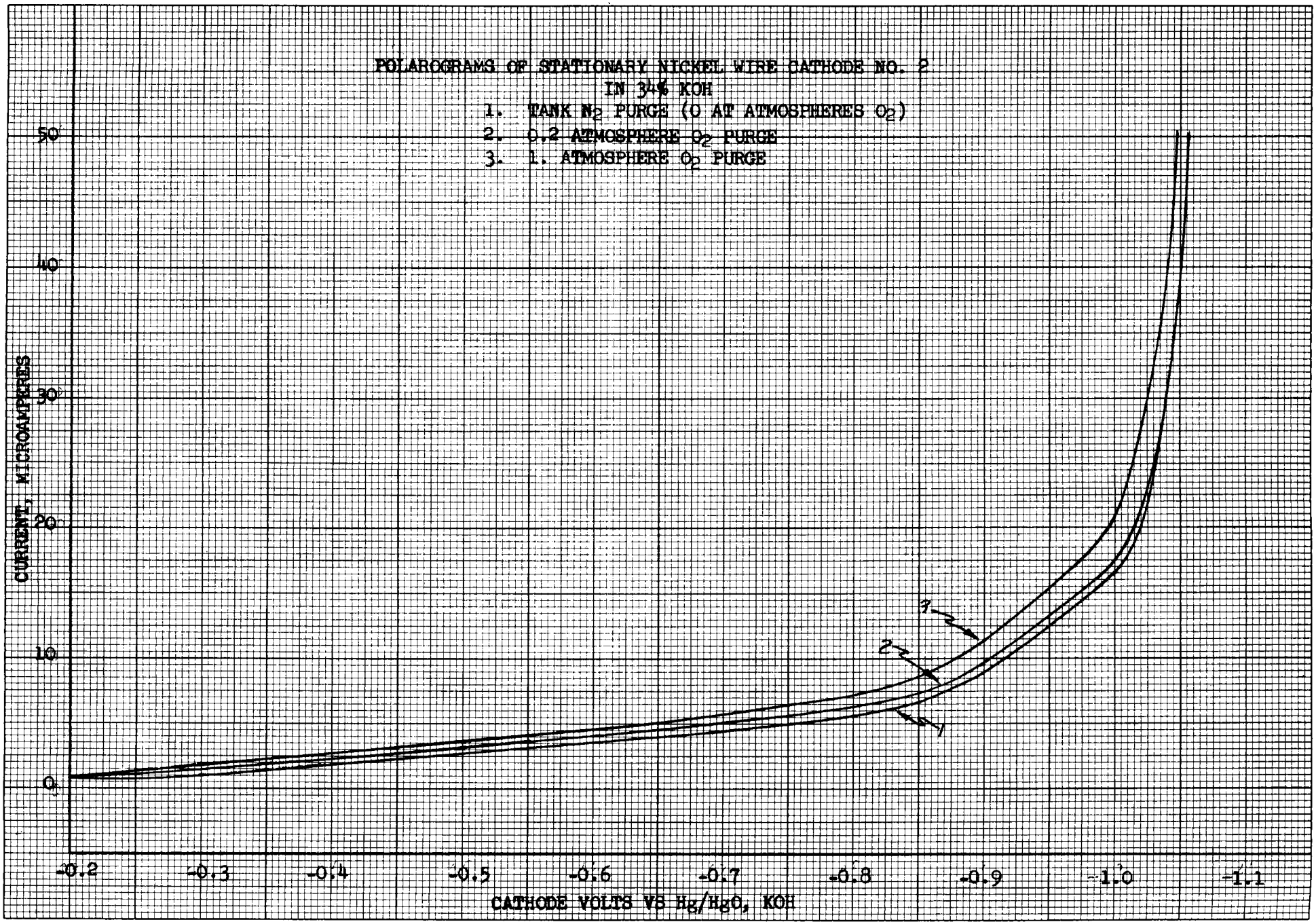

FIG. 48

M1503
AB-3000-E

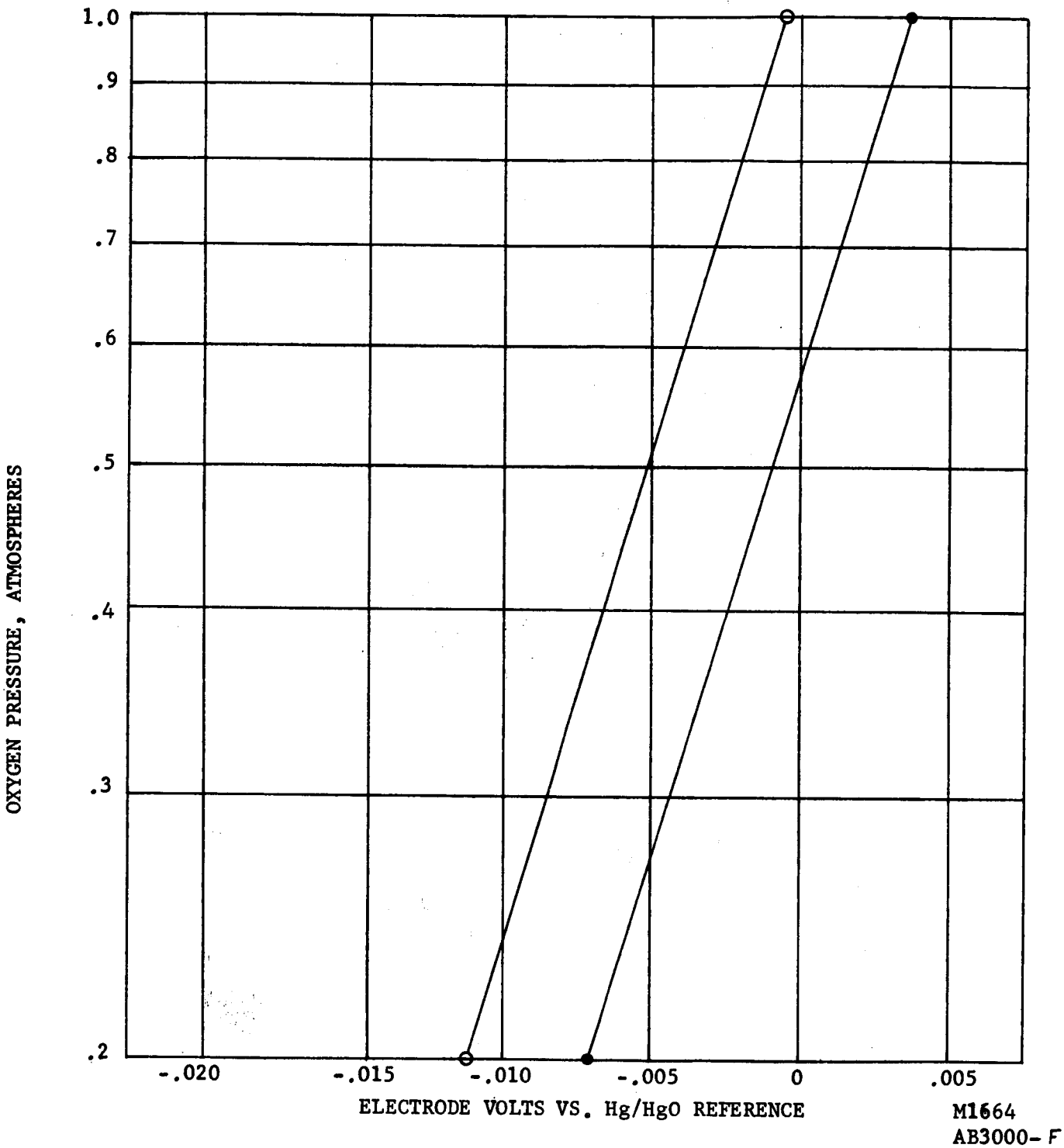

Figure 49 Effect of Pressure on Potential of Selected Hg/HgO - Graphite Pasted Electrodes.

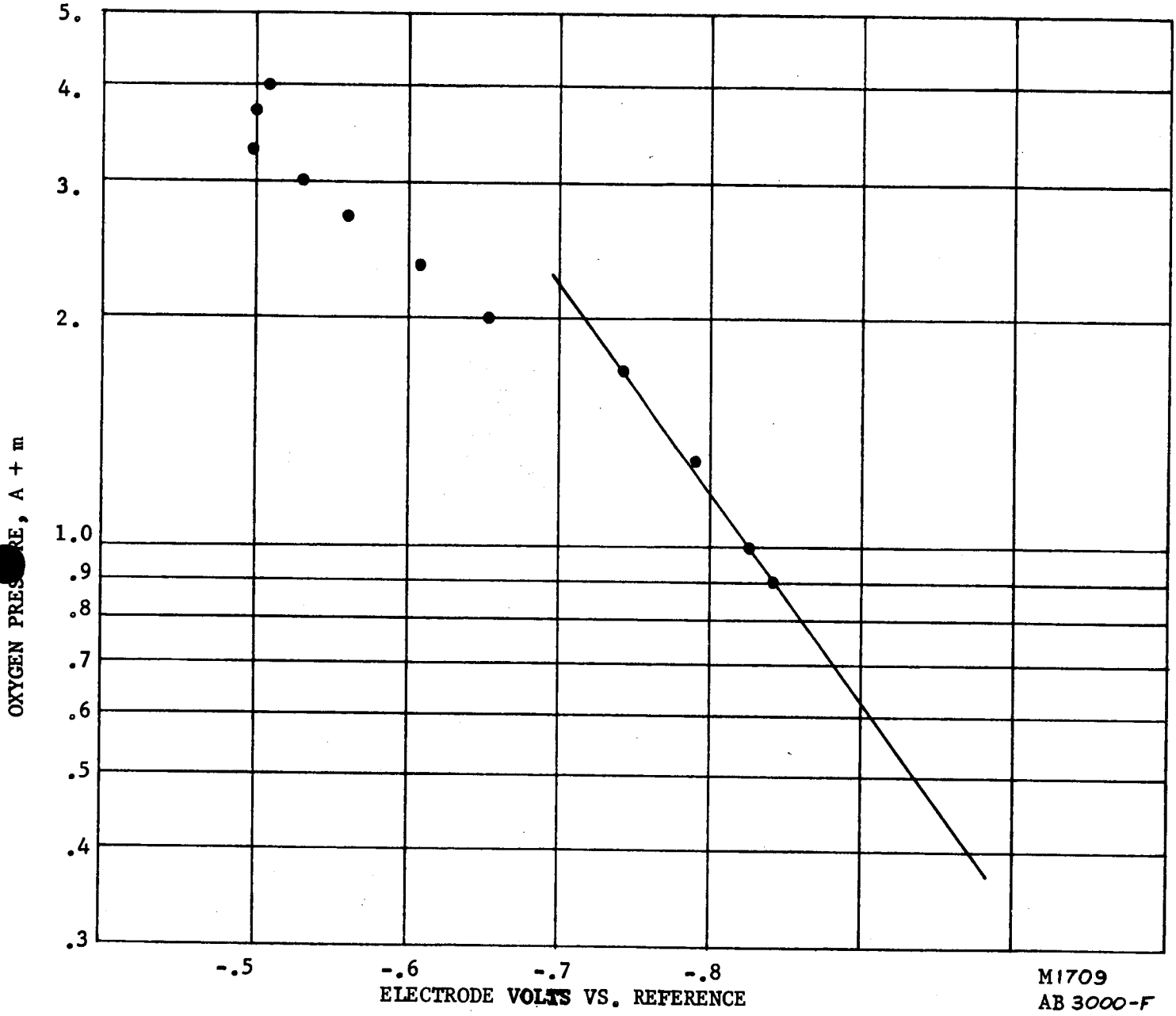

Figure 50 Nernst Relationship of the Oxygen Consuming Ni Electrode During Charge (i = 0.6A, C/10) Cell Ni-Blank (2) Run #1 with Hg/HgO Pressed Electrode, T = 77°F

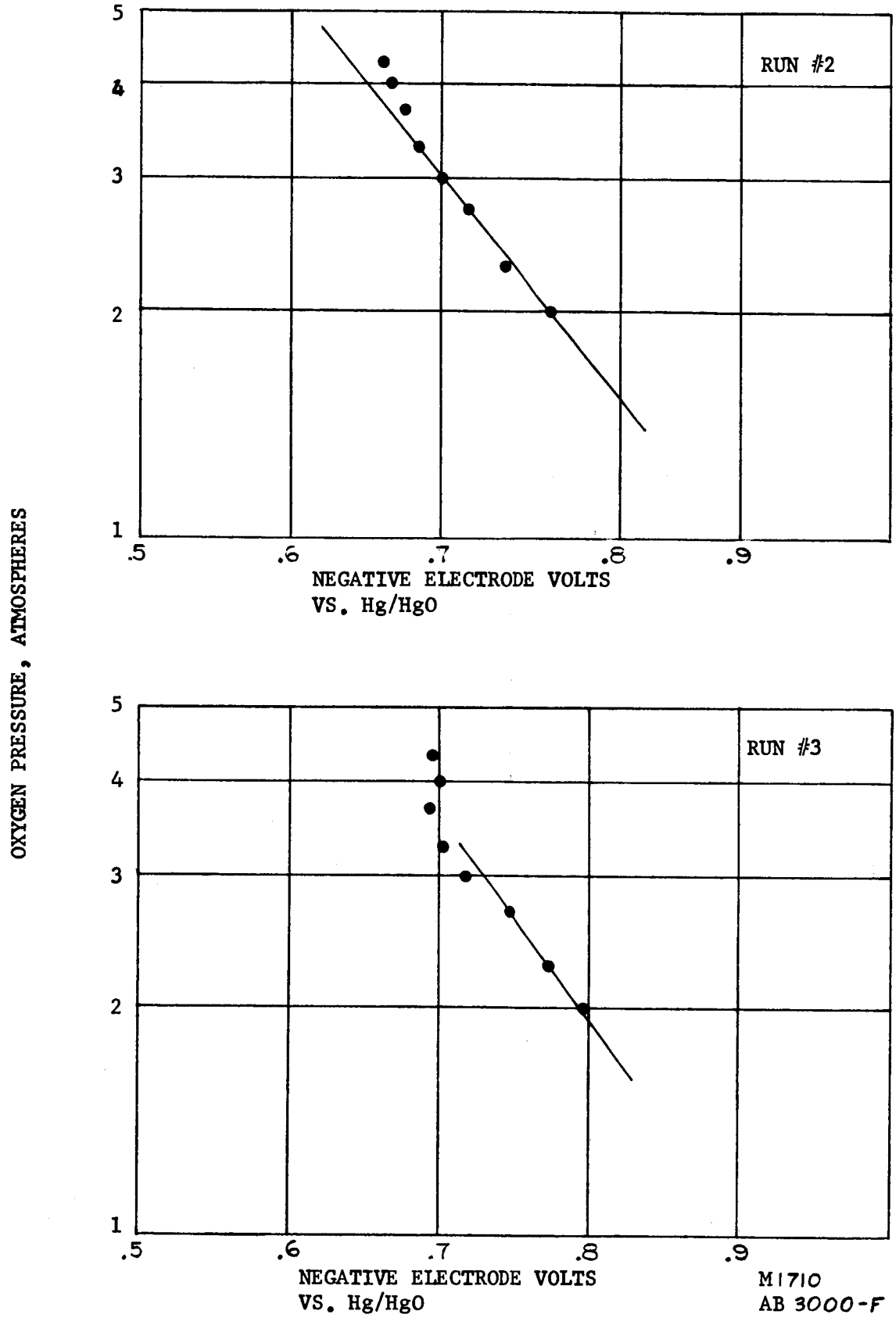

Figure 51 Nernst Relationship of the Oxygen Consuming Ni Electrode During Charge (i = 0.6A, C/10) Cell Ni-Blank (2) Run 2 & 3 with Hg/HgO Pressed Electrode, R = 77°F